

High pressure CO_2/CH_4 separation
with glassy polymer membranes

Aspects of CO_2 -induced plasticization

Alie Bos

**HIGH PRESSURE CO₂/CH₄ SEPARATION
WITH GLASSY POLYMER MEMBRANES**

Aspects of CO₂-induced plasticization

PROEFSCHRIFT

ter verkrijging van
de graad van doctor aan de Universiteit Twente,
op gezag van de rector magnificus,
prof. dr. Th.J.A. Popma,
volgens besluit van het College voor Promoties
in het openbaar te verdedigen
op vrijdag 13 december 1996 te 15.00 uur

door

Aaltje Bos

geboren op 23 maart 1968
te Emmen

Dit proefschrift is goedgekeurd door de promotor prof. dr. ing. H. Strathmann
en de assistent-promotor dr. ing. M. Wessling

Voorwoord

Mijn eerste kennismaking met membranen was tijdens de stage- en afstudeerperiode van het HLO, niet wetende dat ik er nog eens vier jaar onderzoek aan zou wijden. In die vier jaar heb ik naar hartelust membranen kunnen strijken en karakteriseren en aan opstellingen kunnen sleutelen. Het begeleiden van studenten en het bezoeken van congressen waren leuke bijkomstigheden.

De begeleiding van mijn project lag in handen van prof. Heiner Strathmann, van Marcel Mulder in het eerste jaar en van Matthias Wessling de resterende drie jaar.

Voor de technische ondersteuning was er Ineke Pünt. Zij heeft een groot deel van het experimentele werk uitgevoerd. De samenwerking met haar was grandioos. Haar manier van werken sloot feilloos aan bij de mijne. Daarnaast hebben de HTS-studenten Jason Viotty, Eric Brinkers en Johan Gierlings elk een eigen steentje bijgedragen aan dit proefschrift.

Het was ook altijd prettig dat mensen zoals Clemens Padberg, John Heeks en Zandrie Borneman altijd klaar stonden om te helpen. Hetzelfde gold voor Arie Pleiter en Fred ter Borg van het hoge-druk-lab met wie ik een sorptie-opstelling heb kunnen bouwen.

Na drie jaar experimenteren werd het dan tijd eens achter de computer te gaan zitten om alle bevindingen op te schrijven. Daarbij heeft mijn kamergenoot Erik Meuleman mij nog op handige trucjes op de computer kunnen wijzen. Naar mate de tijd verstreek werd mij ineens duidelijk dat 'spelen' op de computer ook z'n nut heeft.

De inhoud van dit proefschrift is mede gegroeid door discussies met Matthias Wessling. Hoewel hij veel van het onderwerp afwist door zijn eigen promotie-onderzoek, heeft hij mij toch mijn eigen weg laten bewandelen. Daarnaast zijn de discussies met collega-a.i.o.'s/o.i.o.'s, postdocs en echtgenoot evenzo belangrijk geweest. In het eerste jaar waren Jeroen Boom en Richard Bouma altijd bereikbaar. De discussies met Josef Thesing hebben een grote bijdrage geleverd aan de FTIR-metingen. En tijdens het schrijven van dit proefschrift heb ik veel gehad aan de inzet van Willem Kools, Nico v.d. Vegt, Matthias Wessling en Ingo Blume. Mede door het enthousiasme waarmee zij mijn werk hebben gelezen, bekritiseerd en bediscussieerd heb ik veel plezier in het schrijven gehad.

En dan kom ik op het punt waar dit voorwoord overgaat in een dankwoord aan alle mensen die ik hierboven heb genoemd, aan de rest van de membraangroep voor de prettige werksfeer, aan familie en vrienden die altijd belangstelling voor mijn werk hebben getoond en aan Ingo in het bijzonder.

Bedankt!



SON/STW is gratefully acknowledged for their financial support.

ISBN 90-3650905-X

Copyright © 1996 A. Bos

All rights reserved.

Printed in the Netherlands by FEBODRUK B.V., Enschede

Contents

1 Gas separation membranes

1.1. Introduction	1
1.2. Gas transport through homogeneous dense membranes	4
1.3. Polyimides as membrane material	8
1.4. Plasticization phenomena	11
1.5. Scope of this thesis	15
1.6. List of symbols	16
1.7. References	17

2 Experimental methods

2.1. Introduction	21
2.2. Materials	22
2.3. Film preparation	24
2.4. Characterization	24
2.4.1. Single and mixed gas permeation	24
2.4.2. High pressure sorption	28
2.4.3. Glass transition and density measurements	31
2.5. Temperature dependence of permeability	32
2.6. Film morphology	35
2.6.1. Effect of film thickness on permeability	35
2.6.2. Effect of casting solvent on permeability	37
2.7. List of symbols	38
2.8. References	39

3 CO₂ - induced plasticization phenomena in glassy polymers

3.1. Introduction	41
3.2. Physical observations related to plasticization	41
3.3. CO ₂ plasticization related to chemical structure	49
3.4. Conclusions	63
3.5. References	64

4 Suppression of CO₂ plasticization

Part 1: Crosslinking by thermal treatment

4.1. Introduction	67
4.2. Background on crosslinking methods	68
4.3. Film preparation	70
4.4. Characterization of the treated Matrimid films	70
4.5. CO ₂ and CO ₂ /CH ₄ permeation behaviour	73
4.6. CO ₂ sorption and diffusion behaviour	78
4.7. Conclusions	81
4.8. References	81

5 Suppression of CO₂ plasticization

Part 2: Blending and semi-interpenetrating polymer networks

5.1. Introduction	85
5.2. Matrimid/P84 and Matrimid/PSF blends	86
5.2.1. Film preparation	86
5.2.2. Characterization of the films	86
5.2.3. CO ₂ permeation, sorption and diffusion behaviour of Matrimid/P84 blend	87
5.2.4. CO ₂ /CH ₄ permeation behaviour	89
5.3. Matrimid/Thermid blends: s-ipns	92
5.3.1. Background on semi-interpenetrating polymer network formation	92
5.3.2. Film preparation	93
5.3.3. Characterization of the films	94
5.3.4. CO ₂ permeation behaviour	96
5.3.5. CO ₂ /CH ₄ permeation behaviour	102
5.4. Conclusions	104
5.5. References	105

6 FTIR study of CO₂ in Matrimid films

6.1. Introduction	107
6.2. FTIR of Matrimid films	108
6.2.1. Background on FTIR spectroscopy	108
6.2.2. Experimental methods	109
6.2.3. Interpretation of the FTIR-spectrum of Matrimid	109
6.3. FTIR in the presence of CO ₂	111
6.3.1. Background on infrared spectra of CO ₂	111
6.3.2. Experimental methods	113
6.3.3. Results and discussion of FTIR in the presence of CO ₂	115
6.4. Conclusions	124
6.5. References	125

7 Process calculations

7.1. Introduction	127
7.2. Permeator analysis	128
7.2.1. Background	128
7.2.2. Results and discussion	132
7.3. Cost accounting	135
7.3.1. Background	135
7.3.2. Results and discussion	137
7.4. Conclusions	142
7.5. List of symbols	143
7.6. References	144
Summary	145
Samenvatting	148
Levensloop	151

1

Gas separation membranes

1.1. Introduction

Membranes

The concept of separating gases with polymeric membranes is more than 150 years old. The first publications related to gas separation membranes are addressed to Mitchell [1,2] and Graham [3]. Mitchell observed that natural rubber balloons filled with hydrogen gas descended after a period of time. He attributed this phenomenon to gas release by diffusion through the balloon wall. Graham repeated Mitchell's experiments with films of natural rubber and made the first quantitative measurements of the rate of gas permeation. However, the widespread use of gas separation membranes has occurred only within the last 20 years. A breakthrough was the introduction of the Prism membrane system of Monsanto in 1979 [4]. These membranes were used for the recovery of hydrogen from process streams in the ammonia synthesis. Since that time, the market for gas separation membranes has expanded enormously. A nice review on the development of gas separation membranes on the market that expanded into more demanding areas is given by Koros and Fleming [5].

Although membranes have proven their usefulness, membrane technology has to compete with conventional techniques such as cryogenics, adsorption and absorption processes, for example pressure swing adsorption and amine treatment [6-9]. Commercialization depends on the development of membranes with sufficient productivity and separating ability to make them economically attractive in industrial applications. Advantages of membranes are low capital investment, ease of operation, low energy consumption, cost effectiveness even at low gas volumes and good weight and space efficiency [6,7]. The latter, for example, comes to the credit of membranes in natural gas cleaning on offshore platforms or environmentally sensitive areas. For this application, amine treatment is still an efficient method, but the amine units are large and heavy.

Despite all the advantages of membranes, it is still difficult to introduce membranes on a market where people are familiar with the conventional separation techniques. But given the number of commercial-scale membrane

suppliers [6,10], there is a growing acceptance of membranes in industry. And considering the recent reviews and books [5,11-15] appeared on polymeric gas separation membranes over the last five years, there is also a tremendous progress in the theoretical and experimental aspects of the gas separation technology.

Membranes can be classified on the basis of their morphology or the separation process [16]. Current gas separation membranes are thin dense films, integrally skinned asymmetric membranes or composites mainly prepared from glassy polymers [6]. Asymmetric membranes have a dense top layer and a porous substructure and are formed by a phase inversion process [17]. Composites have a dense top layer and a porous substructure. The top layer is created in a separate step for example by coating. In both cases, the permselective top layer should be as thin as possible ($<1 \mu\text{m}$) to achieve a high flux. The substructure should have good mechanical strength with negligible gas transport resistance. Thin polymeric films by themselves are too weak to withstand the high differential gas pressures required in gas separation operations. Membranes with a support layer are therefore the most applied ones. The advantage of a composite membrane is that the top layer and the support can be optimized separately.

Membrane processes

The research described in this thesis has mainly been concentrated on the separation of carbon dioxide and methane. In this field, three major applications are distinguished [6,18]:

Enhanced Oil Recovery (EOR)

In enhanced oil recovery, the gas stream exits the field at high pressures, frequently at pressures up to 140 bar. Carbon dioxide is used as injection medium into existing oil fields to increase the oil production. The oil is easily driven to the surface, because its viscosity is lowered by the dissolved CO_2 . Simultaneously with the oil, casing head gas is produced. This gas contains a variety of hydrocarbons including substantial amounts of methane and is mixed with CO_2 at the well. Concentration levels of 40 to 90 mol % carbon dioxide are achieved [6]. The CO_2 must be removed to utilize the hydrocarbons. In this application, the natural gas as well as the carbon dioxide is the desired product, to be used respectively as fuel or for reinjection. In the latter case, a purity of 95 mol % is often sufficient to maintain the solvent power of CO_2 .

Natural gas sweetening

Natural gas sweetening processes remove CO_2 from high-pressure methane stemming from natural gas wells. Many natural gas streams are available at pressures in the range of 28 to 83 bar [19]. Membranes are often used in combination with traditional gas separation processes [6]. The bulk of CO_2 can be separated from the raw gas with membranes and the final purification to pipeline quality gas can be performed by for example an amine absorption

process. Such hybrid processes take advantage of both processes that neither process could achieve separately. For example, a capacity increase of an existing amine plant can be achieved by integrating a membrane unit. One can also think about reduction of the operating costs of the amine unit that can be downsized if most of the CO_2 is removed.

CO₂ recovery from landfill gas

Landfill gas is produced at atmospheric pressures resulting from decomposition of organic material under anaerobic conditions. This biogas contains 40-45 mol % CO_2 , 54-59 mol % CH_4 , some water vapour (1%), nitrogen (4%), oxygen (1%) and traces of H_2S and halogenated hydrocarbons (CFC). When the landfill site is covered, the gas can be collected for use. A possibility is the upgrading of CH_4 for use in the local gas distribution system [20,21]. For this application the toxic trace components H_2S and CFC are removed first by an adsorption process. The remaining gas stream is fed to a membrane system and is often compressed to higher pressures, up to 35 bar, to enhance membrane efficiency.

Research objectives

As can be concluded from the examples for CO_2/CH_4 separation applications, the process conditions are harsh. The high feed pressures require membrane materials that can withstand these conditions. Furthermore, a high total feed pressure also implies a high partial CO_2 pressure. It is known that CO_2 acts as a plasticizer at elevated pressures [22,23]. The absorbed gas weakens the polymer material, which results in a decrease of the separating ability of the membrane. This thesis focuses therefore on two topics:

- (1) understanding of CO_2 -induced plasticization on a molecular level,
- (2) identifying methods to suppress plasticization.

With this knowledge a good membrane material can be developed for the separation of carbon dioxide and methane at high feed pressures.

In the next section, a definition of a gas separation membrane and the basics of gas transport are given. A brief summary about polyimides as membrane material is given in the third section. Because of the harsh process conditions, there is a demand for new membrane materials. Polyimides are good alternatives for polysulfone and cellulose acetate which are currently used. Additional to the good gas separation properties, polyimides also show good mechanical, chemical and thermal stability. Despite of their improved performance, the polyimides of interest are highly susceptible to plasticization. Therefore, CO_2 induced plasticization phenomena are studied. A brief introduction on phenomena related to plasticization is given in the fourth section. A more extensive description will be given in Chapter 3. The fifth section finally will summarize the scope of this thesis.

1.2. Gas transport through homogeneous dense membranes

Definition of a membrane

The most important part of a membrane separation process is the membrane itself. Looking in the published literature, it still seems to be difficult to find an exact definition of a membrane. This is because of the large application area of membranes, not only in gas separation but also in for example purification of liquids. A general definition for gas separation is: "A membrane is a barrier material through which one component of the feed mixture permeates much easier than the others, which leads to a separation of the components". More comprehensive definitions are collected by Lonsdale [24].

Parameters describing membrane performance

To compare membrane properties, two characteristic parameters are given for the performance or efficiency of a gas separation membrane [16]:

- The flow or flux (J) through the membrane, which is the *amount* of gas that permeates through the membrane per unit of time and unit of surface area. A specific *measure* of the gas permeation through a membrane is quantitatively expressed by the permeability coefficient (P).
- The separation factor (α), which is a measure of the separating ability of the membrane.

Gases diffuse through a nonporous membrane due to a chemical potential gradient expressed as a concentration gradient across the membrane. This concentration gradient is the driving force needed for transport. Fick's first law generally describes this transport of gases well. The flux can be expressed by:

$$J_i = -D_i \cdot \frac{dC_i}{dx} \quad (1.1)$$

where D is the diffusion coefficient and dC_i/dx the concentration gradient of a component i in the membrane. The equilibrium concentration (C_i) of a penetrant i in a polymer is related to its ambient pressure (p_i) by:

$$C_i = S_i \cdot p_i \quad (1.2)$$

Equation (1.2) is Henry's law in case the solubility (S_i) is independent of pressure, which means that the concentration is directly proportional to the pressure. And, if a constant diffusion coefficient is assumed, integration of Equation (1.1) over the membrane thickness ($x=0 \rightarrow x=\ell$) and subsequent substitution of Equation (1.2) in (1.1) yields:

$$J_i = \frac{D_i (C_{i,0} - C_{i,\ell})}{\ell} = \frac{D_i \cdot S_i (P_{i,0} - P_{i,\ell})}{\ell} \quad (1.3)$$

where J_i is the gas flux through the membrane of component i , D_i the diffusion coefficient, $C_{i,0}$ and $C_{i,\ell}$ the concentration at, respectively, the upstream and

downstream side of the membrane, S_i the solubility coefficient, $p_{i,0}$ and $p_{i,\ell}$ the pressure at, respectively, the upstream and downstream side of the membrane and ℓ the membrane thickness. The product $D_i \cdot S_i$ is the basic equation for the permeability (P_i) of component i :

$$P_i = D_i \cdot S_i \quad (1.4)$$

If the permeabilities of a gas pair are known, the ideal selectivity (α_{ij}^*) of the membrane is given by the ratio of the individual permeabilities:

$$\alpha_{ij}^* = \frac{P_i}{P_j} \quad (1.5)$$

This *ideal* selectivity (denoted by an asterix) depends only on the nature of the gas-membrane system under consideration and the temperature [25].

The separation factor (α_{ij}) is given by the mole fractions of both components at the downstream (permeate) and upstream (feed) side:

$$\alpha_{ij} = \frac{X_i^p \cdot X_j^f}{X_j^p \cdot X_i^f} \quad (1.6)$$

where X is the mole fraction and the superscripts (p) and (f) refer to the feed and permeate, respectively. The separation factor is related to the ideal selectivity as given in Equation 1.7.

$$\alpha_{ij} = \alpha_{ij}^* \cdot \frac{(X_i^f p^f - X_i^p p^p)}{(X_j^f p^f - X_j^p p^p)} \cdot \frac{X_j^f}{X_i^f} \quad (1.7)$$

If the gases do not interact strongly with each other and with the membrane material and the permeate pressure is kept close to zero, the separation factor will be essentially equal to the ideal selectivity.

Solution-diffusion model

Equation (1.4) is a simplified description of the solution-diffusion mechanism for gases through homogeneous dense membranes first postulated by Graham [3]. According to this model, transport occurs in three successive steps: sorption of the penetrant at the feed side of the membrane, diffusion through the membrane and desorption at the permeate side. However, transport is not as easily described as written here. Equation (1.4) is given for ideal systems, for example for gases that have no interactions with the membrane material, such as O_2 , N_2 , H_2 and He at sufficiently low pressure. The solubility and diffusivity coefficients are often complex functions of many variables, in particular for gases such as carbon dioxide. In general, the diffusion coefficient and the solubility coefficient are functions of temperature and penetrant concentration or pressure.

Diffusion through nonporous membranes is possible because of the existence of free volume [26,27]. These “empty spaces” in the polymer matrix are possible sorption sites for gas molecules. The polymer segments surrounding a sorbed gas molecule can displace by thermal fluctuations. If the displacement is large enough, the trapped molecules jump from one cavity to another in the direction of the concentration gradient [28,29]. With Computer Aided Molecular Modelling the migration of penetrant molecules can be simulated. And as shown by Smit [30] and Gusev et al. [31], diffusion takes place via a discrete jump mechanism.

The transport mechanism is mainly influenced by the molecular structure of the polymer itself. Short range motions in the polymer chains, such as chain bending, bond rotation and phenyl ring flips allow penetrant molecules to proceed into the direction of the lower chemical potential. In contrast to rubbery polymers, which have flexible chains, free segmental rotations of the polymer chains are restricted in the glassy state. The arresting of segmental motions during cooling through the glass transition region creates additional fixed holes or microcavities within the material. This is the reason of the nonequilibrium state of a polymeric glass. The additional free volume, also called excess or unrelaxed free volume, is actually due to a state of lower polymer density. Glassy polymers are therefore able to discriminate between penetrants on the basis of their sizes and shapes, which contributes to an enhanced selectivity compared to rubbery polymers.

The solubility coefficient indicates how much gas can be absorbed by the polymer membrane and depends on the condensibility as well as physical interactions of the penetrants with the particular membrane material. The solubility is determined via the concentration of the sorbed gas per unit polymer volume. The concentration as a function of pressure and at constant temperature shows a sorption isotherms with a characteristic shape that is concave to the pressure axis. Different models are available to describe the sorption of gases in glassy polymers. They all have in common that they try to describe the concave shape of the isotherm.

Sorption models

Here only a few examples of sorption models will be given. A detailed overview of the existing models can be found in the literature [32-44]. All models have their advantages as well as disadvantages. To be able to discriminate between the various models describing gas transport in homogeneous membranes, an intensive study is necessary. This has not been done, because it is not the purpose of this thesis to verify the validity of the existing models.

The first and most widely used model is the dual-mode sorption model [32]. In this model, two different sorption mechanisms are distinguished: sorption in the homogeneous densified matrix described by Henry's law and sorption in microcavities “frozen” into the polymer matrix obeying a Langmuir type of sorption. Equation (1.8) describes the total concentration of component i (C_i)

sorbed by the polymer at equilibrium:

$$C_i = C_{i,D} + C_{i,H} = k_{i,D}p_i + \frac{C_{i,H}b_i p_i}{1+b_i p_i} \quad (1.8)$$

where $C_{i,D}$ is the concentration of component i sorbed in the Henry mode, $C_{i,H}$ the concentration of component i sorbed in the Langmuir mode, $k_{i,D}$ the Henry's law or solubility constant, p_i the pressure, $C_{i,H}$ the Langmuir capacity factor and b_i the hole affinity constant of component i .

This model initially assumed a complete immobilization of the gas molecules sorbed in the Langmuir mode. However, Petropoulos [33] and later Koros and Paul [34] made plausible that these molecules were only partially immobilized. Therefore, the extended dual-mode sorption model assumes two distinct diffusion coefficients, $D_{i,D}$ and $D_{i,H}$, characterizing the mobility of component i in the Henry and Langmuir domains, respectively. Combination of this assumption with the general solution-diffusion equation and Equation (1.8), Petropoulos and Koros and Paul derived an equation for the permeability (P_i) of component i as a function of pressure. The approach of Koros and Paul is given in Equation (1.9) because this one has been applied more extensively [35].

$$P_i = k_{i,D}D_{i,D} \left(1 + \frac{C_{i,H} b_i}{k_{i,D}} \frac{D_{i,H}}{D_{i,D}} \frac{1}{1+b_i p_i} \right) \quad (1.9)$$

The only difference in the two approaches is that Petropoulos suggested a driving force based on chemical potential, whereas Koros and Paul used a concentration gradient. The equation for the overall permeability also differs slightly. But, both show a decreasing permeability as a function of pressure, which approaches a limiting value ($k_{i,D}D_{i,D}$) as $p_i \rightarrow \infty$.

In fitting the concentration of gas sorbed as a function of pressure, the dual-mode sorption theory is so successful because it consists of only three fitting parameters (k_D , C_H and b) which will in most cases result in a good fit. There is some criticism about the validity of the underlying assumptions of the dual-mode theory. For example, no experimental evidence has been found yet for the existence of two distinct modes [49-51]. Furthermore, no interactions between gas and polymer are assumed. This is not likely in case of high sorption or plasticization. There are modifications developed to account for this problem, but the theory remains a phenomenological one without much predictive value.

An alternative of the dual-mode theory, which indeed accounts for gas-polymer interactions, is the gas-polymer-matrix model proposed by Raucher and Sefcik [36]. A single sorption site is assumed to exist and the equation relating the sorption to the applied gas pressures contains only two parameters. However, it seems difficult to correlate the parameters with gas properties in a meaningful way. Kirchheim [37,38] describes sorption in glassy polymers by assuming a Gaussian distribution of free volume hole sizes. He uses Fermi-Dirac statistics to

calculate the fraction of these sites that are occupied at a given pressure.

A completely different approach of describing the sorption behaviour of gases in glassy polymers are the Flory-Huggins based models. The Flory-Huggins theory is developed for sorption of liquids. This theory can also be applied for gases, if it is assumed that the gas in the polymer matrix behaves like a liquid. Examples are the Flory-Huggins model of Vrentas and Vrentas [39] based on the penetrant-induced glass transition temperature depression, the elastic strain corrected lattice model of Bitter [40] and the thermodynamic model of Lipscomb [41] accounting for elastic deformation. Barbari and Conforti [42] developed a lattice-based activity coefficient model for glassy polymer. They combined sorption and dilation data to determine the parameters needed.

1.3. Polyimides as membrane material

Current commercially available gas separation membranes are prepared from various polymers, such as cellulose acetate and polysulfone [6]. These polymers are used because of their commercial availability and their processability combined with acceptable gas separation properties. In particular for CO₂/CH₄ separations better membrane performances are required. The ideal membrane has a high selectivity combined with a high permeability. This can be achieved by developing new tailor made polymers. Rigid aromatic glassy polymers, such as polycarbonates, polyetherimides, sulfonated polysulfones, polyamides, polyamideimides and polyimides are the new generation polymers. In particular polyimides are of interest. Ube already manufactures polyimide membranes, which are also utilized in CO₂/CH₄ separations [52].

Polyimides

The general structure of polyimides is given in Figure 1.1.

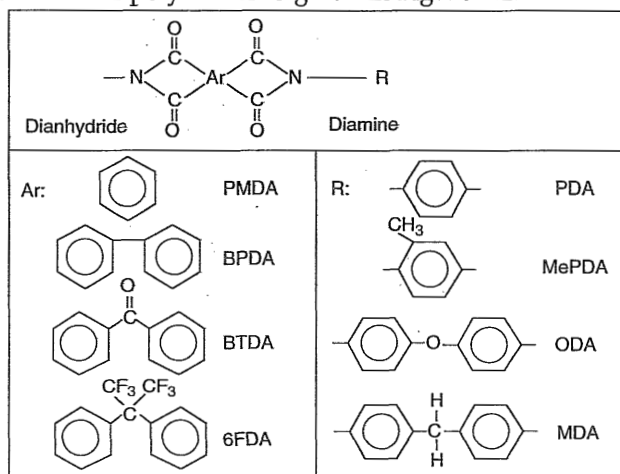


Figure 1.1. Chemical structure of polyimides with a selection of substituents.

Aromatic polyimides are formed in a polycondensation reaction of a dianhydride with a diamine [53-55]. This is a two-step process. In the first step, a tetracarboxylic acid dianhydride is added to a diamine solution leading to a polyamic acid. In the second step, the actual imidization takes place by extended heating at elevated temperature (thermal imidization) or by treatment with chemically dehydrating agents (=chemical imidization). The acronyms identifying the polyimides refer to the dianhydride (first part) and the diamine (second part).

Structure-property relationships

Polyimides are preferable to the many other polymers, because they combine higher selectivities with high permeabilities. The typical trade-off between productivity and selectivity is clearly seen in Figure 1.2. The data are obtained from the literature [13,15,56-59].

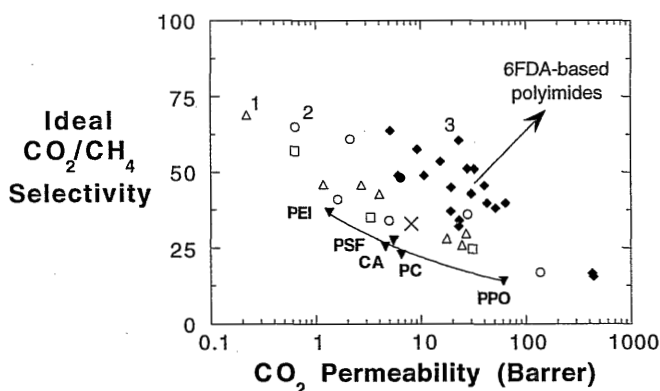


Figure 1.2. CO_2 permeabilities and ideal CO_2/CH_4 selectivities at 35 °C and 10 atm in various polymers [13,15,56-59]. Polyimides: PMDA-based (open triangles), BPDA-based (circles), BTDA-based (open squares) and 6FDA-based (closed diamonds) polyimides with 1. PDMA-ODA, 2. BPDA-ODA, 3. 6FDA-ODA. (The cross refers to BTDA-DAPI (Matrimid 5218)).

The ideal selectivity is plotted versus the CO_2 permeability. Usually, polymers with a high selectivity have a low permeability and vice versa. It was thought that polyimides are an exception to this rule, in particular the 6FDA-based ones. However, the inverse permeability and selectivity relationship still holds but at higher values than for the conventional polymers.

Much research has been done on polymer synthesis to control productivity and selectivity. Fundamental studies on structure-permeability relationships are carried out within different polymer families, such as polyimides [5,11,29,56-59] but also polyamide-imides [60], polyetherimides [61,62], polycarbonates [63,64], polysulfones [65,66], polyoxadiazoles and polytriazoles [67,68]. The chemical structure is systematically altered by the substitution of selected functional groups in the polymer chain and the gas permeabilities are determined. These studies are based on the pioneering work of Hoehn [69]. He stated that polymers which

are useful for gas separation should meet the following criteria concerning their repeat unit of the main chain: rigid subunits connected by nonlinear bonds, bonds with restricted rotation and an overall chemical structure of predominantly aromatic character. To achieve this the most important factors one can vary, by varying the chemical structure, are chain stiffness and packing density. Chain stiffness influences intrasegmental (rotational) mobility and packing density influences the intersegmental spacing. A trade-off should be found in inhibition of chain mobility resulting in higher selectivities due to a molecular sieve mechanism and inhibition of chain packing resulting in higher permeabilities due to an increase in free volume. The bulky $-\text{C}(\text{CF}_3)_2$ groups in the dianhydride structure of the 6FDA-based polyimides meet both conditions. This is why the 6FDA-based polyimides are more permselective than other polyimides with comparable permeabilities.

However, improving the permeability and selectivity by altering the chemical structure has only limited success, as shown by Robeson [70]. Permeability data were taken from over 300 references and included various glassy as well as rubbery polymers. His plots of $\log(\alpha_{i,j})$ versus $\log(P_i)$ for different gas pairs i and j yield an upper bound. This upper bound is an imaginary linear line on the log-log plot above which virtually no data exist. Further structure-property optimization of polymers will shift the upperbound relationship slightly higher, but the inverse permeability-selectivity trade-off is expected to remain the same.

It is beyond the scope of this thesis to discuss the many types of structural modifications of polyimides and their effect on gas separation properties. Although these studies are a large step forward in understanding structural contributions to gas separation properties, these effects are still largely unpredictable and sometimes unexpected. They also may vary considerably from one type of polymer to the other. And more important, a polymer exhibiting the ideal gas separation properties may be useless as it is not easily converted into a cost effective membrane [11].

Only little research has been reported in the literature on the development of (asymmetric) membranes usable for real applications [71-75]. Most field tests on CO_2/CH_4 separations with polyimide membranes reported concern tests with existing Ube-membranes [76-79]. These membranes are prepared from the polyimides BPDA-ODA, BPDA-MDA and BPDA-PDA used as blends or as copolymers. The exact combinations are kept proprietary by Ube. Known Ube films prepared from singular polymers are Upilex R (BPDA-ODA) and Upilex S (BPDA-PDA). Kapton (PMDA-ODA) is a polyimide film manufactured by Dupont.

Polyimide Matrimid 5218

Most polyimides of interest are synthesized on laboratory scale, that is in small quantities. To make a comparison of data possible generated during the whole project, polymer from the same batch is preferred. It was therefore found necessary to search among the few commercial available polyimides. Matrimid 5218 manufactured by Ciba-Geigy was then selected as model polymer. It is a

soluble thermoplastic polyimide and consists of 3,3'-4,4'-benzophenone tetracarboxylic dianhydride (BTDA) and diaminophenylindane (DAPI) [80]. In the synthesis of the DAPI monomer two isomeric products are obtained. The final polyimide is therefore a mixture of the 6-amino and 5-amino isomers of DAPI. The chemical structure of the Matrimid monomer is given in Figure 1.3.

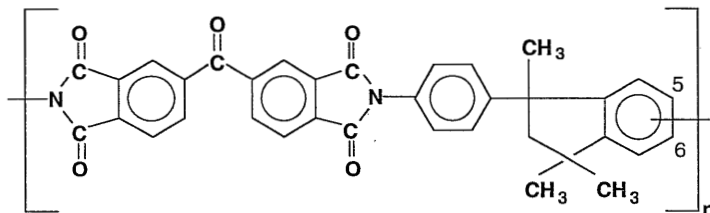


Figure 1.3. Chemical structure of the Matrimid monomer unit.

This polyimide is fully imidized during manufacturing and is soluble in a variety of common solvents, such as *N,N*-dimethyl-acetamide (DMAc), *N*-methylpyrrolidone (NMP), *N,N*-dimethylformamide (DMF), chloroform and methylene chloride. It is believed that the phenylindane ring system is the reason for the extremely high solubility [80,81].

The CO_2/CH_4 gas separation properties are given in Figure 1.2 indicated by the cross. Matrimid is not as permeable as the 6FDA-polyimides of interest. However, in the same way as the 6FDA-polyimides, it has a high tendency to plasticize and is therefore a useful candidate to demonstrate possible effects of suppressing plasticization. Matrimid is originally developed for use in the microelectronic industry [82], but has also found its use as material for gas separation membranes [83-86]. In the patent literature only gas separation properties based on pure gas permeation experiments are reported. Possible CO_2 -plasticization phenomena are not known or not mentioned.

1.4. Plasticization phenomena

Plasticizers generally are organic liquids of low volatility. About 80% of all plasticizers are used in polyvinylchloride (PVC) [87]. They are used to facilitate internal motion of the molecular chains to improve the flexibility of PVC. In the polymers described in this thesis, carbon dioxide acts as plasticizer. Although its plasticizing behaviour is unwanted in CO_2/CH_4 separations, it can also have a practical effect. For example, in the incorporation of additives in polymers, high pressure CO_2 increases the sorption of the polymer-soluble compound whose diffusion into the polymer alone is kinetically limited [88]. In such applications, the polymer film is exposed simultaneously to substance to be incorporated and CO_2 under high pressure. The CO_2 rapidly diffuses into the polymer, plasticizes it and accelerates the absorption of the additive. Upon release of pressure, the CO_2

desorbes quickly, which reduces the degree of plasticization and hence the diffusivity of the additive. With this method, the additive is effectively "trapped" in the polymer. Another example where the CO_2 plasticizing ability can be used is in gas separation itself. By preswelling the membrane with high pressure CO_2 (conditioning), it is possible to increase its permeability without seriously reducing the selectivity [89]. The membrane is swollen to a plasticized state for a certain time. Subsequently, the CO_2 is exchanged with another gas without applying a vacuum. The exchanged gas does not show conditioning effects itself. When the exchanged gas has sufficient solubility, such as methane or air, an increased permeability induced by CO_2 conditioning could be retained.

In many cases, however, plasticization phenomena are not desired. For example in the food packaging industry. Plastic films, such as ethylene vinylalcohol, are used as barrier materials to keep oxygen away from the food. Upon storage, water vapour starts to plasticize the material and simultaneously reduces the resistance to oxygen permeation [90].

In the following, the CO_2 plasticization phenomena observed in CO_2/CH_4 separations are briefly presented. A more extended description about the explanations found in the literature are given in Chapter 3.

CO_2 -induced plasticization effects

In single gas permeation, most glassy polymers show a minimum in the permeabilities as a function of partial CO_2 pressure. This phenomenon is illustrated for a Matrimid film in Figure 1.4. The permeability first decreases with increasing pressure and then increases with further increase of carbon dioxide pressure. The decrease in permeability at low pressures stems from a decreasing solubility with increasing pressure.

The increase of permeability with increasing pressure is typical for plasticization and cannot be described by the existing dual-mode model. The permeability increase results from a high CO_2 concentration in the polymer film that disrupts chain packing. The free volume of the polymer matrix increases, which results in an increased segmental mobility and, hence, permeability. The pressure corresponding to the minimum permeability is called the plasticization pressure, p_{pl} .

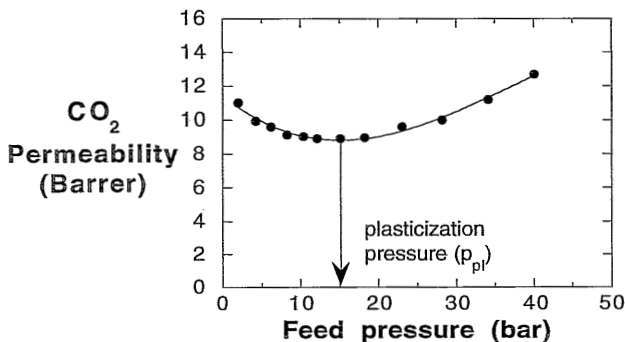


Figure 1.4. CO_2 permeability as a function of pressure for a Matrimid film at 35°C

which correlates to the minimum amount of carbon dioxide necessary to induce plasticization. In case of the Matrimid example, the plasticization pressure is 15 bar at 35 °C. The temperature must be mentioned explicitly, because the plasticization pressure depends on temperature as will be shown in Chapter 2.

Another phenomenon attributed to the carbon dioxide plasticization is the time-dependency of the permeability at pressures above the plasticization pressure [91]. This behaviour is shown for the Matrimid film in Figure 1.5, in which the relative CO₂ permeability at 30 bar is given as a function of time.

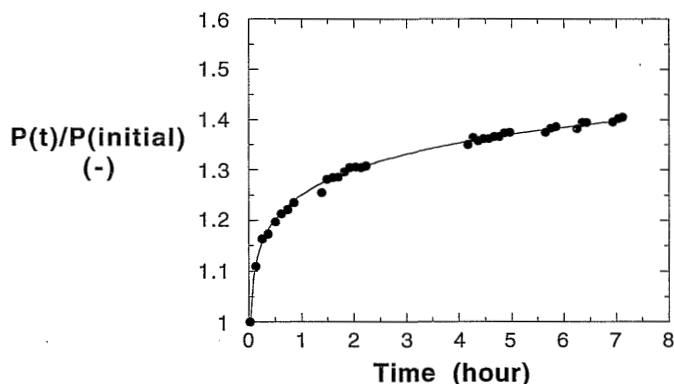


Figure 1.5. Relative CO₂ permeability as a function of time for a Matrimid film at 30 bar and 35 °C.

All permeabilities at time t , $P(t)$, are divided by the permeability determined after 1 minute ($=P_{\text{initial}}$). The relative increase of the permeability is more than 40% after 8 hours and does not reach a steady-state value within the experimentation time. In our laboratory, similar experiments have been carried out earlier over a longer time period. Also 30 bar carbon dioxide was applied on a Matrimid film and three 6FDA-based polyimide films for 18 hours and no steady-state permeability values were reached within that time [92]. Eventually, the permeability may reach a steady-state value. This process, however, may take several days [89].

These plasticization phenomena significantly effect the membrane performance in CO₂/CH₄ separation processes. In a CO₂/CH₄ mixture, the highly sorbed carbon dioxide causes such an increase in free volume that the film starts to permeate methane at a larger extent. The membrane loses its selectivity, because it cannot discriminate anymore on a basis of size and shape. It is said that the molecular sieve mechanism is lost. When the selectivity is determined as a function of feed pressure, a decrease in selectivity is observed. It was thought that this could be attributed to CO₂ plasticization. However, this is not true in all cases as will be illustrated with the help of Figure 1.6.

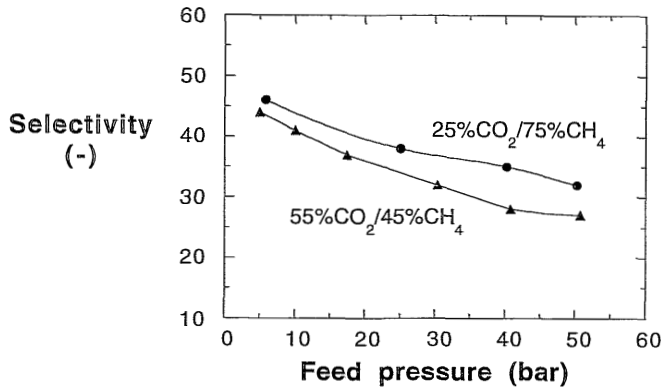


Figure 1.6. Comparison of the selectivity as a function of total feed pressure of a 25/75 mol % CO₂/CH₄ mixture and a 55/45 mol % CO₂/CH₄ mixture for a Matrimid film at 35 °C.

The selectivity as a function of feed pressure of a 25/75 mol % CO₂/CH₄ mixture and a 55/45 mol % mixture for Matrimid is given. In both cases the selectivity decreases with increasing pressure. A decreasing selectivity is actually expected as the dual-mode sorption theory is considered. At lower pressures the permeability of CO₂ and CH₄ decreases with increasing pressure, because the solubility decreases with increasing pressure. And because the decrease is more pronounced for CO₂ than for CH₄, the selectivity decreases. This behaviour must not be confused with plasticization, as the partial CO₂ pressure in the mixture is not high enough to induce plasticization. As was shown in Figure 1.4, a partial CO₂ pressure of at least 15 bar is necessary to induce plasticization. In case of the 25/75 mol % mixture the plasticization pressure is not reached at all in the pressure range examined in Figure 1.6. With further increase of the feed pressure, the dual-mode sorption model predicts a constant selectivity because both gases will then reach a constant permeability. In practice, this will not happen because of plasticization. Also in the case of a 25/75 mol % mixture the plasticization pressure will eventually be reached at elevated pressures, above the range explored here, and the selectivity will decrease further. It was beyond the limits of the capacity of our permeation set-up to prove this experimentally. Therefore, a 55/45 mol % mixture was used to demonstrate this further decrease in selectivity due to plasticization. In this mixture, the plasticization pressure is reached at a total feed pressure of 27.3 bar. Hence, the decrease in selectivity above this pressure can be attributed to plasticization. Normally, the two contributions to the decrease in selectivity cannot be distinguished because the plasticization pressure is not known. Therefore, an analysis of the (partial) permeabilities is necessary in studying the CO₂ plasticization behaviour and the effects of suppressing plasticization on the membrane performance.

1.5. Scope of this thesis

To prevent CO₂ plasticization, an understanding of the phenomenon is required. The two main objectives are: clarifying the plasticization mechanism and searching for methods to suppress it. The phenomenon plasticization itself has been well described in the literature, but it still seems to be difficult to find a fundamental explanation. Furthermore, hardly any report has been found on methods to suppress it. The plasticization problem can be approached in different ways. In understanding plasticization one can find possibilities to suppress it. But the problem can also be considered vice versa. In identifying the possibilities to suppress plasticization, an attempt may be done to understand CO₂-induced plasticization.

The experimental methods for film preparation and characterization are described in *Chapter 2*. Because glassy polymer films are non-equilibrium materials, film morphology may influence the plasticization behaviour of CO₂. The effect of casting solvent and film thickness are therefore studied. Furthermore, the influence of the temperature is discussed.

In *Chapter 3*, CO₂-induced plasticization phenomena in glassy polymers are discussed. The main theories found in the literature are presented. Furthermore, permeation experiments are carried out on eleven different glassy polymers. The main objective was to search for relationships between plasticization pressures and the chemical structure of the polymer. The results are also explained in terms of fractional free volume.

Crosslinking or blending a polymer highly susceptible to plasticization with a polymer that does not plasticize may be two options to suppress plasticization. *Chapter 4* describes the results obtained in crosslinking Matrimid films thermally. It discusses possible crosslink mechanisms and compares treated films with untreated ones on the basis of single as well as mixed gas permeation. Single gas permeation data are combined with sorption experiments to determine diffusion coefficients. Again, treated films are compared with untreated ones.

Chapter 5 describes the influence of blending on plasticization. Matrimid has been blended with polysulfone and P84 (copolyimide BTDA-Me4PDA(80%)/MDA(20%)). Furthermore, Matrimid has been blended with an oligomer with reactive acetylene groups. Upon heating this oligomer polymerizes and simultaneously forms crosslinks resulting in a semi-interpenetrating polymer network. These blended materials are studied with and without further treatment. All films are characterized by single and mixed gas permeation experiments.

In *Chapter 6* a more fundamental interpretation about the mechanism of plasticization and its suppression will be given. The treated as well as untreated films are characterized by Fourier Transform Infrared (FTIR) spectroscopy. Furthermore, FTIR experiments in the presence of CO₂ are carried out for an

untreated Matrimid film and after it has been thermally crosslinked. For this purpose the films are conditioned with CO₂. Subsequently, the desorption of CO₂ in time is recorded in the FTIR experiments.

Membrane process simulations with CO₂/CH₄ gas mixtures are presented in *Chapter 7*. The calculations are based on mixed gas permeation data obtained with an untreated and a thermally crosslinked Matrimid film. In practice, membranes are packed into a module. In gas separation mainly two types are used [6]: a hollow fiber module which contains a bundle of small tubes and spiral wound modules which contain flat sheets manufactured into a sandwich role. For simplicity the module used in the process calculations is considered as a black box. The results give information to what extent a treated film improves a CO₂/CH₄ gas separation process.

1.6. List of symbols

b_i	= Langmuir sorption capacity for component i	cmHg ⁻¹
C_i	= concentration gas sorbed of component i	cm ³ (STP)/(cm ³)
$C_{i,D}$	= conc. gas sorbed of comp. i in the Henry mode	cm ³ (STP)/(cm ³)
$C_{i,H}$	= conc. gas sorbed of comp. i in the Langmuir mode	cm ³ (STP)/(cm ³)
$C_{i,H}$	= Langmuir affinity constant	cm ³ (STP)/(cm ³)
C_i	= concentration of component i	cm ³ (STP)/(cm ³)
$C_{i,0}$	= concentration of component i on upstream side	cm ³ (STP)/(cm ³)
$C_{i,\ell}$	= concentration of component i on downstream side	cm ³ (STP)/(cm ³)
D_i	= diffusion coefficient of component i	cm ² /s
$D_{i,D}$	= mobility of component i in the Henry mode	cm ² /s
$D_{i,H}$	= mobility of component i in the Langmuir mode	cm ² /s
J_i	= flux of component i	cm ³ (STP)/cm ² s)
$k_{i,D}$	= Henry's law constant of component i	$\frac{\text{cm}^3(\text{STP})}{\text{cm}^3 \text{ cmHg}}$
P_i	= permeability coefficient of component i	$\frac{\text{cm}^3(\text{STP}) \text{ cm}}{\text{cm}^2 \text{ s cmHg}}$
p_i	= pressure of component i	cmHg
$p_{i,0}$	= pressure of component i on upstream side	cmHg
$p_{i,\ell}$	= pressure of component i on downstream side	cmHg
p^f	= feed pressure	cmHg
p^p	= permeate pressure	cmHg
S_i	= solubility coefficient of component i	$\frac{\text{cm}^3(\text{STP})}{\text{cm}^3 \text{ cmHg}}$
$X_{i,j}^f$	= mole fraction of component i or j in the feed	(-)
$X_{i,j}^p$	= mole fraction of component i or j in the permeate	(-)

- α_{ij} = separation factor of component i and j (-)
 α_{ij}^* = ideal selectivity of component i and j (-)

1.7. References

- [1] Mitchell, J.K., On the penetrativeness of fluids, *Am. J. Med.*, 13 (1830) 36-67
- [2] Mitchell, J.K., On the penetration of gases, *Am. J. Med., Sci.*, 25 (1833) 100-112
- [3] Graham, T., On the absorption and dialytic separation of gases by colloid septa, *Phil. Mag.*, 32 (1866) 401-420
- [4] Haggin, J., New generation of membranes developed for industrial separations, *Chem. Eng.*, June (1988) 7-16
- [5] Koros, W.J., Fleming, G.K., Membrane-based gas separation, *J. Membrane Sci.*, 83 (1993) 1-80
- [6] Spillman, R.W., Economics of gas separation membranes, *Chem. Eng. Prog.*, 85 (1989) 41-62
- [7] Spillman, R.W., Economics of gas separation membrane processes, in: *Membrane Separation Technology. Principles and Applications*, Noble, R.D., Stern, S.A., (Eds.), Elsevier, Amsterdam, (1995)
- [8] Weber, W.F., Bowman, W., Membranes replacing other separation technologies, *Chem. Eng. Prog.*, 82 (1986) 23-28
- [9] Haselden, G.G., Gas separation fundamentals, *Gas Sep. Purif.*, 3 (1989) 209-215
- [10] Scott, K., *Handbook of industrial membranes*, Elsevier, Oxford, (1995)
- [11] Stern, S.A., Polymers for gas separations: the next decade, *J. Membrane Sci.*, 94 (1994) 1-65
- [12] Ghosal, K., Freeman, B.D., Gas separation using polymer membranes: an overview, *Polym. Adv. Technol.*, 5 (1994) 673-697
- [13] Paul, D.R., Yampol'skii, Y.P., (Eds.), *Polymeric gas separation membranes*, CRC Press, London, (1994)
- [14] Kesting, R.E., Fritzsche, A.K., *Polymeric gas separation membranes*, John Wiley & Sons, New York, (1993)
- [15] Zolandz, R.R., Fleming, G.K., Gas permeation, in: *Membrane Handbook*, Ho, W.S.W., Sirkar, K.K., (Eds.), Van Nostrand Reinhold, New York, (1992) Chapter 2
- [16] Mulder, M., *Basic principles of membrane technology*, Kluwer Academic Publ., Dordrecht, (1991)
- [17] Koros, W.J., Pinnau, I., Membrane formation for gas separation processes, in: *Polymeric gas separation membranes*, Paul, D.R., Yampol'skii, Y.P., (Eds.), CRC Press, (1994) 209-271
- [18] Henis, J.M.S., Commercial and practical aspects of gas separation membranes, in: *Polymeric gas separation membranes*, Paul, D.R., Yampol'skii, Y.P., (Eds.), *Polymeric gas separation membranes*, CRC Press, London, (1994) 441-512
- [19] Bhide, B.D., Stern, S.A., Membrane processes for the removal of acid gases from natural gas. I. Process configurations and optimization of operating conditions, *J. Membrane Sci.*, 81 (1993) 209-237
- [20] Rautenbach, R., Welsch, K., Treatment of landfill gas by gas permeation - pilot plant results and comparison to alternatives, *Gas Sep. Purif.*, 7(1) (1993) 31-37
- [21] Röhr, M., Wimmerstedt, A comparison of two commercial membranes used for biogas upgrading, *Desalination*, 77 (1990) 331-345
- [22] Chern, R.T., Provan, C.N., Gas-induced plasticization and the permselectivity of poly(tetrabromophenolphthalein terephthalate) to a mixture of carbon dioxide and methane, *Macromolecules*, 24 (1991) 2203-2207
- [23] Petropoulos, J.H., Plasticization effects on the gas permeability and permselectivity of polymer membranes, *J. Membrane Sci.*, 75 (1992) 47-59
- [24] Lonsdale, H.K., What is a membrane? Part II, *J. Membrane Sci.*, 43 (1989) 1-3

- [25] Stern, S.A., Walawender, W.P., Analysis of membrane separation parameters, *Sep. Sci.*, 4(2) (1969) 129-159
- [26] Sperling, L.M., Introduction to physical polymer science, John Wiley & Sons, Inc., New York, (1992)
- [27] Van Krevelen, D.W., Properties of polymers, third edition, Elsevier, Oxford, (1990)
- [28] Meares, P., Diffusion of gases through polyvinyl acetate, *J. Am. Chem. Soc.*, (1954) 3415-3422
- [29] Brandt, W.W., Model calculation of the temperature dependence of small molecule diffusion in high polymers, *J. Phys. Chem.*, 63 (1959) 1080-1084
- [30] Smit, E., Modelling of the diffusion of gases through membranes of novel polyimides, Ph-D Thesis, University of Twente, The Netherlands, (1991)
- [31] Gusev, A.A., Müller-Plathe, F., van Gunsteren, W.F., Suter, U.W., Dynamics of small molecules in bulk polymers, *Adv. Polym. Sci.*, 116 (1994) 207-247
- [32] Vieth, W.R., Howell, J.M., Hsieh, J.H., Dual sorption theory, *J. Membrane Sci.*, 1 (1976) 177-220
- [33] Petropoulos, J.H., Quantitative analysis of gaseous diffusion in glassy polymers, *J. Polym. Sci., Part A-2*, 8 (1970) 1797-1801
- [34] Paul, D.R., Koros, W.J., Effect of partially immobilizing sorption on permeability and the diffusion time lag, *J. Polym. Sci., Polym. Phys. Ed.*, 14 (1976) 675-685
- [35] Petropoulos, J.H., Mechanisms and theories for sorption and diffusion of gases in polymers, in: *Polymeric gas separation membranes*, Paul, D.R., Yampol'skii, Y.P., (Eds.), *Polymeric gas separation membranes*, CRC Press, London, (1994) 17-81
- [36] Raucher, D., Sefcik, M.D., Sorption and transport in glassy polymers. Gas-polymer-matrix model, in: *Industrial gas separations*, Whyte, T.E., Yon, C.M., Wagener, E.H., (Eds.), *ACS Symp. Series No 223*, Washington, DC (1983)
- [37] Kirchheim, R., Sorption and partial molar volume of small molecules in glassy polymers, *Macromolecules*, 25 (1992) 6952-6960
- [38] Kirchheim, R., Partial molar volume of small molecules in glassy polymers, *J. Polym. Sci., Polym. Phys. Ed.*, 31 (1993) 1373-1382
- [39] Vrentas, J.S., Vrentas, C.M., Sorption in glassy polymers, *Macromolecules*, 24 (1991) 2404-2412
- [40] Bitter, J.G.A., Transport mechanisms in membrane separation process, Plenum Press, New York, (1991)
- [41] Lipscomb, G.G., Unified thermodynamic analysis of sorption in rubbery and glassy materials, *AIChE J.*, 36 (1990) 1505-1516
- [42] Barbari, T.A., Conforti, R.M., The effect of lattice compressibility on the thermodynamics of gas sorption in polymers, *J. Polym. Sci., Polym. Phys. Ed.*, 30 (1992) 1261
- [43] Barbari, T.A., Conforti, R.M., Recent theories of gas sorption in polymers, *Polym. Adv. Techn.*, 5 (1994) 698-707
- [44] Petropoulos, J.H., Some fundamental approaches to membrane gas permeability and permselectivity, *J. Membrane Sci.*, 53 (1990) 229-258
- [45] Vieth, W.R., Diffusion in and through polymers. Principles and applications, Hanser Publishers, Munich, (1991)
- [46] Frisch, H.L., Sorption and transport in glassy polymers - A review, *Polym. Eng. Sci.*, 20 (1980) 2-13
- [47] Matson, S.L., Lopez, J., Quinn, J.A., Separation of gases with synthetic membranes, *Chem. Eng. Sci.*, 18 (1983) 503-524
- [48] Banerjee, T., Lipscomb, G.G., Mixed gas sorption in elastic solids, *J. Membrane Sci.*, 96 (1994) 241-258
- [49] Sefcik, M.D., Schaefer, J., Solid-state ^{13}C NMR Evidence for gas-polymer interactions in the carbon dioxide-poly(vinyl chloride) system, *J. Polym. Sci., Polym. Phys. Ed.*, 21 (1983)

- 1055-1062
- [50] Cain, E.J., Wen, W.-Y., Jones, A.A., Inglefield, P.T., Cauley, B.J., Bendler, J.T., A dual-mode interpretation of spin relaxation for $^{13}\text{CO}_2$ sorbed in polycarbonate, *J. Polym. Sci., Polym. Phys. Ed.*, 29 (1991) 1009-1020
- [51] Higuchi, A., Nakagawa, T., Infrared spectroscopic studies of CO_2 sorbed in glassy and rubbery polymeric membranes, *J. Polym. Sci., Polym. Phys. Ed.*, 32 (1994) 149-157
- [52] Nakamura, A., Gas and vapor dehydration with the polyimide membranes, A.I.S.T.-A.F.M.E. expert meeting on energy conservation technology, (1989)
- [53] Dinehart, R.A., Wright, W.W., Preparation and fabrication of aromatic polyimides, *J. Appl. Polym. Sci.*, II (1967) 609-627
- [54] Husk, G.R., Cassidy, P.E., Gebert, K.L., Synthesis and characterization of a series of polyimides, *Macromolecules*, 21 (1988) 1234-2238
- [55] Wilson, D., Stenzenberger, H.D., Hergenrother, P.M., (Eds.), *Polyimides*, Blackie & Son, Glasgow, (1990)
- [56] Kim, T.H., Koros, W.J., Husk, G.R., O'Brien, K.C., Relationship between gas separation properties and chemical structure in a series of aromatic polyimides, *J. Membrane Sci.*, 37 (1988) 45-62
- [57] Stern, S.A., Mi, Y., Yamamoto, H., Structure/permeability relationships of polyimide membranes. Applications to the separation of gas mixtures, *J. Polym. Sci., Polym. Phys. Ed.*, 27 (1989) 1887-1909
- [58] Tanaka, K., Kita, H., Okano, M., Okamoto, K.-I., Permeability and permselectivity of gases in fluorinated and non-fluorinated polyimides, *Polymer*, 33 (1992) 585-593
- [59] Hirayama, Y., Yoshinaga, T., Kusuki, Y., Nimomiya, K., Sakakibara, T., Tamari, T., Relation of gas permeability with structure of aromatic polyimides, *I. J. Membrane Sci.*, 111 (1996) 169-182; *II. J. Membrane Sci.*, 111 (1996) 183-192
- [60] Fritsch, D., Peinemann, K.-V., Novel highly permselective 6F-poly(amide-imide)s as membrane host for nano-sized catalysts, *J. Membrane Sci.*, 99 (1995) 29-38
- [61] Eastmond, G.C., Paprotny, J., Webster, I., Isomeric poly(ether imide)s: synthesis, thermal properties and permeabilities, *Polymer* 34 (1993) 2865-2874
- [62] Eastmond, G.C., Page, P.C.B., Paprotny, J., Richards, R.E., Shaunak, R., Poly(ether imide)s with hindering substituents in the anhydride moiety: synthesis, properties and gas permeabilities, *Polymer*, 35 (1994) 4215-4227
- [63] Hellums, M.W., Koros, W.J., Husk, G.R., Paul, D.R., Fluorinated polycarbonates for gas separation applications, *J. Membrane Sci.*, 46 (1989) 93-112
- [64] Muruganandam, N., Paul, D.R., Gas sorption and transport in substituted polycarbonates, *J. Polym. Sci., Polym. Phys. Ed.*, 25 (1987) 1999-2026
- [65] McHattie, J.S., Koros, W.J., Paul, D.R., Gas transport properties of polysulphones: 1. Role of symmetry of methyl group placement on bisphenol rings, *Polymer*, 32 (1991) 840-850
- [66] McHattie, J.S., Koros, W.J., Paul, D.R., Gas transport properties of polysulphones: 3. Comparison of tetramethyl-substituted bisphenoles, *Polymer*, 33 (1992) 1701-1711
- [67] Gebben, B., Thermally stable and chemically resistant polymer membranes. Aromatic polyoxadiazoles and polytriazoles, Ph-D Thesis, University of Twente, The Netherlands, (1988)
- [68] Hensema, E., Polyoxadiazole and polytriazole gas separation membranes. Synthesis and properties, Ph-D Thesis, University of Twente, The Netherlands, (1991)
- [69] Hoehn, H.H., Heat treatment of membranes of selected polyimides, polyesters and polyamides, US Patent 3,822,202, (1974)
- [70] Robeson, L.M., Correlation of separation factor versus permeability for polymeric membranes, *J. Membrane Sci.*, 62 (1991) 165-185

- [71] White, L.S., Blinka, T.A., Kloczewski, H.A., Wang, I-F., Properties of a polyimide gas separation membrane in natural gas streams, *J. Membrane Sci.*, 103 (1995) 73-82
- [72] Pinnau, I., Koros, W.J., Gas-permeation properties of asymmetric polycarbonate, polyester carbonate, and fluorinated polyimide membranes prepared by the generalized dry-wet phase inversion process, *J. Appl. Polym. Sci.*, 46 (1992) 1195-1204
- [73] Chung, T.-S., Kafchinski, E.R., Foley, P., Development of asymmetric hollow fibers from polyimides for air separation, *J. Membrane Sci.*, 75 (1992) 181-195
- [74] Chung, T.-S., Kafchinski, E.R., Vora, R., Development of a defect-free 6FDA-durene asymmetric hollow fiber and its composite hollow fibers, *J. Membrane Sci.*, 68 (1994) 21-36
- [75] Yanagishita, H., Nozoye, H., Nakane, T., Preparation of 6FDA-based polyimide composite membrane by CVDP process, *Desalination*, 90 (1993) 55-63
- [76] Haray, K., Obata, K., Itoh, N., Shndo, Y., Hakuta, T., Yoshitome, H., Gas permeation and separation by an asymmetric polyimide hollow fiber membrane, *J. Membrane Sci.*, 41 (1989) 23-35
- [77] Iwakami, Y., CO₂ removal: field test using a cellulose acetate membrane and a polyimide membrane, *ICOM, Heidelberg*, (1993)
- [78] Higashijima, T., Ohaya, H., Tsuchiya, Y., Tokunaga, H., Aihara, M., Negishi, Y., Separation of supercritical fluid mixtures of CO₂ and petroleum components with an asymmetric polyimide membrane, *J. Membrane Sci.*, 93 (1994) 165-173
- [79] Chung, I.-J., Lee, K.-R., Hwang, S.-T., Separation of CFC-12 from air by polyimide hollow-fiber membrane module, *J. Membrane Sci.*, 105 (1995) 177-185
- [80] Bateman, J., Gordon, D.A., Soluble polyimides derived from phenylindane diamines and dianhydrides, *US Patent 3,856,752*, (1974)
- [81] Bateman, J., Gordon, D.A., Phenylindane diamine mixture and epoxy resin therewith, *US Patent 3,983,092*, (1976)
- [82] Falcigno, P., Masola, M., Williams, D., Jasne, S., Comparison of properties of polyimides containing DAPI isomers and various dianhydrides, in: *Polyimides: Materials, chemistry and characterization*, Proc. of the third international conference on polyimides, Feger, C., Khojasteh, M.M., McGrath, J.E., Ellenville, New York, (1989)
- [83] Ekiner, O.M., Hayes, R.A., Va, W., Phenylindane-containing polyimide gas separation membranes, *US Patent 5,015,270*, (1991)
- [84] Wang, I-F., Minhas, B.S., Asymmetric polyimide membranes, *US Patent 5,067,970*, (1991)
- [85] Simmons, J.W., Ekiner, O.K., Polyimide and polyamide-imide gas separation membranes, *US Patent 5,232,472*, (1993)
- [86] Macheras, J.R., Bikson, B., Nelson, J.D., Method of preparing membranes from blends of polyetherimide and polyimide polymers, *US Patent 5,443,728*, (1995)
- [87] Selinger, B., *Chemistry in the marketplace*, Harcourt Brace Jovanovich, Sydney, fourth edition, (1991) 198
- [88] Berens, A.R., Huvard, G.S., Korsmeyer, R.W., Kunig, F.W., Application of compressed carbon dioxide in the incorporation of additives into polymers, *J. Appl. Polym. Sci.*, 46 (1992) 231-242
- [89] Koros, W.J., Jordan, S.M., Fleming, G.K., Processes to condition gas permeable membranes, *US Patent 4,755,192*, (1988)
- [90] Alger, M.M., Stanley, Pay, J., Retortable food packages containing water-sensitive oxygen barrier, in: *Barrier polymers and structures*, Koros, W.J., (Ed.), ACS Symp. Series No. 423, (1990), Washington, D.C., Chapter 10
- [91] Wessling, M., Huisman, I., van den Boomgaard, Th., Smolders, C.A., Time-dependent permeation of carbon dioxide through a polyimide membrane above the plasticization pressure, *J. Appl. Polym. Sci.*, 58 (1995) 1959-1966
- [92] Final report BRITE Project RI/B-0098/NL, Membrane separation of CO₂ and H₂S from mixtures with gaseous hydrocarbons, (1988)

2

Experimental methods

2.1. Introduction

Polyimides are selected as membrane material for gas separation because of their significantly better permselective performance than membranes made from conventional glassy polymers [1]. However, a disadvantage of polyimides is their tendency to plasticize. To prevent plasticization, a fundamental understanding of the phenomenon is required. Our research therefore focuses on understanding plasticization on a molecular level and on identifying methods, such as crosslinking, to suppress plasticization. To carry out the first task, permeation properties of different glassy polymers were characterized. Because of the limited availability of different polyimides, also other glassy polymers are included. Nonetheless, the results are useful for understanding plasticization. To perform the second task, mainly the polyimide Matrimid 5218 is used. This polymer is chosen as model polymer. Its gas separation properties are comparable with those of polysulfone. It has the advantage that it is commercially available and soluble in many common solvents. It was found possible to prepare a network structure of Matrimid either by thermal treatment at 350 °C or by formation of a semi-interpenetrating polymer network with the oligomer Thermid FA-700. These possibilities to change the polymer structure into a network make Matrimid useful to demonstrate the effect of the modifications on the suppression of plasticization.

This chapter describes all experimental methods used to characterize the properties of the polymer films used in Chapter 3 to 5. The different glassy polymers selected are classified in groups by their chemical structure. From all polymers, homogeneous dense films are prepared and characterized by single and mixed gas permeation and sorption experiments. Furthermore, densities and glass transition temperatures are determined. The effect of operating temperature on the permeation behaviour is presented. And finally, the effect of film morphology on plasticization is investigated by using different casting solvents and varying film thickness to elucidate their effect on the plasticization.

2.2. Materials

Polymers

To investigate plasticization fundamentally, different glassy polymers were classified in groups by their chemical structure. All polymers used are listed in Table 2.1.

The following reasons underlay the classification:

Group A consists of PSF, PES and PEI. All three polymers have an ether linkage in the polymer backbone in common. Moreover, PES is closely related to PSF because both have a sulfur dioxide group between two benzene rings. For PSF and PEI an additional similarity is the isopropylidene group between two benzene rings.

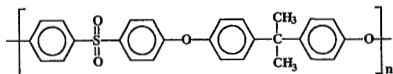
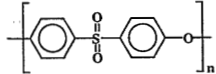
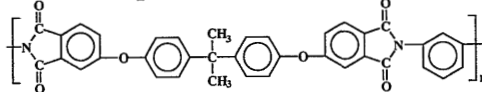
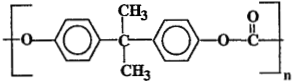
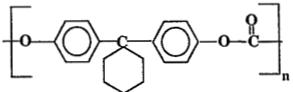
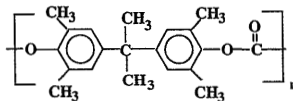
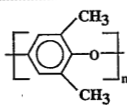
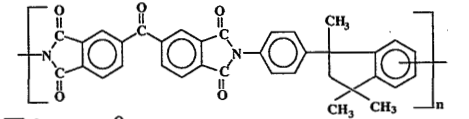
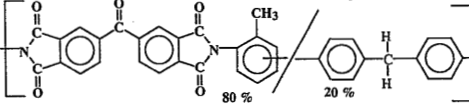
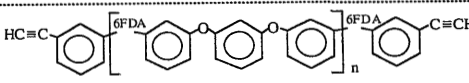
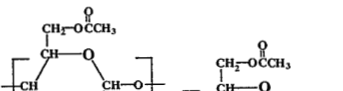
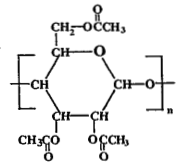
Group B consists of a series of polycarbonates and PPO. The polycarbonates are based on the bisphenol A moiety (2,2-bis(4-hydroxyphenyl)-propane) [2]. In BPA-PC, the repeat unit consists of a bisphenol unit (4,4-isopropylidene-bisphenol) and of a carbonate unit. Replacing the isopropylidene group in BPA-PC by an cyclohexylidene ring results in the BPZ-PC structure. Substituting four methylgroups on the bisphenol unit of BPA-PC results in the TMBPA-PC structure. PPO has been added into this group because the monomer can be recognized in the tetramethyl substituted polycarbonate.

Group C consists of polyimides. Two polymers based on benzophenone-tetracarboxylic dianhydride (BTDA) and an oligomer based on hexafluoro-isopropylidene bis(phthalic anhydride) (6FDA). The BTDA-polyimides differ only in their diamine structure. The diamine structure in Matrimid 5218 is 5(6-amino-1-(4'-aminophenyl)-1,3-trimethylindane). P84 is a copolymer containing 80% methyl substituted phenylenediamine and 20% methylenedianiline. The difference in dianhydride structure of the polymers compared to the oligomer consists of the bridging group between the benzene rings. The BTDA-based polyimides have a carboxyl-group (-C=O) as bridging group and the 6FDA-polyimide has a hexafluoro-isopropylidene group (-C(CF₃)₂).

Group D consists of cellulose derivatives. The CA structure is a secondary acetate. The manufacturer indicates that 55-56% acetic acid was added, which results in a secondary acetate according to the literature [3]. Addition of 60-62 % acetic acid results in a triacetate (CTA).

PSF is manufactured by Amoco, PES by BASF and PEI by General Electric. The polycarbonates (group B) are supplied by Bayer. PPO is synthesized at the Research Institute of Chemical Industry in Novosibirsk (Russia). CA is manufactured by BDH Chemicals and CTA by Aldrich. P84 (copolyimide of 3,3'4,4'-benzophenone tetracarboxylic dianhydride and 80% methylphenylenediamine + 20% methylene diamine) is obtained from Lenzing, Matrimid (polyimide of 3,3'4,4'-benzo-phenone tetracarboxylic dianhydride and diamino-phenylindane) from Ciba-Geigy and Thermid FA-700 (polyimide oligomer of

Table 2.1. *Polymers used for homogeneous dense film preparation.*

	Name	Acronym	T _g (°C)	Chemical structure
A	Polysulfone (Udel P3500)	PSF	182	
	Polyethersulfone (Ultrason E 6010P)	PES	222	
	Polyetherimide (ULTEM 1000)	PEI	199	
B	Bisphenol A polycarbonate (Macrolon 3200)	BPA-PC	151	
	Bisphenol Z polycarbonate	BPZ-PC	175	
	Tetramethyl Bisphenol A polycarbonate	TMBPA-PC	193	
	Poly(2,6 dimethyl-p-phenylene) oxide	PPO	210	
C	Polyimide (Matrimid 5218)	BTDA-DAPI	313	
	Copolyimide (P84))	BTDA-Me4PDA/ MDA	300	
	Polyimide oligomer (Thermid FA-700)	6FDA-TPE-Q/APA	175	 (see also Figure 5.5)
D	Cellulose acetate	CA	187	
	Cellulose triacetate	CTA	185	

4,4'-hexafluoroisopro-pylidene bis(phthalic anhydride) and 1,4-bis(4-amino-phenoxy)benzene and 3 aminophenylacetylene endcaps) from National Starch & Chemical Corporation.

Solvents

N,N-dimethylacetamide (DMAc), N-methylpyrrolidone (NMP), chloroform (CHCl_3) and methylene chloride (CH_2Cl_2) were purchased from Merck (analytical grade) and used as received. For density measurements, absolute ethanol was used, purchased from Merck and used as received.

Gases

Carbon dioxide (>99.99%) and methane (>99.9%) were purchased from Union Carbide and were used in the pure permeation and/or sorption experiments. From these gases a mixture with the composition of 55 mol % CO_2 and 45 mol % CH_4 was prepared. Furthermore, a 25 mol % CO_2 and 75 mol % CH_4 gas mixture was purchased from Union Carbide.

2.3. Film preparation

Homogeneous dense films

Polymer solutions were made with concentrations ranging from 10 to 20 wt %. All solutions were filtered over a 1 μm glass fiber filter (Whatman) combined with a metal filter of 5 μm (Bekaert Fibre Technologies) to remove undissolved material and dust particles. The filtered polymer solution was cast on a glass plate. Depending on the desired final thickness of the film and concentration of the polymer solution casting knives with slit heights ranging from 150 - 250 μm were used. The cast film was dried in a nitrogen atmosphere at room temperature for at least 16 hours. Subsequently, the film was removed from the glass plate with a small amount of water and further dried in a vacuum oven (Heraeus, RVT 220/180) at 150 $^\circ\text{C}$ for at least four days. Final film thicknesses were determined with a micrometer screw gauge (Mitutoyo) and ranged from 10 to 40 μm . The accuracy of the micrometer was 1 μm .

2.4. Characterization

2.4.1. Single and mixed gas permeation

The high pressure gas permeation set-up used is schematically given in Figure 2.1. The set-up consists of two permeation cells. Initially, permeation experiments were done at room temperature. Later double-walled permeation cells allowed permeation at elevated temperature. The cells are thermostated with water pumped around by a Colora thermostate bath. The permeation experiments are carried out at room temperature and 35 $^\circ\text{C}$. Room temperature

varied from 21 to 27°C.

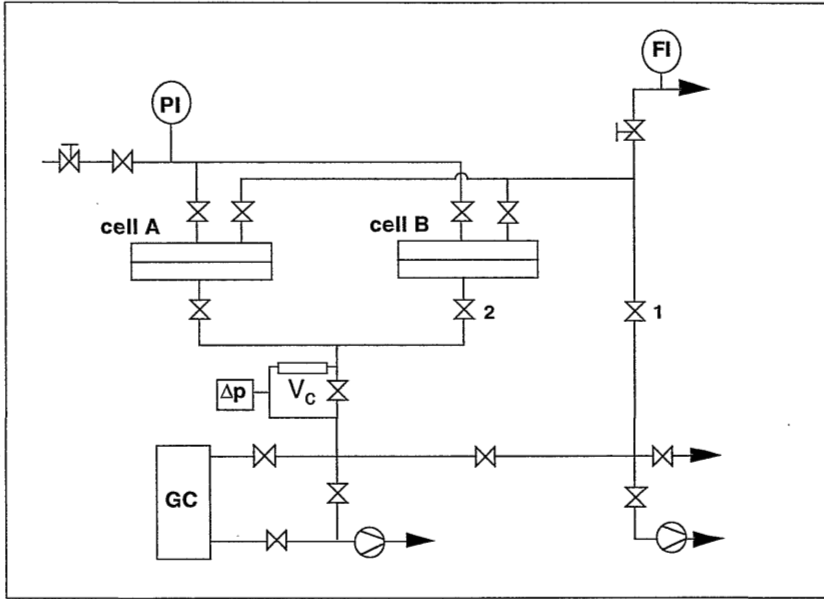


Figure 2.1. Gas permeation set-up. PI is an absolute pressure indicator, Δp is a differential pressure indicator, V_c a calibrated volume, FI is a flow meter and GC is the gas chromatograph.

A single gas permeation measurement starts with evacuation of the whole set-up by two vacuum pumps (Edwards). A feed pressure is applied on top of the films, while the feed and permeate side are separated by closing valve 1. A pressure difference across the film is maintained by keeping the permeate site at vacuum pressure. Two films can be equilibrated simultaneously, but the permeability of the films are determined separately. To use cell A, cell B is disconnected on the permeate site by closing valve 2. In a closed calibrated volume (V_c), the pressure increases with time due to the permeating gas molecules. The volume was calibrated with helium by expansion from a known externally calibrated volume.

The permeability is calculated from the slope of the steady state pressure increase $\Delta p_p / \Delta t$ in the calibrated volume with Equation (2.1).

$$P = \frac{\Delta p_p}{\Delta t (p_f - p_p)} \frac{V_c \ell}{RT A} V_m \quad (2.1)$$

where V_c is the calibrated volume, R the universal gas constant, T the experimental temperature, ℓ the membrane thickness, A the membrane surface

area, V_m the molar volume at standard temperature and pressure (STP) and $(p_f - p_p)$ the pressure difference across the membrane. The permeate pressure (p_p) is negligibly small with respect to the feed pressure (p_f), therefore, the driving force ($p_f - p_p$) is assumed to be equal to p_f . The feed pressure is measured with an absolute pressure indicator (Druck Nederland b.v.) at a range of 0 - 60 bar and the permeate pressure with a differential pressure indicator (Druck Nederland b.v.) at a range of 0 to 150 mbar. The standard unit to quantify the permeability is Barrer, which is defined as:

$$1 \text{ Barrer} = 10^{-10} \frac{\text{cm}^3(\text{STP}) \text{ cm}}{\text{cm}^2 \text{ s cmHg}} \quad (2.2)$$

A considerable amount of data is available on the permeation of pure gases through nonporous polymeric films, but less on the permeation of mixtures. Permeation data of mixtures are necessary, because from the data obtained with pure gases one cannot always predict the permeation behaviour of a mixture [4-9]. Possible competition for sorption sites or interactions between the components in a mixture are not taken into account in pure gas permeation experiments. In particular, plasticization effects of CO_2 are not considered. For the few studies done on gas mixtures, the permeation data are often fitted with existing permeability models. The models often do not fit the data precisely. The CO_2 permeability is often lower than predicted from the model and the CH_4 permeability higher [4]. Apparently, the presence of a less permeable gas, such as CH_4 , can reduce the permeability of a more permeable gas, such as CO_2 . The opposite is also valid. The presence of a more permeable gas can increase the permeability of a less permeable gas. This then results in a lower actual selectivity compared to the ideal selectivity obtained from the pure gas permeabilities. Donohue et al. [6] give an explanation for this phenomenon observed in cellulose acetate membranes. The solubilities of both gases, CO_2 and CH_4 , decrease in the presence of each other. But more important, the diffusivity of CO_2 decreases due to the presence of CH_4 and the diffusivity of CH_4 increases because of CO_2 plasticization. Because the diffusivity of CH_4 increases more than the solubility of CH_4 decreases, the CH_4 permeability is higher in a mixture compared to the pure gas permeability at the corresponding partial pressure and the CO_2 permeability is lower. Kumazawa et al. [10] ascribe the decreased CO_2 permeability in the gas mixture to a reduction of free volume due to a hydrostatic pressure effect. Some models also do consider plasticization effects of CO_2 [11,12], but these studies demonstrate the difficulty to describe plasticization in transport models. Raymond et al. [8] even deny the use of any model because such models do not consider 'history' effects.

Pure gas and mixed gas permeation experiments differ in two points.

1) In mixed gas experiments, the feed flows along the film and the permeate flows perpendicular to the film (crossflow configuration) whereas in pure permeation experiments a dead-end configuration is used. The feed flow is

measured with a Sho Rate flow meter (FI) (Brooks Instruments).

2) The composition of the permeate as well as the feed has to be determined in mixed gas experiments. This is done online by gas chromatography on a Varian 3300 gas chromatograph which is connected with a LDC/Milton Roy integrator. The following paragraphs describe briefly the equations governing the calculations of the mixed gas permeation. O'Brien et al. [13] described a similar measuring procedure as it is used here. Symbols are explained in detail in Section 2.7.

The permeate flow (Q_P) is calculated from the product of the total permeance (P_{tot}/l), feed pressure (p_f) and membrane area (A):

$$Q_P = (P_{tot}/l) * p_f * A \quad (2.3)$$

The separation factor is calculated with the ratio of the mole fractions in the permeate (X_i^p) divided by the ratio of the mole fractions in the feed (X_i^f):

$$\alpha = \frac{X_{CO_2}^p \cdot X_{CH_4}^f}{X_{CH_4}^p \cdot X_{CO_2}^f} \quad (2.4)$$

Since the permeate pressure is kept close to zero, the separation factor will further be referred to as the selectivity. Furthermore, Equation (2.4) is only valid if the feed composition is constant during permeation. This is achieved if the feed flow (Q_F) is much higher than the permeate flow (Q_P). Or in other words, the stage cut should be kept as small as possible. The stage cut θ is the fraction of the feed permeating through a film defined by:

$$\theta = \frac{Q_P}{Q_F} \quad (2.5)$$

The stage cut can vary between 0 and 1. A stage cut of one means no separation at all. All the feed is transported through the membrane. The highest concentration of the more permeable component in the permeate is obtained at a stage cut near zero.

The total permeability (P_{tot}) of the gas mixture is determined as given by Equation (2.1). The CO_2 permeability in the mixture (P_{CO_2}) and CH_4 permeability in the mixture (P_{CH_4}) are then calculated from the total permeability by Equation (2.6), where (X_i^p) is the mole fraction in the permeate and (X_i^f) in the feed. Dividing by the mole fraction in the feed is necessary to obtain the permeabilities at the partial pressures of the gases in the mixture.

$$P_{CO_2} = \frac{P_{tot} * X_{CO_2}^p}{X_{CO_2}^f} \quad \text{and} \quad P_{CH_4} = \frac{P_{tot} * X_{CH_4}^p}{X_{CH_4}^f} \quad (2.6)$$

Error analysis

The error in the calculated permeability is dominated by random errors in the measuring instruments and the reading thereof. If the permeability (P) is calculated by Equation (2.1), a probable error in the permeability is approximately the sum of the products of the errors in each term times the effect that term has on the value of the permeability [14]. The error in the gas constant (R) and the molar volume (V_m) is neglected. The probable error is given in Equation (2.7):

$$\begin{aligned} \Delta P = & \Delta(\Delta p) \cdot \left. \frac{\partial P}{\partial \Delta p} \right|_{\Delta t, p_f, V_c, R, T, \ell, A, V_m} + \Delta(\Delta t) \cdot \left. \frac{\partial P}{\partial \Delta t} \right|_{\Delta p, p_f, V_c, R, T, \ell, A, V_m} + \\ & \Delta(p_f) \cdot \left. \frac{\partial P}{\partial p_f} \right|_{\Delta p, \Delta t, V_c, R, T, \ell, A, V_m} + \Delta(V_c) \cdot \left. \frac{\partial P}{\partial V_c} \right|_{\Delta p, \Delta t, p_f, R, T, \ell, A, V_m} + \\ & \Delta(T) \cdot \left. \frac{\partial P}{\partial T} \right|_{\Delta p, \Delta t, p_f, V_c, R, \ell, A, V_m} + \Delta(\ell) \cdot \left. \frac{\partial P}{\partial \ell} \right|_{\Delta p, \Delta t, p_f, V_c, R, T, A, V_m} + \\ & \Delta(A) \cdot \left. \frac{\partial P}{\partial A} \right|_{\Delta p, \Delta t, p_f, V_c, R, T, \ell, V_m} \end{aligned} \quad (2.7)$$

Working out the partial derivatives of P with respect to each of the terms in Equation (2.1) and dividing the whole equation through the absolute value of P , Equation (2.7) becomes Equation (2.8):

$$\frac{\Delta P}{|P|} = \frac{\Delta(\Delta p)}{|\Delta p|} + \frac{\Delta(\Delta t)}{|\Delta t|} + \frac{\Delta p_f}{|p_f|} + \frac{\Delta V_c}{|V_c|} + \frac{\Delta T}{|T|} + \frac{\Delta \ell}{|\ell|} + \frac{\Delta A}{|A|} \quad (2.8)$$

The estimated errors of the different terms are :

$\Delta p_f = 0.1$ bar (accuracy of applying the pressure), $\Delta V_c = 0.05$ cm³ (standard deviation of ten calibration measurements), $\Delta T = 1$ K, $\Delta \ell = 1$ μm, $\Delta A = 0.005$ cm², $\Delta(\Delta p) = 0.1$ - 0.5 mbar and $\Delta(\Delta t) = 1$ - 3 sec. The estimated errors in Δp and Δt are dependent on the feed pressure and are dominated by reading off the recorder paper. The recorder scale was adjusted to the measured fluxes. The absolute values of the different terms are: $V_c = 35.2$ cm³, $T =$ room temperature (≈ 298 K) or 308 K, $\ell = 10$ - 40 μm, $A = 11,95$ cm², $\Delta(\Delta p) = 6$ - 130 mbar and $\Delta(\Delta t) = 3$ - 15 minutes. The calculated probable error $\left(\frac{\Delta P}{|P|}\right)$ ranged from 0.04 - 0.10 , which is an error of 4 to 10% in the permeability value being larger at lower pressures.

2.4.2. High pressure sorption

A sorption equipment similar to the one designed by Koros and Paul [15] was built for the sorption experiments and is schematically drawn in Figure 2.2. The set-up consists of two cells, one sample cell and an empty expansion cell. The sample cell is a Cajon long tube butt weld with an VCR female nut and male plug (Swagelok, Amsterdam Valve & Fitting b.v.). For each experiment a new

stainless steel gasket was used to seal the cell. The expansion cell is a closed stainless steel tube. The cells as well as the expansion cell and the gas cylinder are separated by stainless steel Nupro diaphragm valves (Amsterdam Valve & Fitting b.v.). These valves seal at vacuum pressure and resist pressures up to 241 bar. The absolute pressure in both cells are determined with pressure indicators P1 and P2. The pressure transducers (PCDR 911, Druck Nederland b.v.) range from 0 to 60 bar and have an inaccuracy of 0.030% of the full pressure range. The volumes of both cells are calibrated with helium by expansion from an externally calibrated expansion cell. During the sorption experiments the cells are thermostated in a Colora thermostate bath.

The principle of the measurement is as follows. To remove all sorbed gas molecules from the sample, the two cells are evacuated to vacuum pressure for one night with an Edward vacuum pump. After evacuation the cells are separated by closing valve L1 between the cells and the expansion cell is pressurized. The actual pressure can be read from the pressure indicator P2. Subsequently, the gas will be expanded into the sample cell by closing valve L2 and opening valve L1.

The initial number of moles transferred into the sample cell can be determined exactly from the initial and final pressure in the expansion cell. The number of moles sorbed by the polymer sample will then be calculated from the difference of the equilibrium pressure indicated by pressure indicator 1 and the calculated initial pressure in the sample cell.

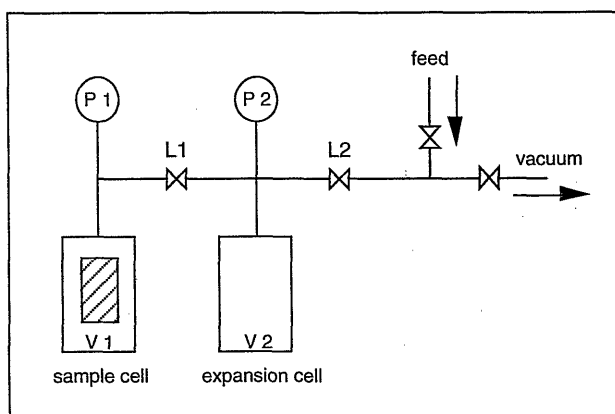


Figure 2.2. High pressure sorption set-up. P1 and P2 are absolute pressure indicators. V1 and V2 are the calibrated volumes of the sample cell and the expansion cell, respectively.

To increase accuracy, the sorption isotherms are measured with incremental pressure steps of at least 5 bar. The size of the polymer sample ($\sim 1 \text{ cm}^3$) and the step size should be as large as possible due to the limited accuracy of the absolute

pressure transducers. Over a pressure range of 0 to 60 bar registration of pressure differences as a result of sorption should be in the order of millibars. The pressure read out (DPI 280, Druck Nederland b.v.) consist of a 4 digit display. The transducers and the read out are calibrated and the measured inaccuracy was 0.030 % of the full pressure range. According to Koros and Paul [15] a volume ratio of $V_2/(V_1-V_p)$ of about 10 or smaller is good enough to do accurate sorption experiments with CO_2 in polycarbonate. However, this volume ratio shows a scatter in their results for N_2 in polycarbonate. For gases with low solubilities, such as N_2 , a volume ratio of $V_2/(V_1-V_p)$ of about 1.5 gives much better results. Here, the volume ratio $V_2/(V_1-V_p)$ is about 1. Hence, if the ratio of 1.5 is enough for accurate sorption with a low soluble gas in a glassy polymer than a ratio of 1 should be perfect for CO_2 sorption experiments.

The expressions to calculate the number of moles of gas sorbed by the polymer sample are given by Equation (2.9). The subscripts i and f stand for initial and final, respectively, and the numbers 1 and 2 for cell 1 and cell 2, respectively. V_p refers to the volume of the polymer sample. Since CO_2 cannot be considered as an ideal gas, the compressibility factor $Z (=pV/RT)$ should be taken into account in calculating the number of moles sorbed.

$$n_{\text{sorbed}} = n_{\text{initial}} - n_{\text{final}} \quad (2.9)$$

$$n_{\text{initial}} = n_{2i} - n_{2f} = \frac{V_2}{RT} \left(\frac{P_{2i}}{Z_{2i}} - \frac{P_{2f}}{Z_{2f}} \right) \quad (2.9a)$$

$$n_{\text{final}} = \frac{(V_1')}{RT} \left(\frac{P_{1f}}{Z_{1f}} \right) \quad \text{with } V_1' = (V_1 - V_p) \quad (2.9b)$$

The compressibility factor expresses the non-ideality of the gas [16]. Equations of state for CO_2 can be found in literature [16-18]. The virial coefficients are solely a function of temperature. We used the tabulation of Van Huff et al. [18]. They determined the compressibility factor of CO_2 by combining the data of Michels and Michels [18a], MacMormack and Schneider [18b], and Kennedy [18c] by volume-explicit equations of state in the range 0 to 600 °C and 0 to 150 atm with an average deviation of 0.09 % and a maximum deviation of 0.5 % over the whole range. No compressibility factors are tabulated for pressures above 40 bar and temperatures below 40 °C, because the gas state is near the two-phase region. It appears to be difficult to calculate compressibility factors accurately in the proximity of that region. Hence, the sorption experiments are carried out up to a maximum pressure of 40 bar.

The concentration of CO_2 in the polymer sample at standard temperature and pressure (STP) per volume of polymer (V_p) can be calculated with Equation (2.10). V_m refers to the molar volume at standard temperature and pressure.

$$\Delta c = \frac{n_{\text{sorbed}} * V_m}{V_p} \quad (2.10)$$

Error analysis

The probable error in the calculation of the CO₂ concentration in the polymer film is dominated by the error in the determination of the number of moles CO₂ sorbed by the polymer film. The largest contribution to this error is found to be the determination of the pressure difference due to sorption in the sample cell.

Calculation of the probable error in the concentration is not as straightforward as in the permeability. The error in n_{sorbed} is the sum of the absolute errors of the initial and final number of moles. And as the number of moles of gas sorbed in the second sorption step is added to the number of moles sorbed in the first step, the error in n_{sorbed} of the first sorption step should therefore be added to n_{sorbed} of the second step. The error in n_{sorbed} of the second and first sorption step should then be added to n_{sorbed} of the third step. Writing out all the calculations is therefore complicated. Furthermore, it was found not justified to count the error in V_1 , V_2 , V_p and T in each calculation of the error in the number of moles. The probable error is therefore estimated by a simplified equation as given by Equation (2.11):

$$\frac{\Delta n_{\text{sorbed}}}{|n_{\text{sorbed}}|} = \frac{\Delta V_1}{|V_1|} + \frac{\Delta V_2}{|V_2|} + \frac{\Delta V_p}{|V_p|} + \frac{\Delta T}{|T|} + \left(\frac{\Delta Z}{|Z|}\right)_s + \sum_{i=1}^s \left(\frac{\Delta(\Delta p)_{\text{sorbed}}}{|\Delta p_{\text{sorbed}}|}\right)_i \quad (2.11)$$

where s is the number of sorption steps. The errors in V_1 , V_2 , V_p and T are accounted for once. Furthermore, the total error in the Z -factors of one sorption step is the sum of the relative errors in the Z -factors corresponding to the initial pressure in cell 2 and the final pressures in cell 1 and 2 of that particular sorption step. And the error in Δp_{sorbed} is considered as cumulative going from the first to the last sorption step. The errors in the gas constant (R) and molar volume (V_m) are again neglected.

The absolute values of the different terms are: $V_1 = 14.47 \text{ cm}^3$, $V_2 = 15.37 \text{ cm}^3$, $V_p \approx 1 \text{ cm}^3$, $T = 294 - 300 \text{ K}$, $\Delta p_{\text{sorbed}} = \sim 1500 \text{ mbar}$ (first sorption step: 0 to 4 bar) to $\sim 500 \text{ mbar}$ (last sorption step: 26 to 33 bar) and $Z = \sim 0.98$ at 4 bar CO₂ to ~ 0.75 at 40 bar CO₂. The estimated errors of the different terms are: $\Delta V_1 = 0.03 \text{ cm}^3$ and $\Delta V_2 = 0.02 \text{ cm}^3$ (standard deviation of five calibration measurements), $\Delta V_p = 0.03 \text{ cm}^3$, $\Delta T = 1 \text{ K}$, $\Delta p_{\text{sorbed}} = 18 \text{ mbar}$ (0.03% of 60 bar) and $\Delta Z = 0.09$ to 0.5 % of Z -value over the whole pressure and temperature range.

The relative error in ΔC is estimated to be $\sim 5 \%$ in the first sorption step and $\sim 17\%$ in the last sorption step.

2.4.3. Glass transition and density measurements

Glass transition

Glass transition temperatures of the polymer films are determined on a Perkin Elmer DSC-7 calorimeter with a heating rate of 30 °C/min. In most cases no transitions were observed in the first heating run. The glass transition

temperatures were therefore taken from the second run. The average glass transition temperature determined from two samples prepared from the same cast film has a standard deviation of ± 1 °C.

Density

The density of the films was measured with a buoyancy technique [19]. A well dried film sample was first weighed in air. It is then immersed in ethanol at room temperature and the difference in weight upon immersion is determined. The volume of the sample is calculated from the weight difference of the measurements divided by the density of ethanol. From the weight in air and the volume, the density of the polymer film (ρ_p) is calculated as given in Equation 2.12.

$$\rho_p = \frac{m_p}{V_p} = m_p * \frac{\rho^{\text{EtOH}}}{m_p - m_p^{\text{EtOH}}} \quad (2.12)$$

where m_p is the mass of the polymer film weighted in air, ρ^{EtOH} the density of ethanol at room temperature and m_p^{EtOH} the mass of the polymer film weighed in ethanol. For each density measurement, three pieces of polymer film are cut from the same cast film. The final density of that particular film is the average of the three measurements. The standard deviation varied from 0.005 to 0.01.

2.5. Temperature dependence of permeability

Permeation of gases is an activated process and is therefore temperature dependent. A higher permeability is expected at increasing temperature. The temperature dependence of the permeability is given by an Arrhenius type equation [20]:

$$P = P_0 e^{-E_p/RT} \quad (2.13)$$

where P_0 is the pre-exponential factor, E_p the activation energy for permeation, R the gas constant and T the temperature. The activation energy for permeation can easily be obtained from the slope of $\ln(P)$ as a function of $1/T$.

Because a number of the permeation experiments described in this thesis were carried out at room temperature, which varied between 21 and 27 °C, it was found necessary to check the influence of small changes in temperature on the permeability. In Figure 2.3, four permeation curves are given for Matrimid films cast from DMAc. Two samples (1a and 1b) from the same cast film are measured on different days. Room temperature was 27 °C on the first measuring day and 21 °C on the second day, two weeks later. Furthermore, the experiments are repeated with a newly cast film. Two permeation curves (2a and 2b) were obtained simultaneously and room temperature was 22 °C.

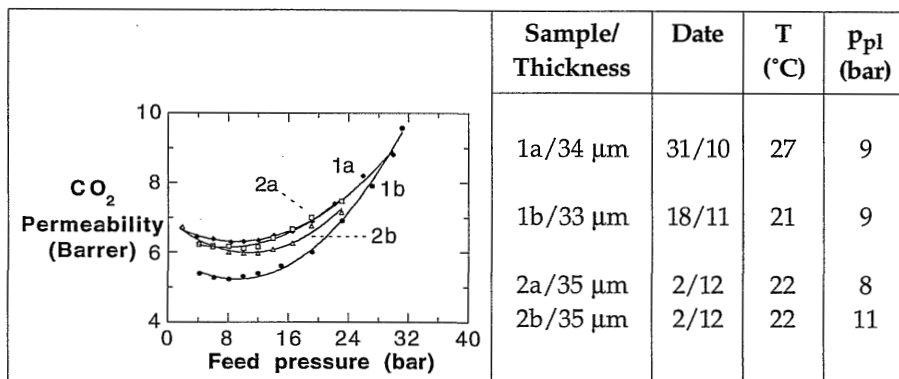


Figure 2.3. CO_2 permeability as a function of pressure at room temperature of Matrimid films cast from DMAc. In the table, the sample thickness, date of experiment, temperature and the plasticization pressure of the different samples are given.

The difference in permeability of sample 1a and 1b at 4.2 bar CO_2 pressure is 1 Barrer. As it is considered that most permeation experiments at room temperature were carried out in a range of 22–25 °C, the permeability differences due to differences in temperature will be smaller than 20%. To get an indication of the variation in permeability, the activation energy and the pre-exponential factor are determined at 4.2 bar CO_2 pressure of the first sample. An activation energy of 21.6 kJ/mol and a pre-exponential factor of 3.8×10^{-6} Barrer were found. A permeability of 5.6 to 6.1 is then calculated at 22 and 25 °C, respectively. In this case, the difference in permeability is only 0.5 Barrer (9% with respect to 5.6 Barrer). In general for glassy polymers no dramatic changes in the absolute value of the permeability are observed [21–23]. Differences in permeability are more pronounced at temperature differences of 100 °C. It is striking that the permeabilities of the second sample obtained at 22 °C correspond with the permeabilities of the first sample obtained at 27 °C. Although it was thought that the samples were prepared in the same way, there must be some influence due to differences in film history. As will be clear from the next section, the influences of different film history on the permeability are larger than the differences due to temperature variations. No trend was therefore found in the different absolute permeabilities as a function of temperature.

The plasticization pressures derived from the permeation isotherms cover the variation found in the plasticization pressure (8–12 bar) of the different Matrimid films measured at room temperature. No trend was found in the plasticization pressure as a function of temperature.

Although the small changes in temperature do not seem to influence the permeation experiments much, it was decided to implement new permeation

test cells with double walls to allow for a better temperature control. The main reason was that a constant temperature is necessary if permeation and sorption data are combined to calculate diffusion data (see Chapter 3). Most permeation experiments with the new cells were carried out at 35 °C, because most of the literature data are available at this temperature. This temperature is just above the critical temperature of carbon dioxide ($T_c = 31$ °C).

To check whether a temperature difference of 10 °C higher than room temperature influences CO₂ plasticization, the permeability as a function of pressure is measured at 24 and 35 °C. Two Matrimid films cast from DMAc with equal thicknesses (22 μm) are used. The permeation curves are given in Figure 2.4.

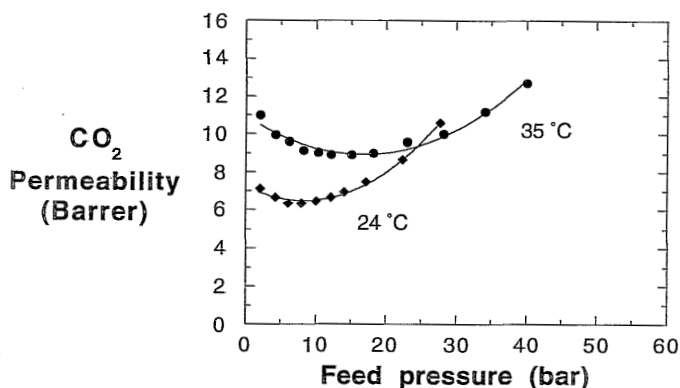


Figure 2.4. Permeation-pressure curves of Matrimid films cast from DMAc with a thickness of 22 μm measured at 24 and 35 °C.

The plasticization effect is somewhat less at 35 °C. The onset of plasticization is at 15 bar instead of the 8-12 bar found in all other measurements at room temperature. A similar shift to a higher plasticization pressure is also observed by Okamoto et al. [24]. They compared the plasticization behaviour of a polyimide film at 35 and 50 °C. The plasticization pressure was increased from 10 to 15 atm. Furthermore, the increase in permeability of the 35 °C-isotherm above the plasticization pressure is less pronounced than the increase of the 24 °C-isotherm. An explanation of this phenomenon is the lower solubility of carbon dioxide in the glassy polymer at higher temperatures [21-23]. The higher absolute permeability value for the 35 °C-isotherm is explained by the increase in diffusivity. The diffusivity increase with increasing temperature outweighs the solubility decrease. The permeability increases therefore with increasing temperature.

2.6. Film morphology

Glassy polymers are not in a thermodynamic equilibrium state [25]. In a normal process, a polymer is cooled from the melt through the glass transition into the glassy state. At the glass transition, a rapid decrease in molecular mobility occurs. The polymer molecules are not able to reach their equilibrium conformation and packing with respect to the cooling rate. The molecules are therefore "frozen" into a nonequilibrium state of higher energy and volume relative to the corresponding equilibrium state at that same temperature. The same occurs in the drying process of solvent cast polymer films. The polymer passes its glass transition in going from a completely dissolved state to a dry polymer film. As solvents are used with different volatility, for example DMAc and CHCl_3 , the rate of passage through the glass transition is different. This eventually leads to different nonequilibrium states or film morphologies. It is also plausible that different film thicknesses lead to different film morphologies.

Because of the nonequilibrium state of the polymer film, there is a thermodynamic potential or driving force to undergo further packing and/or conformational rearrangement in order to approach equilibrium. This process is called physical aging [26]. The aging process results in a redistribution of free volume. These phenomena make comparison of intrinsic permeability, solubility and diffusivity data of films prepared from the same polymer more difficult. It is important how the film has been prepared, and what history it has experienced before the permeation or sorption experiments are carried out [27-31]. The 'history' of the films should be the same for all films to make reliable comparison possible.

To check whether differences in film history influence the study of CO_2 plasticization, the permeability as a function of pressure is determined for Matrimid films with different film thicknesses and films cast from different solvents. The results are given in subsections 2.6.1 and 2.6.2.

2.6.1. Effect of film thickness on permeability

Matrimid films were cast from DMAc with thicknesses ranging from 14 to 34 μm . The permeability of carbon dioxide as a function of pressure is shown in Figure 2.3. These experiments are carried out at room temperature that varied from 21 to 27 $^\circ\text{C}$. No clear trend can be observed in the permeability behaviour of the films with thicknesses ranging from 14 to 34 μm . The permeability curve for the 14 μm thick film falls between the curves for the 21-22 μm and 33-34 μm films. Furthermore, no trend is found in the plasticization pressure in relation to film thickness.

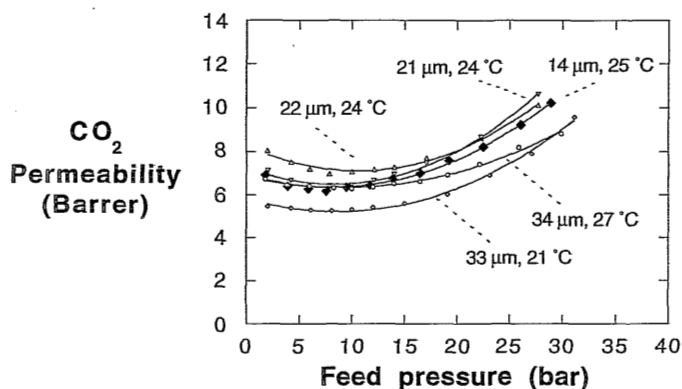


Figure 2.5. Permeability-pressure curves of Matrimid films cast from DMAc with thicknesses varying from 14 to 34 μm measured at room temperature.

Pfromm [32] also did not find significant differences on films with an even broader range in thickness. He obtained similar permeation results for polysulfone and polyimide films with thicknesses of 2.54 μm (intermediate) and 25 μm (thick). Both polymers are amorphous. However, for thin films ($\sim 0.5 \mu\text{m}$) he found decreasing permeabilities and increasing selectivities as a function of time that surpassed those of intermediate and thick films. These phenomena are attributed to an accelerated physical aging of thin glassy polymer films, which results in a densification of the polymer matrix [32,33]. Thin films show a densification of the polymer matrix due to aging. In addition to aging processes in the bulk of the polymer, there is an elimination of excess free volume that takes place in part at the surface of the sample. These surface effects cannot be neglected in very thin films. The large surface area with respect to the film thickness causes an acceleration of the physical aging. Rezac observed similar phenomena for thin polycarbonate layers coated on a ceramic support [34]. The films used in this work are thick, so accelerated physical aging does not influence the transport properties of the film. Another advantage of using thick films is that it is easy to prepare pinhole free films.

A recent publication about the effect of film thickness (5 - 100 μm) on gas transport is from Shishatskii et al. [35]. Dense films of poly(vinyltrimethyl silane) (PVTMS) and poly(trimethylsilyl norbornene) (PTMSNB) were tested. They found that the density was inversely proportional to the film thickness, but did not find significant differences in permeability coefficients. As density is related to free volume, a decrease in permeability with increasing density could be expected [36]. However, the findings of Shishatskii et al. are in accordance with the results of Pfromm, where the whole thickness range (5-100 μm) is classified as intermediate to thick.

Considering the changes in density, Shishatskii et al. [35] emphasise that the polymers chosen have a relatively high free volume. The polymers are comparable with poly(1-(trimethylsilyl)-1-propyne) (PTMSP) and are very susceptible to physical aging. Hence, the density of a film with a certain thickness will probably change in time, too.

2.6.2. Effect of casting solvent on permeability

Matrimid films are cast from three different solvents: CHCl_3 , DMAc and NMP. The permeability of carbon dioxide is measured as a function of feed pressure at room temperature. The permeation curves are given in Figure 2.6.

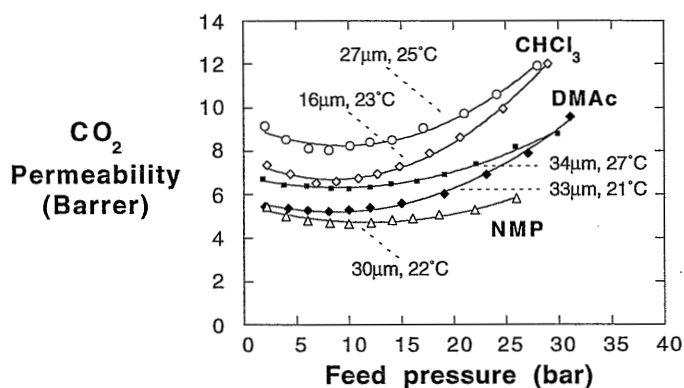


Figure 2.6. Permeation-pressure curves of Matrimid films cast from CHCl_3 , DMAc and NMP measured at room temperature.

The permeabilities of the chloroform cast films are slightly higher than the permeabilities of the DMAc and NMP cast ones. This can be explained by the volatility of chloroform. The drying of the solution cast film is faster if chloroform is used instead of DMAc or NMP. It is possible that due to this fast drying process a larger free volume arises in the dry film. It is also found that the permeability increases with increasing free volume [36]. This explanation also holds for DMAc compared to NMP. DMAc is more volatile than NMP. The permeabilities of the DMAc cast films are also slightly higher than the NMP cast ones. However, considering the probable error in the permeability of 4 to 10% and the small differences in thickness and temperature, it is difficult to indicate the significance of these differences.

In the literature, it has been reported that differences in morphology due to the casting solvent used are more significant in case of (semi-) crystalline polymers [37,38]. Mohr and Paul [37], for example, have shown that the casting solvent influences the crystalline modification formed and the spatial arrangement of

the crystallites within the film. The CO₂ permeability of a poly(4-methyl-1-pentene) film varied from 15 to 94 Barrer at 2 bar and 35 °C depending on the casting solvent used [37].

There is no clear trend found in the plasticization behaviour in relation to the casting solvent used. For example, one does not observe a trend in the shift of the plasticization pressure. From these results it is therefore concluded that changing casting solvent or film thickness does not influence the CO₂-induced plasticization phenomena.

Studying the effects of suppressing plasticization, it is important to evaluate differences in the observed trends. For example, a polymer film may be changed in such a way that its permeability-pressure curve shows a significant shift in the plasticization pressure or does not show a plasticization effect at all.

2.7. List of symbols

A	=	membrane area	cm ²
c	=	concentration of the gas sorbed	cm ³ (STP)/cm ³
E _p	=	activation energy for permeation	J/mol
l	=	thickness	cm
m _p	=	mass of polymer film	g
m _p ^{EtOH}	=	mass of polymer film in ethanol	g
n _{initial}	=	initial number of moles	mol
n _{final}	=	final number of moles	mol
n _{sorbed}	=	number of moles sorbed	mol
P	=	permeability of component i	cm ³ (STP) cm/(cm ² s cmHg)
P ₀	=	pre-exponential permeability factor	cm ³ (STP) cm/(cm ² s cmHg)
p _f	=	feed pressure	cmHg
p _p	=	permeate pressure	cmHg
p _{1f}	=	final pressure in cell 1	Pa
p _{2f}	=	final pressure in cell 2	Pa
p _{2i}	=	initial pressure in cell 2	Pa
Q _F	=	feed flow	cm ³ /s
Q _P	=	permeate flow	cm ³ /s
R	=	universal gas constant	J/mol K
T	=	temperature	K
t	=	time	s
V _c	=	calibrated measuring volume	cm ³ /mol
V _m	=	molar volume	cm ³ /mol
V _p	=	volume of polymer sample	cm ³ /mol
X _{CO₂} ^f	=	mole fraction of CO ₂ in feed	–
X _{CH₄} ^f	=	mole fraction of CH ₄ in feed	–
X _{CO₂} ^f	=	mole fraction of CO ₂ in permeate	–

$X_{\text{CH}_4}^p$	=	mole fraction of CH_4 in permeate	-
Z	=	compressibility factor	-
α	=	separation factor	-
ρ	=	density	g/cm^3
θ	=	stage cut	-

2.8. References

- [1] Koros, W.J., Walker, D.R.B., Gas separation membrane material selection criteria: weakly and strongly interacting feed component situations, *Polymer J.*, 23 (1991) 481-490
- [2] Sommer, K., et al., Correlation between primary chemical structure and property phenomena in polycondensates, *Adv. Mater.* 3 (1991) 590-599
- [3] Roff, W.J., Scott, J.R., *Fibres, films, plastics and rubbers. A handbook of common polymers*, London, Butterworths, (1971), Section 14
- [4] Barbari, T.A., Koros, W.J., Paul, D.R., Polymeric membranes based on bisphenol-a gas separations, *J. Membrane Sci.*, 42 (1989) 69-86
- [5] Chern, R.T., Koros, W.J., Yui, B., Hopfenber, H.B., Stannett, V.T., Selective permeation of CO_2 and CH_4 through Kapton polyimide: Effects of penetrant competition and gas-phase nonideality, *J. Polym. Sci.: Part B: Polym. Phys.*, 22 (1984) 1061-1084
- [6] Donohue, M.D., Minhas, B.S., Lee, S.Y., Permeation behavior of carbon dioxide-methane mixtures in cellulose acetate membranes, *J. Membrane Sci.*, 42 (1989) 197-214
- [7] Story, B.J., Koros, W.J., Comparison of three models for permeation of CO_2/CH_4 mixtures in poly(phenylene oxide), *J. Polym. Sci.: Part B: Polym. Phys.*, 27 (1989) 1927-1948
- [8] Raymond, P.C., Koros, W.J., Paul, D.R., Comparison of mixed and pure gas permeation characteristics for CO_2 and CH_4 in copolymers and blends containing methyl methacrylate units, *J. Membrane Sci.*, 77 (1993) 49-57
- [9] Chern, R.T., Koros, W.J., Sanders, E.S., Yui, R., "Second component" effects in sorption and permeation of gases in glassy polymers, *J. Membrane Sci.*, 15 (1983) 157-169
- [10] Kumazawa, H., Inamori, K., Messaoudi, B., Sada, E., Permeation behavior for mixed gases in poly(4-methyl-1-penten) membrane near the glass transition temperature, *J. Membrane Sci.*, 92 (1994) 7-12
- [11] Stern, S.A., Saxena, V., Concentration-depended transport of gases and vapors in glassy polymers, *J. Membrane Sci.*, 7 (1980) 47-59
- [12] Zhou, S., Stern, S.A., The effect of plasticization on the transport of gases in and through glassy polymers, *J. Polym. Sci., Part B, Polym. Phys.*, 27 (1989) 205-222
- [13] O'Brien, K.C., Koros, W.J., Barbari, T.A., A new technique for the measurement of multicomponent gas transport through polymeric films, *J. Membrane Sci.*, 29 (1986) 229-238
- [14] Bevington, P.R., *Data reduction and error analysis for the physical sciences*, McGraw-Hill, (1969) 57
- [15] Koros, W.J., Paul, D.R., Design considerations for measurement of gas sorption in polymers by pressure decay, *J. Polym. Sci., Part B: Polym. Phys.*, 14 (1976) 1903-907
- [16] Reid, R.C., Prausnitz, J.M., Sherwood, T.K., *The properties of gases and liquids*, McGraw Hill, New York, (1977)
- [17] Pitzer, K.S., Lippmann, D.Z., Curl, R.F., Huggins, C.M., Petersen, D.E., The volumetric and thermodynamic properties of fluids. II. Compressibility factor, vapor pressure and entropy of vaporization, *J. Am. Chem. Soc.*, 77 (1955) 3433-3440
- [18] Van Huff, N.E., Houghton, G., Coull, J., Equation of state and compressibilities for gaseous carbon dioxide in the range of 0 °C to 600 °C and 0 to 150 atm., *J. Chem. Eng. Data*, 8 (1963)

- 336-340
- [18a] Michels, A., Michels, C., Proc. Roy. Soc. (London), Ser. A. 160 (1937) 358
- [18b] MacCormack, K.E., Schneider, W.G., J. Chem. Phys., 18 (1950) 1269
- [18c] Kennedy, G.C., Am. J. Sci., 252 (1954) 225
- [19] Standard test methods for specific gravity (relative density) and density of plastics by displacement, in: ASTM annual book of standards, (1993), D-792
- [20] Stannett, V., Simple Gases, in: Diffusion in polymers, Crank, J., Park, G.S., (Eds.), Academic press, London, (1968) chapter 2
- [21] Kim, T.-H., Koros, W.J., Husk, G.R., Temperature effects on gas permselection properties in hexafluoro aromatic polyimides, J. Membrane Sci., 46 (1989) 43-56
- [22] Costello, L.M., Koros, W.J., Temperature dependence of gas sorption and transport properties in polymers: measurement and applications, Ind. Eng. Chem. Res., 31 (1992) 2708-2714
- [23] Costello, L.M., Koros, W.J., Comparison of pure and mixed gas CO₂ and CH₄ permeabilities in polycarbonate: effect of temperature, Ind. Eng. Chem. Res., 32 (1993) 2277-2280
- [24] Okamoto, K.-i., Tanaka, K., Shigematsu, T., Kita, H., Nakamura, A., Kusuki, Y., Sorption and transport of carbon dioxide in a polyimide from 3,3',4,4'-biphenyltetracarboxylic dianhydride and dimethyl-3,7-diaminodibenxothiophene-5,5'-dioxide, Polymer, 31 (1990) 673-678
- [25] Tant, M.R., Wilkes, G.L., An overview of the nonequilibrium behavior of polymer glasses, Polym. Eng. Sci., 21(14) (1981) 874-895
- [26] Struik, L.C.E., Physical aging in amorphous polymers and other materials, Elsevier, Amsterdam, (1978)
- [27] Wessling, M., Relaxation phenomena in dense gas separation membrane, Ph-D Thesis, University of Twente, Enschede, The Netherlands, (1993)
- [28] Hopfenberg, H.B., The effect of film thickness and sample history on the parameters describing transport in glassy polymers, J. Membr. Sci., 3 (1978) 215-230
- [29] Wonders, A.G., Paul, D.R., Effect of CO₂ exposure history on sorption and transport in polycarbonate, J. Membr. Sci., 5 (1979) 63-75
- [30] O'Brien, K.C., Koros, W.J., Husk, G.R., Influence of casting and curing conditions on gas sorption and transport in polyimide films, Polym. Eng. Sci., 27(3) (1987) 211-217
- [31] Moe, M., Koros, W.J., Hoehn, H.H., Husk, G.R., Effects of film history on gas transport in a fluorinated aromatic polyimide, J. Appl. Polym. Sci., 36 (1988) 1833-1846
- [32] Pfromm, P.H., Gas transport properties and aging of thin and thick films made from amorphous glassy polymers, Ph.D. Thesis, University of Texas, Austin, USA, (1994)
- [33] Pfromm, P.H., Koros, W.J., Accelerated physical aging of thin glassy polymer films: evidence from gas transport measurements, Polymer, 36(12) (1995) 2379-2387
- [34] Rezac, M.E., Update on the aging of a thin polycarbonate-ceramic composite membrane, Ind. Eng. Chem. Res., 34 (1995) 3170-317
- [35] Shishatskii, A.M., Yampol'skii, Yu.P., Peinemann, K.-V., Effects of film thickness on density and gas permeation parameters of glassy polymers, J. Membrane Sci., 112 (1996) 275-285
- [36] Yampol'skii, Yu. P., Platé, N.A., Is it possible to predict transport properties of polymers on the basis of the chemical structure of the chains: a review, Polym. Sci., 11 (1994) 1599-1609
- [37] Mohr, J.M., Paul, D.R., Effect of casting solvent on the permeability of poly(4-methyl-1-pentene), Polymer, 32(7) (1991) 1236-1243
- [38] Ma, S.P., Sasaki, T., Sakurai, K., Takahashi, T., Morphology of solution-cast thin films of wholly aromatic thermoplastic polyimides with various molecular weights, Polymer, 35(26) (1994) 5618-5625

3

CO₂ - induced plasticization phenomena in glassy polymers

3.1. Introduction

CO₂-induced plasticization phenomena observed in permeation experiments have been briefly described in Chapter 1 of this thesis. These phenomena are:

- a minimum in the CO₂ permeability as a function of pressure,
- time dependency of the permeability at CO₂ pressures above the plasticization pressure, and
- a decreasing CO₂/CH₄ selectivity at elevated pressures.

The experiments in which “plasticization phenomena” are observed must be explicitly mentioned because it is not possible to give an unambiguous definition of plasticization. Plasticization occurs when the concentration of the penetrant molecules in the polymer matrix is high enough to facilitate polymer segmental motion. The increase in chain mobility can be observed, for example, by a depression of the glass transition temperature of the polymer-penetrant mixture. However, a decrease in the glass transition temperature is not always a sufficient condition to cause an increase in permeability. This example illustrates that plasticization covers different phenomena and that one phenomenon does not automatically imply another one.

In the next section, plasticization related phenomena found in the literature are summarized. There was no general rule found that can predict whether a polymer will be plasticized by a penetrant or not. In this chapter, an attempt is made to find relationships between the plasticization pressure and the chemical structure within a series of polymers. The CO₂ permeability and solubility as a function of pressure of eleven different glassy polymers have been measured. The results are presented in Section 3.3.

3.2. Physical observations related to plasticization

CO₂ permeation behaviour

Typically, three types of pressure-dependencies of the CO₂-permeability in glassy

polymers can be distinguished:

- 1) a decreasing permeability (P) as a function of pressure over the pressure range considered,
- 2) a minimum in the permeability as a function of pressure, and
- 3) a progressive increase in permeability with increasing feed pressure.

The three types of permeation behaviour are schematically given in Figure 3.1.

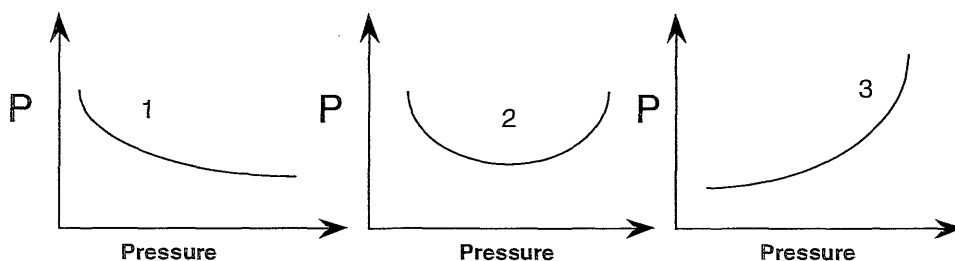


Figure 3.1. Schematic representation of the possible shapes of the permeability (P) versus pressure curves.

The three trends are found among polymers that differ over an order of magnitude in permeability [1]. Polysulfone (PSF) and polycarbonate (PC), for example, show type 1 permeation behaviour for pressures up to 30 bar [1]. Matrimid, as was shown in Chapter 1, shows a permeation curve represented by type 2. A relatively low partial CO_2 pressure is necessary to induce plasticization. In this case, plasticization is defined as the increase in permeability with increasing feed pressure above a certain threshold pressure value. Type 3 has been found for polyarylates, such as polymethyl-methacrylate (PMMA) [1] and polyethylmethacrylate (PEMA) [2] and cellulose acetate (CA) [1,3]. Although these polymers are in the glassy state, they show a similar permeation behaviour as found for rubbers. Much research has been done to find an explanation for type 3 permeation behaviour [1-10], because this knowledge may also be useful in explaining the increase in permeability of the type 2 curve.

Considering the solution-diffusion model, the increase in permeability is attributed to the concentration dependence of the diffusion coefficient [11,12]. The pressure dependence of the solubility coefficient is comparable for different polymers. Hence, differences in permeability are determined mainly by the diffusivity. Furthermore, the diffusivity generally increases with increasing pressure, whereas the solubility decreases. An increase in permeability is therefore possible because the diffusion coefficient increases with concentration much more rapidly than the solubility coefficient decreases with pressure. However, this does not imply that the solubility of a penetrant is unimportant. On the contrary, solubility indirectly contributes to the increase in diffusivity. Ultimately, the diffusion coefficient can only increase because the CO_2 concentration in the polymer increases.

Polarity of the polymer chain

It was thought that in PMMA, PEMA and CA *polar* and *flexible* pendant groups, such as $-\text{OCOCH}_3$ or COOCH_3 , attribute to the plasticization behaviour of CO_2 [1-10]. CA also contains polar hydroxyl groups, but it is speculated that the ester unit is more important in the plasticization process since both CA and the polyarylates have this functional group in common. The polar groups of the polymer could have dipolar interactions with the polarizable carbon dioxide molecules. Pilato [13] already suggested a dipole-induced-dipole interaction between CO_2 and the sulfone group in polysulfone. Based on this idea, Koros [5] found a relation between the concentration of carbonyl and sulfone groups in the polymer structure and the solubility selectivity of a CO_2/CH_4 gas pair. The solubility selectivity increased with increasing concentration of the polar groups. It was therefore thought that the carbonyl group in the ester moiety is responsible for the high plasticization responses in CA and the polyarylates. However, this is not supported by the study of Puleo et al. [7]. They compared the CO_2 permeation and sorption behaviour of a methoxy ($-\text{OCH}_3$) and an acetoxymethyl ($-\text{OCOCH}_3$) substituted para-polystyrene. Both polymers exhibited the same extent of plasticization by CO_2 . Hence, the carbonyl part of the ester unit is not the sole cause for the plasticization responses in CA and the polyarylates.

It is also found that introducing polar groups not always results in an increased solubility for CO_2 . Additional to polymer-gas interactions, the solubility is also determined by free volume. As demonstrated by Ghosal [14], the substitution of a small number of nitrate groups in the polysulfone backbone initially resulted in a decreasing solubility with increasing nitrate content. The large nitrate groups reduce the free volume available for sorption. Apparently, a critical number of substituents is necessary to cause an increase in solubility. Furthermore, the *position* of the polar group is sometimes more important than differences in polarity [5,15]. For example, the polyimide Kapton (PMDA-ODA) has a high concentration of carbonyl groups in the polymer matrix but has a very low solubility selectivity for a CO_2/CH_4 gas pair [5]. An explanation for this fact could be that the carbonyl groups are not fully accessible for the CO_2 molecules [5].

Polarity should also be considered in the sense that polar groups in the polymer chain can cause specific interactions between chain segments. This can result in a denser packing of the polymer matrix. In case plasticization occurs the CO_2 molecules are able to overcome the intersegmental interactions of the polar groups. Several researchers have studied specific polar interactions in polymers [3,9,16,17]. Kamide et al. [9] observed strong hydroxyl-hydroxyl interactions in CA by nuclear magnetic resonance and found that these interactions were partly or fully destroyed by addition of a solvent. Puleo et al. [3] used Fourier transform infrared spectroscopy to study the effect of sorbed CO_2 on the interactions between the chain segments in CA. They found that the sorbed CO_2 molecules disrupt the hydroxyl-acetyl and acetyl-acetyl interaction. CO_2 is able to do that because it will interact with the polar acetyl group. Furthermore, they observed that the intersegmental interactions slowly reformed on removal of CO_2 and

interpreted this in such a way that plasticization is a reversible process. Fried and Li [17] support the findings of Puleo et al. [3]. They indicated weak dipole-dipole interactions between the ester groups in PMMA, which are disrupted by sorbed CO₂.

Summarizing, the interactions of CO₂ with polar groups in the polymer chain are stronger than the interactions between chain segments. Thus, CO₂ breaks these interactions, which provides additional diffusion pathways for the CO₂ molecules. Now, it is also clear why it is suggested that the pendant group should be flexible in addition to being polar. As the interactions between the pendant groups is broken, the polymer segments become highly mobile, which provides more opportunities for penetrant molecules to execute diffusive jumps. As was shown by Wessling et al. [18], the activation energy for diffusion decreases with increasing concentration of the penetrant sorbed.

Influence of sorbed CO₂ on T_g

As may be clear from the above discussion, gas transport is mainly influenced by chain packing density, segmental mobility and interactions between chain segments. These factors also effect the glass transition temperature (T_g). An increased chain mobility correlates with a decrease in T_g. And, as plasticization refers to an increase in chain mobility, the depression of the glass transition temperature can also be used as a measure for the extent of plasticization. Sometimes an *increase* in glass transition is observed. This is attributed to CO₂-induced crystallization [19-21]: CO₂ plasticization causes an increase in polymer segmental motion in such a way that rearrangement into crystals is kinetically favoured.

The decrease in glass transition temperature has been observed by several researchers [1,8,18,22-27] and depends on the polymer and the pressure of CO₂ applied. For example, Chiou et al. [8] equilibrated different polymers with CO₂ at 20 atm and found with differential scanning calorimetry measurements a decrease in T_g of 18 °C for PVC, 32 °C for polystyrene, 51 °C for polycarbonate and 22 °C for PET. Wessling et al. [27] describe a method in which they could relate the skin thickness of foams to CO₂-induced glass transition depression. They observed that high T_g polymers such as the 6FDA-based polyimides showed T_g-depressions of 198 °C at 50 bars CO₂.

Polymers can even change from the glassy into the rubbery state. If the T_g is not much higher than the operating temperature, the concentration of CO₂ may be high enough to reduce the T_g to the temperature of the experimental study. Evidence for the glass-rubber transition is found in the alteration of the sorption isotherm. The sorption isotherm of a low T_g polymer shows an inflection point, at which the curve changes from a nonlinear curve to a straight line. This is schematically shown in Figure 3.2.

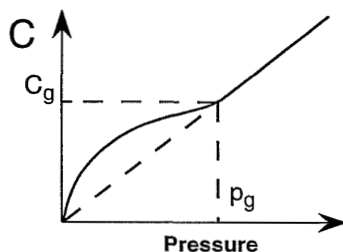


Figure 3.2. Schematic representation of a CO_2 sorption isotherm of a low T_g polymer: concentration (C) as a function of pressure. C_g is the concentration at which the polymer undergoes glass transition and p_g the corresponding pressure.

The isotherm is concave to the pressure axis at low pressures, which is characteristic for gas sorption in glassy polymers. The isotherm becomes linear at higher pressures and can be extrapolated back to the coordinate origin. The latter type of sorption behaviour is characteristic for sorption of gases in rubbery polymers. These types of sorption isotherms are found, for example, for PEMA [2,10,28], polyvinylbenzoate (PVB) [29] and PET [30] and are only observed for CO_2 and not for gases such as N_2 , O_2 , H_2 , CH_4 , He and Ar.

Sanders [1] studied the CO_2 -induced changes in polyethersulfone (PES). He observed that the T_g depressed 76°C after equilibration with CO_2 at 7.8 atm and 100°C as the pressure was increased to 35 atm . From these results it is concluded that PES is highly plasticized by CO_2 . The CO_2 plasticization is believed to be the source of the pressure-dependent permeability behaviour of type 2 at elevated pressures and of type 3. However, Sanders did not measure an increase in CO_2 permeability for PES at pressures up to 27 atm at 25°C . Comparing the T_g depression of various polymers that cover the three types of permeation behaviour shown in Figure 3.1, Sanders concluded that in their study all polymers appeared to be plasticized to similar extents by dissolved CO_2 and that the CO_2 -induced T_g depression appeared to be independent of the permeation behaviour exhibited by the polymer. This phenomenon was interpreted as: molecular motions that are responsible for the plasticization of the bulk physical and mechanical properties of glassy polymers are not necessarily responsible for diffusion of small penetrants in glassy polymers. The T_g , often called α -relaxation, is a parameter of the bulk polymer and refers to long-range chain motions [31]. Some motions in PES, however, are restricted to rocking of the benzene rings, rotation about the ether bonds or to the less energetic motions involving the sulfone group. These motions, also called sub- T_g motions, are referred to as β -relaxations and occur at lower temperatures than the long-range chain motions. Large-scale segmental mobility of the PES backbone does not occur. This is supported by the findings of Kamps et al. [32]. Nitrated PES and PSF

showed lower diffusion coefficients than unmodified PES and PSF. Furthermore, the amount of β -relaxations, measured as the area under the relaxation curve, also decreased. These observations were interpreted as restriction of sub- T_g motions by the substituted nitro-groups. Seymour and Light [33] found a correlation between the amount of β -relaxation and the diffusion coefficient of O_2 in a series of modified polyesters. The diffusivity, and also the permeability, decreased with a decreasing amount of β -relaxation. The same was found for CO_2 . Main chain modifications restrict low-temperature relaxations and thereby the diffusivity and permeability. This emphasizes that sub- T_g motions may have a larger impact on diffusivity than long-range chain motions. In CA or PMMA, which are highly susceptible to plasticization, sub- T_g motions are also possible. The pendant acetate and ester groups are not restricted in their movement by chemical bonds that do exist for groups in the main chain. Plasticization of the polymer matrix should facilitate these motions. It is possible that the movement of these pendant groups perturbs the local packing density sufficiently to allow the penetrant to execute a diffusional jump.

Conditioning and hysteresis effects

Exposure of a glassy polymer to high pressure CO_2 is called "conditioning". The increase in permeability as a function of time is a direct effect of the CO_2 conditioning. During exposure, the polymer matrix is loosened by the CO_2 molecules. The larger free volume can be maintained by exchange of a gas with sufficient solubility as described in Chapter 1. Other results of the conditioning are the hysteresis effects found in permeation and sorption measurements by comparing pressurization and depressurization steps. Significantly higher sorption and steady state permeability values are measured as the pressure is decreased stepwise after high pressure CO_2 exposure [3,7,11,12,30]. This is also observed for polymers that do not show plasticization in the sense that they exhibit an increase in permeability at elevated pressures [7]. The hysteresis effects in the permeation and sorption isotherms upon depressurization are schematically shown in Figure 3.3.

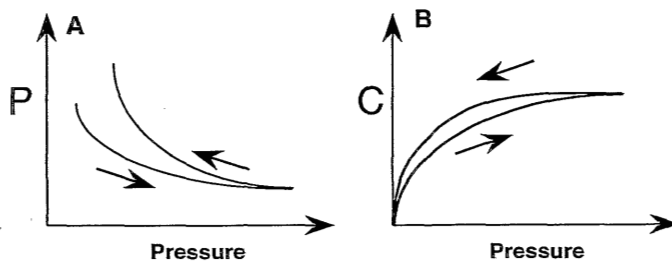


Figure 3.3. Schematic representation of the hysteresis effects upon depressurization in: A. permeation (P =permeability) and B. sorption (C =concentration).

The permeability shows an increase as expected in decreasing the pressure in both the pressurization and depressurization step, but the values are higher in the depressurization step. CO₂ conditioning may cause some redistribution of the excess free volume. Upon release of CO₂ the polymer chains do not relax back to a denser matrix in the time scale of the measurements, which results in higher concentration of CO₂ sorbed in the polymer matrix at the same pressure as in the pressurization step. Wessling et al. [34], present a qualitative physical model which describes these hysteresis effects. The model is based on dilation and consolidation experiments with CO₂ in polyimides. They found that consolidation relaxations can be so slow on the experimental time scale that residual dilation can be observed.

In the literature, such hysteresis phenomena are also attributed to plasticization. However, no clear definition of the term 'plasticization' is given.

Plasticizing ability of 'inert' gases

It is thought that only highly sorbing gases such as CO₂, SO₂ and NO₂ have plasticizing potential due to their polar nature. However, evidence has been found in the literature that even inert gases such as argon show plasticization effects at elevated pressures. These observations support the results described later that polar interactions between CO₂ and the polymer is not a first requirement for the polymer to plasticize. Assink [35] demonstrated this for polydimethyl-siloxane (PDMS) by nuclear magnetic resonance relaxation measurements. PDMS was plasticized by Ar sorbed at 500-2000 atmospheres. Furthermore, Mizoguchi et al. [36] explained the effect of sorbed gas on the crystallization rate of PET on the basis of the plasticization ability of various gases, such as CO₂, C₂H₄, C₂H₆, CH₄ and Ar at pressures of 30 or 50 atm. All gases showed an increase in the crystallization rate compared to air at atmospheric pressure. Argon showed the lowest increase in crystallization rate, but the fact that it could increase the crystallization rate was taken as an indication of its plasticizing ability. A plot of the crystallization rate versus the concentration of the gases in PET showed a steady increase in crystallization rate with increasing gas concentration. From this plot the authors suggested that the plasticization effect of the gas on the crystallization rate only depends on concentration and is independent of the gas species. Kamiya et al. [37,38] concluded from their dielectric relaxation studies that CO₂ and Ar molecules have the same ability to plasticize PEMA above T_g although the solubilities of the gases are very different. The maximum of the dielectric loss tangent (tan δ) increased with increasing CO₂ pressure and was shifted to higher frequencies. The frequency at which the maximum appears (f_{max}) corresponds to the average frequency of molecular motion [31]. Hence, enhanced molecular motion has been observed with increasing CO₂ pressure. The hydrostatic pressure effect resulted in less than 10% decrease of the increase in f_{max}. The plasticizing ability of Ar was actually observed in estimating this hydrostatic pressure effect. A polymer film was pressurized with the inert gases Ar and He. A pronounced effect of hydrostatic pressure on the dielectric relaxation was expected because of the low solubility of

Ar and He compared to CO₂. Log(f_{\max}) as a function of pressure increased linearly for Ar and decreased for He with increasing pressure. Since there is always a competition between the plasticization effect and the hydrostatic pressure effect, the former may be larger than the latter in case of Ar. For helium the hydrostatic pressure effect dominates due to the extremely low solubility of He in polymers.

However, one remark should be made. Kamiya et al. [38] explicitly say that PEMA can be plasticized *above its* T_g by Ar. PEMA has a glass transition temperature of 69 °C and their conclusions are based on experiments carried out at 105 °C, which is well above T_g . This is also the case in the work of Mizoguchi et al. [36]. Their measurements on PET were carried out at 85 °C, which is also above the T_g of 75 °C. Striking fact is that the polymers mentioned are studied in the rubbery state. PDMS is a rubber and the glassy polymers are brought above their T_g by increasing the temperature. The polymer chains are already relatively flexible because they are in the rubbery state. Plasticization should then be defined as a phenomenon that makes flexible chains even more flexible. It is said that Ar can effect this in a similar manner as CO₂, however it requires higher pressures. It is not clear from these findings whether Ar can plasticize a polymer in the *glassy* state too.

Thin versus thick films

As mentioned in Chapter 2, films with thicknesses below 1 μm show different permeation behaviour than intermediate ($\sim 2.5\mu\text{m}$) or thick films ($>14\mu\text{m}$). Wessling [39] has observed a different permeation behaviour of polyimide films with a thickness of about 3 μm compared to thick films of similar polymers. He prepared bi-layer films using the polyimide 6FDA-4PDA as the highly selective top layer and the highly permeable poly(trimethyl silylpropene) (PTMSP) or poly(dimethylsiloxane) (PDMS) as a supporting layer. The CO₂/CH₄ selectivity for both membranes correspond with the selectivity obtained from a thick polyimide film. However, the permeability as a function of pressure progressively increases with increasing pressure in the thin film (type 3 permeation behaviour, see Figure 3.1), whereas thick film equivalents showed type 2 behaviour. These findings may indicate different plasticization behaviour of thin films compared to thick films prepared from the same polymer.

In case of asymmetric or composite membranes, the separating layer is often an (ultra) thin layer. Plasticization of the thin skin layer of an asymmetric membrane may also proceed in a different manner compared to thick films [40-42]. Jordan et al. [40] found that an asymmetric polyimide membrane could be conditioned (preswollen) at much lower pressures than the dense film prepared from the same polymer. The membrane also appeared to reach a much higher plasticization state than the thick film, that is, a more pronounced increase in permeance (permeability per unit of thickness= P/ℓ). Pfromm et al. [41] studied thick films and asymmetric membranes prepared from polysulfone, polycarbonate and polyester carbonate. The P/ℓ of CO₂ increased with pressure in

the asymmetric membranes, whereas the permeabilities of the thick films prepared from the same polymer decrease in the same pressure range. Furthermore, the permeance becomes time dependent at much lower pressures in the asymmetric membranes than in thick films.

Hence, it seems that asymmetric membranes and probably also composites are more sensitive to plasticization effects than thick films. It is beyond the scope of this thesis to explain these phenomena. In general, gas transport properties are studied on homogeneous dense films because it is extremely difficult to prepare asymmetric membranes with a defect-free top layer or composites with a defect-free ultra-thin toplayer [43,44]. In this thesis, plasticization phenomena are also studied on thick homogeneous dense films. This is justified, because at least the observed phenomena are comparable. The CO₂ permeability increases with increasing pressure and the permeability becomes time dependent in a thick film as well as in the thin skin-layer of an asymmetric membrane. It is therefore assumed that the methods identified to suppress plasticization in thick films will also be successful in suppressing plasticization in asymmetric or composite membranes.

3.3. CO₂ plasticization related to chemical structure

Permeation results

Homogeneous dense films were prepared from all polymers mentioned in Table 2.1. The film thicknesses varied from 18 to 45 μm. Permeation experiments were carried out at CO₂ pressures of up to 40 bars. The resulting permeation curves are summarized in Figure 3.4 and are organized according to the classification in Chapter 2. All polymers show the typical trend of a decreasing permeability with increasing pressure at low pressures and an increasing permeability with further increase of pressure. Because of the differences in absolute permeability of the polymers presented in one figure, the minima of the poorer permeable films are not clearly visible on the permeability scale used. For example, PEI, BPZ-PC and P84 show a clearly visible and defined minimum when the data are plotted on a permeability scale of 0 to 2 Barrers.

The permeability values were fitted by a second order polynomial ($y=a+bx+cx^2$). The plasticization pressure is obtained by determining the minimum of the curve fit. Furthermore, the permeability at zero pressure is determined by extrapolating the curve fit to zero pressure. This permeability is purely empirical, but it is of use to obtain an impression to what extent the permeability at the plasticization pressure has decreased with respect to the permeability at very low pressures. In Table 3.1, this is given by the ratio of $P(p=p_{pl})$ and $P(p=0)$. The decrease in permeability varies from 11% for CA to 37% for BPA-PC.

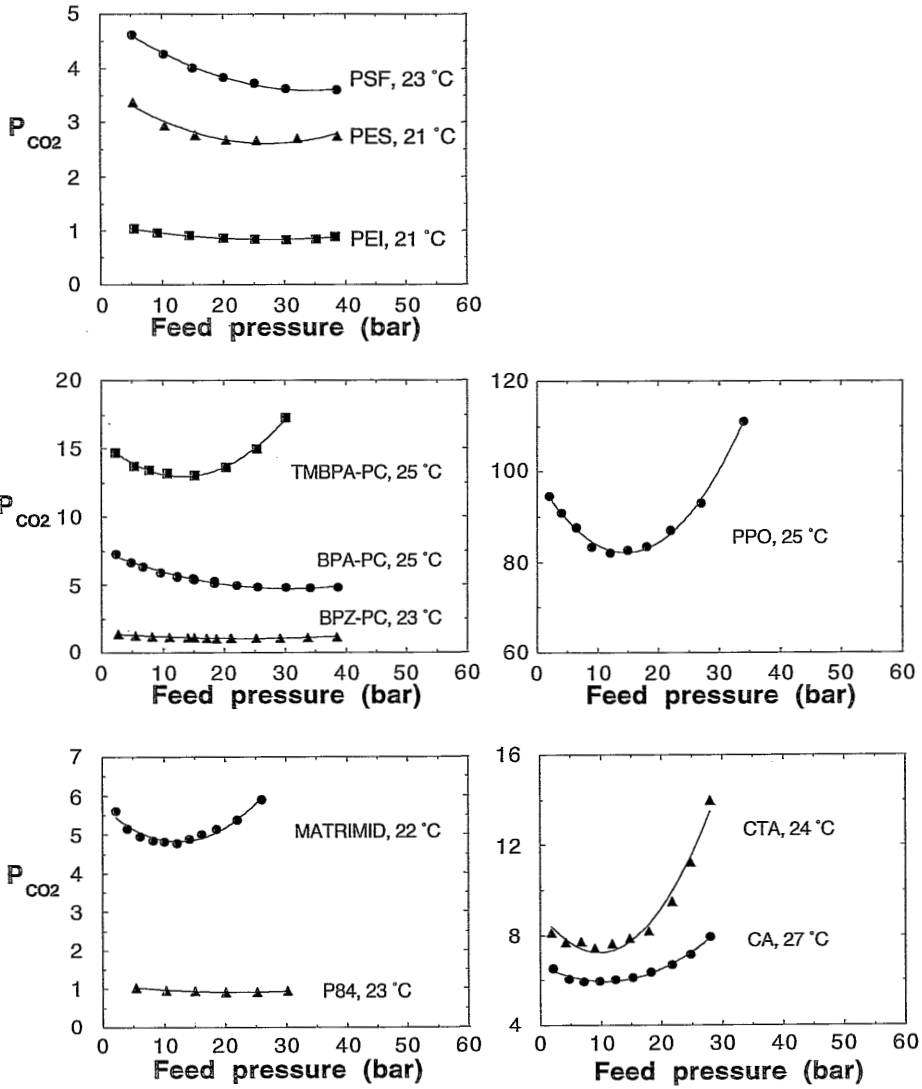


Figure 3.4. CO_2 permeabilities (Barrer) as a function of CO_2 pressure for the different polymers at room temperature, classified as described in Chapter 2.

Table 3.1. Plasticization pressure (p_{pl}), permeability at the plasticization pressure ($P(p_{pl})$) and zero pressure ($P(p=0)$) and the ratio $P(p_{pl})/P(p=0)$ obtained from the permeation curves in Figure 3.4.

Group		Polymer name	p_{pl} (bar)	$P(p_{pl})$ (Barrer)	$P(p=0)$ (Barrer)	$P(p_{pl})/P(p=0)$ (-)
A	1	PSF	34	3.6	5.0	0.72
	2	PES	27	2.6	3.7	0.71
	3	PEI	28	0.84	1.1	0.74
B	4	BPA-PC	31	4.7	7.5	0.63
	5	BPZ-PC	24	1.0	1.4	0.73
	6	TMBPA-PC	13	13	16	0.83
	7	PPO	14	82	99	0.83
C	8	Matrimid 5218	12	4.8	5.7	0.84
	9	P84	22	0.92	1.1	0.82
D	10	CA	11	6.0	6.7	0.89
	11	CTA	10	7.3	9	0.82

Using the plasticization pressure as a measure of the tendency to plasticize, the following qualitative conclusions can be drawn from Table 3.1:

- The polymers in group A, PSF, PES and PEI, show high plasticization pressures compared to the other polymers and, hence, a low tendency to plasticize.
- Comparing the polycarbonates in group B, the plasticization pressure varies from 13 to 31. The tetramethyl substitution apparently causes a higher tendency to plasticize. The suggestion that PPO is similar in its permeation behaviour to TMBPA-PC is justified on the basis of their similar plasticization pressures of 14 and 13 bar, respectively.
- Changing the diamine structure in a BTDA-based polyimide changes the plasticization behaviour. In group C, P84 has a higher plasticization pressure and has therefore a lower tendency to plasticize than Matrimid.
- In group D, the cellulose derivatives show the same tendency to plasticize. Compared to the other groups the tendency of these polymers is the highest.

No obvious trends between the plasticization pressure and the absolute value of the permeability can be found. However, an empirical correlation has been found between the plasticization pressure and the ratio $P(p=p_{pl})/P(p=0)$, as is shown in Figure 3.5.

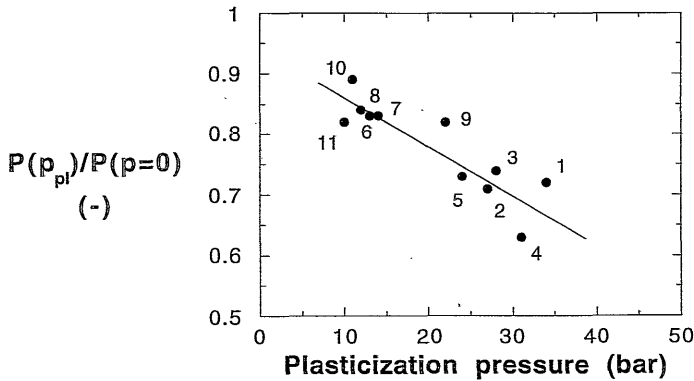


Figure 3.5. Relation between the plasticization pressure, p_{pl} , and the ratio of the permeability at the plasticization pressure and at zero pressure. The numbers refer to the polymers listed in Table 3.1.

As described earlier, the decrease in permeability at low pressures is dominated by a decrease in solubility with increasing pressure. On the other hand, the diffusivity increases with pressure. From Figure 3.5, it seems that a polymer with a lower tendency to plasticize decreases more in permeability with increasing pressure: the higher the plasticization pressure the larger the relative decrease in the permeability at p_{pl} ($P(p=p_{pl})$) with respect to $P(p=0)$. This implies that the diffusivity changes more strongly with increasing concentration as the tendency to plasticize increases. The permeability can therefore decrease less. In the extreme case, the permeability increases immediately and $P(p=p_{pl})/P(p=0)$ would not exist.

Free volume analysis

In a first approach to correlate the plasticization pressure and physico-chemical quantities no clear correlations were found by comparing glass transition temperature or density of the film with the plasticization pressure. Therefore, since transport depends on free volume, fractional free volume calculations are done. The fractional free volume (FFV) is calculated using Equations (3.1):

$$FFV = \frac{V - V_0}{V} \quad (3.1)$$

$$V = M/\rho \quad (3.1a)$$

$$V_0 = 1.3V_w \quad (3.1b)$$

where V is the total molar volume of the monomer unit (cm^3/mole), M the molar mass (g/mole) of the monomer unit and ρ the density of the film (g/cm^3), which is determined experimentally. V_0 is the volume occupied by the chains.

The most closely related value for V_0 is the zero point molar volume of the most stable condensed phase at 0 K (cm^3/mole). V_0 is assumed to be impermeable for diffusing gas molecules. V_w is the van der Waals volume which can be obtained by a group contribution method. According to Bondi [45] a good approximation of the relation between V_0 and V_w is given by Equation (3.1b). The factor 1.3 is estimated from the packing density of molecular crystals at 0 K and accounts for the fact that the volume at 0 K is greater than the molecular volume. The free volume available for gas diffusion in a structural unit is therefore represented by the difference between the total molar volume and the zero point molar volume ($V-V_0$).

According to the additivity principle, many properties or combinations of properties can be calculated by summation of either atomic, group or bond contributions [46]. The contribution of end groups can be neglected because the mass percentage is so small that the repeating unit determines the properties. The van der Waals volume of the monomer unit can be obtained by using such an additivity principle.

The monomer unit is composed of atoms, which are considered as spheres with an atomic radius R , the so-called van der Waals radius [45]. However, the volume of the monomer unit is not just the sum of each atomic volume. If reaction takes place, the total atomic volume will be significantly smaller. Therefore, van der Waals radii and bond lengths are estimated as a function of their atomic surroundings. The total van der Waals volume of that monomer unit can be determined from the volumes of the composing structural groups in a monomer unit. Bondi [44] was the first who calculated the contributions of about 60 structural groups to the van der Waals volume. Later Slonimskii [47] and Askadskii [48,49] also derived group contributions of about 100 values of atomic increments in different surroundings. Slonimskii and Askadskii as well as Bondi used the same calculation method. Van Krevelen used these values to calculate the van der Waals volumes of larger group increments. This makes further calculations less time consuming. Therefore, the tabulation of van Krevelen has been used [46,50,51]. The results are given in Tabel 3.2. The FFV varied from 0.138 for BPZ-PC to 0.225 for Matrimid.

Lee [52] was the first who correlated the permeability of various polymers to their specific free volume ($\{V_f = (V-V_0)/M\}$). He used the following equation for the diffusivity as a function of the polymer free-volume:

$$D_i = A \cdot \exp\left(\frac{-B}{V_f}\right) \quad (3.2)$$

where A and B are empirical constants equal for all polymers, but dependent on the type of gas. Substitution of Equation (3.2) in $P_i = D_i S_i$ gives:

$$P_i = S_i \cdot A \exp\left(\frac{-B}{V_f}\right) \quad \text{or} \quad \ln(P_i) = \ln(S_i) + \ln(A) - \left(\frac{B}{V_f}\right) \quad (3.3)$$

Table 3.2. *Results of fractional free volume calculations*

Group	Polymer name	M	ρ	V_w	V_0	V	FFV
A	1 PSF	442.5	1.233	234.2	304.5	358.9	0.152
	2 PES	232.2	1.355	111.9	145.5	171.4	0.152
	3 PEI	592.6	1.278	292.6	380.4	463.7	0.180
B	4 BPA-PC	254.3	1.209	136.2	177.1	210.3	0.158
	5 BPZ-PC	308.4	1.21	169.1	219.8	254.9	0.138
	6 TMBPA-PC	310.4	1.083	180.8	235.0	286.6	0.180
	7 PPO	120.2	1.060	70.62	91.8	113.4	0.190
C	8 Matrimid	568.6	1.241	273.1	355.0	458.2	0.225
	9 P84	423.6	1.336	194.5	252.9	317.1	0.203
D	10 CA	246.2	1.306	121.0	157.3	188.5	0.166
	11 CTA	288.3	1.292	143.2	186.2	223.1	0.166

Units: M in (g/mole); ρ in (g/cm³); V_w , V_0 and V in (cm³/mole); Fractional free volume (-).

Lee assumed $\ln(S_i)$ to vary only little with respect to $\ln(D_i)$ since the solubility varies less with pressure than the diffusivity. In most polymers, the gas diffusivity covers about six orders of magnitude while the gas solubility varies within two orders of magnitude [52]. Equation (3.3) is then simplified by:

$$\ln(P_i) = \ln(A) - \left(\frac{B}{V_f} \right) \quad (3.4)$$

At a given temperature, $\ln(P_i)$ is proportional to the inverse free volume ($1/V_f$) provided that the solubility does not strongly depend on V_f . Lee found this relation to hold for 13 different polymers for the CO₂ as well as O₂ permeability. However, this linear relation is not unambiguous. Hensema [53] made a similar plot including polyimides and polyoxadiazoles and polytriazoles and found different values for A and B. For some polymers with equal chemical nature but different chain conformation, the diffusivity of O₂ and N₂ increased with decreasing free volume. This phenomenon was attributed to differences in the distribution of the free volume.

In this thesis, the fractional free volume is used, because then the influence of the total volume is compensated and comparison of different polymers is more realistic. An attempt has been made to correlate the fractional free volume to (a) the permeability at the plasticization pressure and (b) the plasticization pressure itself.

In Figure 3.6, the logarithm of the permeability at the plasticization pressure, p_{pl} , has been plotted versus the fractional free volume. Equal symbols refer to polymers from the same group. Figure 3.6 shows that for most polymers a linear relation exists between FFV and the logarithm of the CO_2 permeability at p_{pl} . The permeability increases with increasing free volume, which is in agreement with the findings of Lee [52].

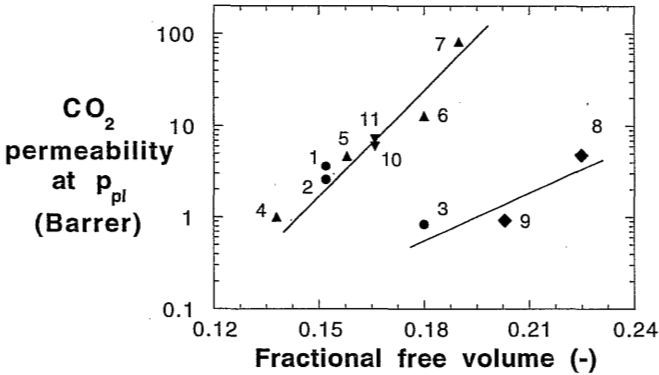


Figure 3.6. CO_2 permeability at the plasticization pressure (p_{pl}) versus FFV of different polymer films. Equal symbols refer to polymers from the same group as classified in Chapter 2. The numbers refer to the different polymers.

The polyimides (8) and (9) do not fit to the general line, but seem to fall on a different line. PEI (3) could be classified in the polyimide group too. This can be justified as they all have the imide group in common.

Carbonyl or sulfone density

Although CO_2 solubility is not the main cause of the increase in permeability at elevated pressures, it indirectly contributes to the increase in diffusivity. A certain number of CO_2 molecules should dissolve to some extent in the polymer matrix to be able to influence chain flexibility. As indicated by several investigators, CO_2 solubility is favoured in the presence of polar groups in the main chain [5,13,14]. Therefore, the carbonyl and/or sulfone density of the polymers listed in Table 3.1 are calculated in the same way as was done by Koros [5]. And because pressure can be related to a concentration in the polymer, the plasticization pressure was plotted versus the carbonyl or sulfone density. The result is given in Figure 3.7.

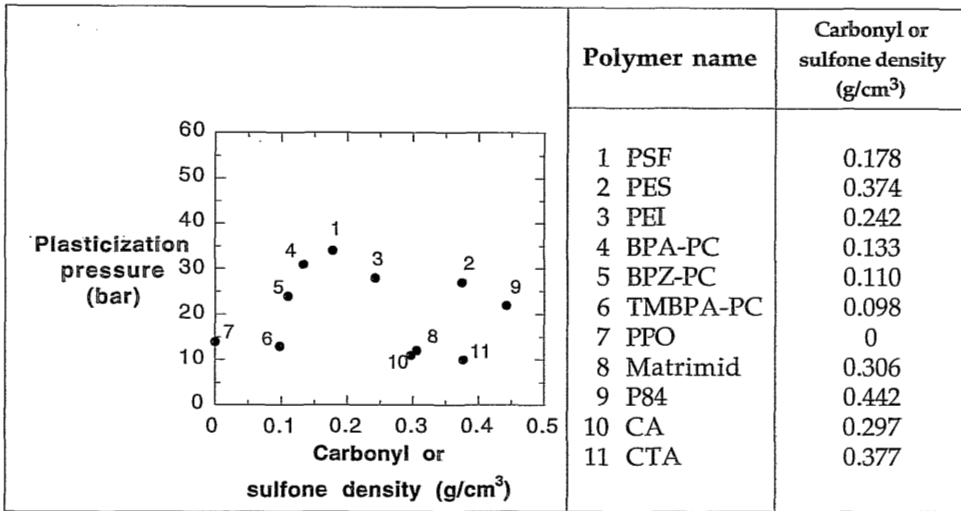


Figure 3.7. Carbonyl or sulfone density versus the plasticization pressure of the different polymers tested.

It is clear from Figure 3.8, that there is no correlation between the carbonyl or sulfone density and the plasticization pressure. P84 has a high carbonyl density but only a moderate plasticization pressure, whereas PPO with no carbonyl or sulfone groups at all plasticizes at a pressure of 14 bar. Apparently, in P84 the carbonyl groups are less accessible for the CO₂ as was pointed out earlier for Kapton. PPO, however, has a polar and flexible ether linkage, which can also contribute to enhanced solubility, but this is not considered here. These results support the findings of Puleo et al. [7] that not only the carbonyl groups are important in explaining plasticization.

Concentration of sorbed gas molecules

To get more insight in the effect of the concentration of sorbed CO₂ on plasticization, the plasticization pressure should be correlated with the concentration of CO₂ sorbed by the polymer at the plasticization pressure. It is hypothesized that each polymer needs the same concentration CO₂ to induce plasticization, but that each polymer requires a different pressure (the plasticization pressure) to reach this concentration. The easiest way to illustrate this, is to take a polymer series from one family. The polycarbonate family considered in this thesis consists of only three polymers, therefore, literature data were used to get a larger number of polymers from one family.

The CO₂ concentration sorbed at the plasticization pressure has been determined for a series of polyimides. The plasticization pressures of the polyimides cover the same range as found in this work. To minimize variations due to film history, care was taken that the combined permeation and sorption data came from the same source. The results are given in Table 3.3 and Figure 3.8.

Table 3.3. Plasticization pressure, concentration at the plasticization pressure and FFV found in the literature for a polyimide series.

Polyimide name	Plasticization pressure (bar)	C at $p=p_l$, 35 °C ($\text{cm}^3(\text{STP})/\text{cm}^3$)	FFV (-)	Ref.
a. 6FDA-6FpDA	15	57	0.190	[54]
b. 6FDA-6FmDA	29	57	0.175	[54]
c. BPDA-6FpDA	14	58	0.161	[54]
d. BTDA-6FpDA	18	45	0.156	[54]
e. 6FDA-DAF	12	55	0.159	[55]
f. BPDA-DDBT	10	47	0.125	[56]

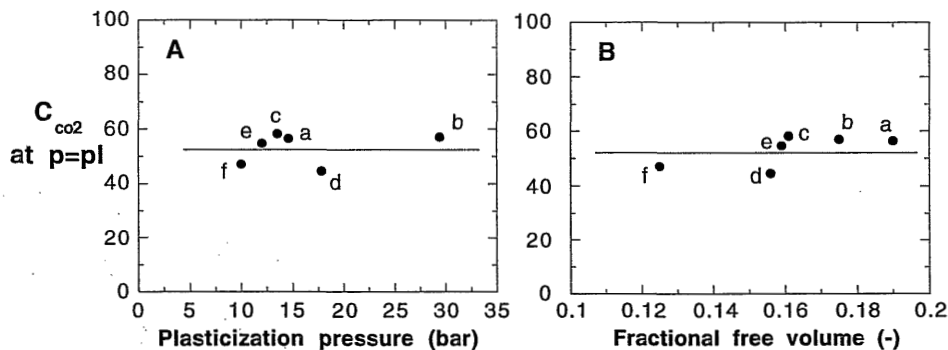
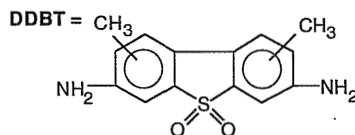
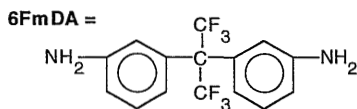
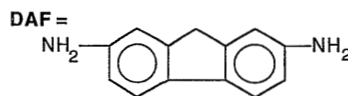
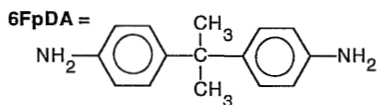


Figure 3.8. CO₂ concentration ($\text{cm}^3(\text{STP})/\text{cm}^3$) at the plasticization pressure for the polyimide series listed in Table 3.3 versus: A. Plasticization pressure and B. Fractional free volume.

The results given in Figure 3.8 support the hypothesis that the polymers require similar CO₂ concentrations before plasticization is induced. At least, this is valid within the polyimide series. The concentration required is $53 \pm 6 \text{ cm}^3(\text{STP})/\text{cm}^3$. Koros and Hellums [57] report similar findings for the concentration required in polycarbonates at which the diffusion coefficients starts to increase due to plasticization. The concentration found in that case was $\sim 35 \text{ cm}^3(\text{STP})/\text{cm}^3$.

Furthermore, there seems to be no correlation of FFV with the concentration of CO₂ in the polymer at $p=p_1$. A high FFV does not contribute necessarily to an increase in plasticization effect. FFV may not be a sufficient measure for the free volume available for CO₂ sorption. The free volume *distribution* may be more important [53,58,59], but is difficult to determine.

It might be possible that each polymer family has its own 'critical' CO₂ concentration to induce plasticization. Therefore, to see whether the hypothesis also holds among polymers from different families similar measurements were done with the polymers listed in Table 3.4. Five polymers were selected which cover the whole range of plasticization pressures found. The polymers used are listed in Table 3.4. As in Figure 3.8, the CO₂ concentration at the plasticization pressure versus plasticization pressure and fractional free volume (FFV) are given in Figure 3.9. Room temperature was 23 or 25 °C.

Table 3.4. Plasticization pressure, CO₂ concentration at the plasticization pressure and FFV for five glassy polymers at room temperature.

Polyimide name	Plasticization pressure (bar)	C at $p=p_1$ (cm ³ (STP)/cm ³)	FFV (-)	Room temp. (°C)
1. PSF	34	47	0.152	23
5. BPZ-PC	24	32	0.138	23
6. TMBA-PC	13	36	0.180	25
8. Matrimid	12	47	0.225	25
9. P84	22	48	0.203	23

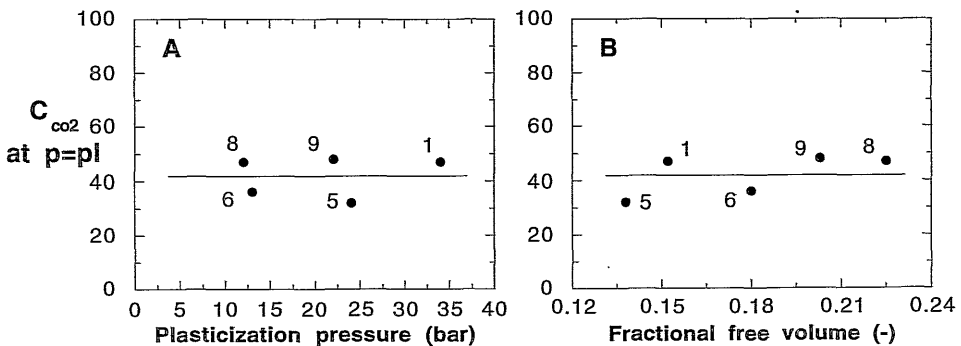


Figure 3.9. CO₂ concentration (cm³(STP)/cm³) at the plasticization pressure for the polymers listed in Table 3.4 versus: A. Plasticization pressure and B. Fractional free volume.

Figure 3.9 shows similar trends as observed for the polyimide series shown in Figure 3.8. No correlation has been found of FFV or plasticization pressure with the concentration of CO₂ at the plasticization pressure either. Furthermore, all polymers appear to require a similar CO₂ concentration to induce plasticization. The average critical CO₂ concentration is $42 \pm 7 \text{ cm}^3(\text{STP})/\text{cm}^3$. The standard deviation of $\pm 7 \text{ cm}^3(\text{STP})/\text{cm}^3$ is comparable to the standard deviation of $\pm 6 \text{ cm}^3(\text{STP})/\text{cm}^3$ found for the polyimides. However, one should be cautious about drawing conclusions from only five polymers. It is still possible that each polymer family has its own critical CO₂ concentration. The polycarbonates (5) and (6) show, for example, a slightly lower critical CO₂ concentration than PSF (1) and the polyimides (8) and (9). But if so, the absolute values of the critical CO₂ concentrations are of the same order of magnitude.

Diffusion

As described in Chapter 1, the diffusion coefficient of CO₂ in a glassy polymer cannot simply be calculated by the ratio of the permeability and solubility. Equation (1.4) is only valid as the diffusion and solubility coefficients are constants. In case of CO₂, both coefficients are concentration dependent. Therefore, to describe the diffusion behaviour of CO₂, an equation should be derived without the simplifying assumption that the diffusion and solubility coefficients are constant.

Since the permeability (P_i) is defined as the flux (J_i) normalized for the pressure difference across the membrane ($p_{2i}-p_{1i}$) and membrane thickness (ℓ), one can write down an equation for the permeability without any assumption by:

$$P_i = \frac{J_i}{(p_{2i}-p_{1i})/\ell} = - \frac{D(C_i) dC_i / dx}{(p_{2i}-p_{1i})/\ell} \quad (3.5)$$

where the flux (J_i) is given by Equation (1.1), p_{2i} and p_{1i} are the pressures at the upstream (feed) and downstream (permeate) side of the membrane, respectively, $D(C_i)$ is a local concentration-dependent diffusion coefficient of a penetrant at any arbitrary point between the feed and permeate side of the membrane and dC_i/dx is the local concentration gradient at the same point in the membrane [57]. Because the steady-state permeability is a constant for fixed upstream and downstream conditions, the product of $D(C_i)$ and dC_i/dx is constant at each point in a membrane. Integration of Equation (3.5) over the membrane thickness ($x=0 \rightarrow x=\ell$) gives:

$$(p_{2i}-p_{1i}) \frac{P_i}{\ell} \int_0^\ell dx = - \int_{C_{2i}}^{C_{1i}} D(C_i) dC_i \quad (3.6)$$

which results in Equation (3.7) for negligible downstream pressure.

$$P_i = \frac{1}{p_{2i}} \int_0^{C_{2i}} D(C_i) dC_i \quad (3.7)$$

Multiplying the numerator and denominator of Equation (3.7) by C_{2i} gives for the permeability (P_i):

$$P_i = \left(\int_0^{C_{2i}} \frac{D(C_i) dC_i}{C_{2i}} \right) \left(\frac{C_{2i}}{P_{2i}} \right) = \bar{D}_i \cdot S_i \quad (3.8)$$

where \bar{D}_i is the *average* diffusion and S_i the solubility coefficient. If the permeability coefficient and average solubility coefficient are determined at the same pressure and temperature an *average* diffusion coefficient can be calculated from the ratio of the permeability and average solubility coefficients.

If complete permeation and sorption isotherms are measured at the same temperature, a local concentration-dependent diffusion coefficient at any arbitrary point between the feed and permeate side can be determined. Differentiation of Equation (3.7) to C_i gives:

$$\frac{dP_i}{dC_i} = \frac{d\left(\frac{1}{P_{2i}}\right)}{dC_{2i}} \int_0^{C_{2i}} D(C_i) dC_i + \frac{1}{P_{2i}} \frac{d}{dC_{2i}} \left(\int_0^{C_{2i}} D(C_i) dC_i \right) \quad (3.9)$$

By applying the chain rule on $\frac{d\left(\frac{1}{P_{2i}}\right)}{dC_{2i}}$ in the first term, differentiation of the integral in the second term and subsequent rearrangement the result in Equation (3.10) is obtained [60].

$$D(C_i) = \left[P(p_{2i}) + P_{2i} \left(\frac{dP_i}{dp_{2i}} \right) \right] \left[\frac{dp_{2i}}{dC_{2i}} \right] \quad (3.10)$$

where $P(p_{2i})$ is the permeability at pressure (p_{2i}), dP_i/dp_{2i} is the slope of the permeation isotherm at pressure p_{2i} and dp_{2i}/dC_{2i} is the reciprocal slope of the sorption isotherm at pressure p_{2i} . Simple polynomial fits of the permeation and sorption isotherms would suffice to evaluate the slopes for use in Equation (3.10). This is a phenomenological approach of describing the phenomenon in question without considering its physical bases [60].

For the polymers listed in Table 3.4, the local concentration-dependent diffusion coefficient is determined at the plasticization pressure by using Equation (3.10). The permeation isotherms were fitted with a second order polynomial ($y=a+bx+cx^2$) and the sorption isotherms with a function similar to the dual-mode sorption equation: $y=ax+bx/(1+cx)$. The results are given in Table 3.5 as well as the permeability, concentration and average solubility at the plasticization pressure. The average solubility at the plasticization pressure is obtained by dividing the concentration at the plasticization pressure by the plasticization pressure ($(C(p=pl)/p_{pl})$).

Table 3.5. *Permeability, concentration, solubility and diffusivity at the plasticization pressure of several polymers.*

Polymer name	P_{pl}	$P(p=pl)$	$C(p=pl)$	$\bar{S}(p=pl)$	$D(C)_{(p=pl)} * 10^{-8}$
1. PSF	34	3.6	47	1.4	2.6
5. BPZ-PC	24	1.0	32	1.3	1.0
6. TMBPA-PC	13	13	36	2.8	5.0
8. Matrimid	12	4.8	47	3.9	1.7
9. P84	22	0.92	48	2.2	0.63

Units: permeability (Barrer), concentration ($\text{cm}^3(\text{STP})/\text{cm}^3$), solubility ($\text{cm}^3(\text{STP})/\text{cm}^3 \text{ bar}$) and diffusivity (cm^2/s)

As was hypothesized, the polymers may require similar concentrations of CO_2 to induce plasticization, but need different pressures to reach this concentration. The reason for this is that the CO_2 solubility in each polymer is different. This is indicated by the average solubility coefficient in Table 3.5. No trend in solubility as a function of the plasticization pressure among the five polymers is found. Within one polymer family, a higher solubility is observed for the polymer with the higher tendency to plasticize. The same is valid for the local diffusion coefficient. There is no trend found in the diffusion coefficient as a function of plasticization pressure for the five polymers considered. But within one family, the diffusion coefficient at the plasticization pressure is higher for the most plasticized polymer.

More interesting is the change in the concentration dependent diffusion coefficient $D(C_i)$ with concentration. To allow comparison among the different polymers, $D(C_i)$ is expressed as the ratio of the local diffusion coefficient $D(C_i)$ (calculated with Equation (3.10)) and the diffusion coefficient at infinite dilution (D_0) as a function of the CO_2 concentration. In Figure 3.10, $D(C_i)/D_0$ is given as a function of the concentration for the five polymers considered above.

All curves show the general trend at low concentration. According to the dual-mode theory, the diffusion coefficient increases with increasing concentration. This increase reflects the saturation of the excess free volume, which levels off at higher concentrations [59]. The relative increase in the local diffusion coefficient after the plateau value is attributed to plasticization. These measurements support the fact that the CO_2 plasticization increases segmental mobility and thereby diffusivity.

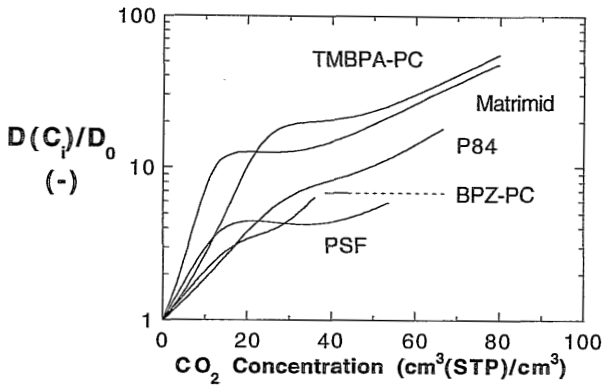


Figure 3.10. The ratio of the local diffusion coefficient ($D(C_i)$) and the diffusion coefficient at zero pressure (D_0) as a function of concentration for the five polymers listed in Table 3.5.

Furthermore, a trend can be observed in magnitude of the ratio $D(C_i)/D_0$ among the five polymers. The ratio of $D(C_i)/D_0$ determined at the concentration corresponding with the plasticization pressure is higher for the polymers having a higher tendency to plasticize. This is illustrated in Figure 3.11, in which the ratio $D(C_i)/D_0$ at the plasticization pressure is plotted versus the plasticization pressure of the different polymers.

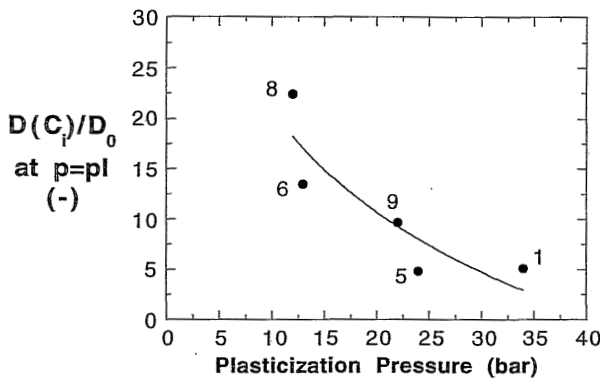


Figure 3.11. The ratio $D(C_i)/D_0$ at the plasticization pressure versus the plasticization pressure of the polymers listed in Table 3.5.

The ratio $D(C_i)/D_0$ decreases with increasing plasticization pressure. Hence, as the tendency to plasticize increases the more the diffusivity changes with increasing concentration. This is exactly what was interpreted from the

correlation found between the plasticization pressure and the ratio $P(p=p_{pl})/P(p=0)$ as shown in Figure 3.5.

3.4. Conclusions

Permeation

Permeability measurements at various CO₂ pressures have been carried out on 11 different glassy polymer films. From the permeability curves, the plasticization pressure (p_{pl}), the corresponding permeability ($P(p=p_{pl})$) and the permeability at zero pressure ($P(p=0)$) have been determined. Additionally, fractional free volume calculations have been done.

- A linear correlation was found between $P(p=p_{pl})/P(p=0)$ and the plasticization pressure of the eleven polymers tested: the higher the plasticization pressure the larger the relative decrease in permeability with increasing pressure. As the changes in solubility are assumed to be similar for all polymers, this implies that the diffusivity changes more strongly with increasing concentration for those polymers showing a larger tendency to plasticize. The latter is supported by the determination of the local concentration-dependent diffusion coefficient as a function of the concentration of five different polymers.
- The logarithm of $P(p=p_{pl})$ correlated with fractional free volume. However, the polyimides did not fit to the same general line.
- The plasticization pressure did not depend on the polar carbonyl or sulfone density of the polymers considered.

Sorption and diffusion

Five different polymers have been selected for sorption experiments. The plasticization pressures of the polymers covered the whole range of plasticization pressures found for the complete series of polymers. Sorption isotherms are measured at the same temperatures as the permeation isotherms. The combined sorption and permeation data allowed calculations of local concentration-dependent diffusion coefficients.

- The CO₂ concentration at the plasticization pressure is constant, independent of the value of the plasticization pressure. We suggest that all polymers need a similar CO₂ concentration to plasticize, but require different pressures to reach it. A critical CO₂ concentration of $42 \pm 7 \text{ cm}^3(\text{STP})/\text{cm}^3$ has been found for our series of polymers studied.
- The local diffusion coefficients showed a clear increase with concentration above the concentration corresponding to the plasticization pressure.
- The relative increase of the local diffusion coefficient was higher for polymers with a higher tendency to plasticize.

3.5. References

- [1] Sanders, E.S., Penetrant-induced plasticization and gas permeation in glassy polymers, *J. Membrane Sci.*, 37 (1988) 63-80
- [2] Chiou, J.S., Paul, D.R., Gas sorption and permeation in poly(ethyl methacrylate), *J. Membrane Sci.*, 45 (1989) 167-189
- [3] Puleo, A.C., Paul, D.R., Kelley, S.S., The effect of degree of acetylation on gas sorption and transport behavior in cellulose acetate, *J. Membrane Sci.*, 47 (1989) 301-332
- [4] Raymond, P.C., Paul, D., Sorption and transport of pure gases in random styrene/methyl methacrylate copolymers, *J. Polym. Sci., Polym. Phys. Ed.*, 28 (1990) 2079-2102
- [5] Koros, W.J., Simplified analysis of gas/polymer selective solubility behavior, *J. Polym. Sci., Polym. Phys. Ed.*, 23 (1985) 1611-1628
- [6] Raymond, P.C., Paul, D.R., Kinetics of CO₂ conditioning of copolymers and blends containing MMA units, *J. Polym. Sci., Polym. Phys. Ed.*, 28 (1990) 2213-2223
- [7] Puleo, A.C., Muruganandam, N., Paul, D.R., Gas sorption and transport in substituted polystyrenes, *J. Polym. Sci., Polym. Phys. Ed.*, 27 (1989) 2385-2406
- [8] Chiou, J.S., Barlow, J.W., Paul, D.R., Plasticization of glassy polymers by CO₂, *J. Appl. Polym. Sci.*, 30 (1985) 2633-2642
- [9] Kamide, K., Okajima, K., Saito, M., Nuclear magnetic resonance study of thermodynamic interaction between cellulose acetate and solvent, *Polymer J.*, 13 (1981) 115-125
- [10] Kamiya, Y., Mizoguchi, K., Hirose, T., Naito, Y., Sorption and dilation in poly(ethyl methacrylate)-carbon dioxide system, *J. Polym. Sci., Polym. Phys. Ed.*, 27 (1989) 879-892
- [11] Vieth, W.R., Dao, L.H., Pederson, H., Non-equilibrium microstructural and transport characteristics of glassy poly(ethylene terephthalate), *J. Membrane Sci.*, 60 (1991) 41-62
- [12] Fleming, G.K., Koros, W.J., Dilation of polymers by sorption of carbon dioxide at elevated pressures. I. Silicone rubber and unconditioned polycarbonate, *Macromolecules*, 19 (1986) 2285-2291
- [13] Pilato, L.A., Litz, L.M., Hargitay, B., Osborne, R.C., Farnham, A.G., Kawakami, J.H., Fritze, P.E., McGrath, J.E., Polymers for permselective membrane gas separations, *Polym. Prepr. Am. Chem. Soc. Div. Polym. Chem.*, 16 (1975) 41-46
- [14] Ghosal, K., Chern, R.T., Freeman, B.D., Savariar, R., The effect of aryl nitration on gas sorption and permeation in polysulfone, *J. Polym. Sci., Polym. Phys. Ed.*, 33 (1995) 657-666
- [15] Story, B.J., Koros, W.J., Sorption and transport of CO₂ and CH₄ in chemically modified poly(phenylene oxide), *J. Membrane Sci.*, 67 (1992) 191-210
- [16] Sefcik, M.D., Schaefer, J., Solid-state ¹³C NMR evidence for gas-polymer interactions in the carbon dioxide-poly(vinyl chloride) system, *J. Polym. Sci., Polym. Phys. Ed.*, 21 (1983) 1055-1062
- [17] Fried, J.R., Li, W., High-pressure FTIR studies of gas-polymer interactions, *J. Appl. Polym. Sci.*, 41 (1990) 1123-1131
- [18] Wessling, M., Schoeman, S., van den Boomgaard, Th., Smolders, C.A., Plasticization of gas separation membranes, *Gas Sep. Purif.*, 5 (1991) 222-228
- [19] Mizoguchi, K., Hirose, T., Naito, Y., Kamiya, Y., CO₂-induced crystallization of poly(ethylene terephthalate), *Polymer*, 28 (1987) 1298-1302
- [20] Chiou, J.S., Barlow, J.W., Paul, D.R., Polymer crystallization induced by sorption of CO₂ gas, *J. Appl. Polym. Sci.*, 30 (1985) 3911-3924
- [21] Handa, Y.P., Capowski, S., O'Neill, M., Compressed-gas-induced plasticization of polymers, *Thermochimica Acta*, 226 (1993) 177-185
- [22] Wissinger, R.G., Paulaitis, M.E., Glass transitions in polymer/CO₂ mixtures at elevated pressures, *J. Polym. Sci., Polym. Phys. Ed.*, 29 (1991) 631-633
- [23] Handa, Y. P., Lampron, S., O'Neill, M.L., On the plasticization of poly(2,6-dimethyl

- phenylene oxide) by CO₂, *J. Polym. Sci., Polym. Phys. Ed.*, 32 (1994) 2549-2553
- [24] Wang, W.-C., Kramer, E.J., Sachse, W.G., Effects of high-pressure CO₂ on the glass transition temperature and mechanical properties of polystyrene, *J. Polym. Sci., Polym. Phys. Ed.*, 20 (1982) 1371-1384
- [25] Fried, J.R., Liu, H.-C., Zhang, C., Effect of sorbed carbon dioxide on the dynamic mechanical properties of glassy polymers, *J. Polym. Sci., Part C: Polym. Lett.*, 27 (1989) 385-392
- [26] Chow, T.S., Molecular interpretation of the glass transition temperature of polymer-diluent systems, *Macromolecules*, 13 (1980) 362-364
- [27] Wessling, M., Borneman, Z., van den Boomgaard, Th., Smolders, C.A., Carbon dioxide foaming of glassy polymers, *J. Appl. Polym. Sci.*, 53 (1994) 1497-1512
- [28] Chiou, J.S., Maeda, Y., Paul, D.R., Gas and vapor sorption in polymers just below T_g, *J. Appl. Polym. Sci.*, 30 (1985) 4019-4029
- [29] Kamiya, Y., Mizoguchi, K., Naito, Y., Hirose, T., Gas sorption in poly(vinyl benzoate), *J. Polym. Sci., Polym. Phys. Ed.*, 24 (1986) 535-547
- [30] Kamiya, Y., Hirose, T., Naito, Y., Mizoguchi, K., Sorptive dilation of polysulfone and poly(ethylene terephthalate) films by high-pressure carbon dioxide, *J. Polym. Sci., Polym. Phys. Ed.*, 26 (1988) 159-177
- [31] Sperling, L.H., Introduction to physical polymer science, second edition, John Wiley & Sons, New York, (1992)
- [32] Kamps, K.M.P., Teunis, H.A., Wessling, M., Smolders, C.A., Gas transport and sub-T_g relaxations in unmodified and nitrated polyarylethersulfones, *J. Membrane Sci.*, 74 (1992) 193-201
- [33] Light, R.R., Seymour, R.W., Effect of sub-T_g relaxations on the gas transport properties of polyesters, *Polym. Eng. Sci.*, 22 (1982) 857-864
- [34] Wessling, M., Huisman, I., v.d. Boomgaard, Th., Smolders, C.A., Dilation Kinetics of glassy, aromatic polyimides induced by carbon dioxide sorption, *J. Polym. Sci., Polym. Phys. Ed.*, 33 (1995) 1371-1384
- [35] Assink, R.A., Plasticization of poly(dimethyl siloxane) by high-pressure gases as studied by NMR relaxation, *J. Polym. Sci., Polym. Phys. Ed.*, 12 (1974) 2281-2290
- [36] Mizoguchi, K., Terada, K., Hirose, T., Kamiya, Y., Crystallization of poly(ethylene terephthalate) under high-pressure gases, *Polymer Comm.*, 31 (1990) 146-148
- [37] Kamiya, Y., Mizoguchi, K., Naito, Y., A dielectric relaxation study of plasticization of polyethylmethacrylate by carbon dioxide, *J. Polym. Sci., Polym. Phys. Ed.*, 28 (1990) 1955-1964
- [38] Kamiya, Y., Mizoguchi, K., Naito, Y., Plasticization of poly(ethyl methacrylate) by dissolved argon, *J. Polym. Sci., Polym. Phys. Ed.*, 30 (1992) 1183
- [39] Wessling, M., Relaxation phenomena in dense gas separation membranes, Ph-D Thesis, University of Twente, The Netherlands, (1993)
- [40] Jordan, S.M., Henson, M.A., Koros, W.J., The effects of carbon dioxide conditioning on the permeation behavior of hollow fiber asymmetric membranes, *J. Membrane Sci.*, 54 (1990) 103-118
- [41] Pfromm, P.H., Pinnau, I., Koros, W.J., Gas transport through integral-asymmetric membranes: a comparison to isotropic film transport properties, *J. Appl. Polym. Sci.*, 48 (1993) 2161-2171
- [42] White, L.S., Blinka, T.A., Kloczewski, H.A., Wang, I-F., Properties of a polyimide gas separation membrane in natural gas streams, *J. Membrane Sci.*, 103 (1995) 73-82
- [43] Koros, W.J., Pinnau, I., Membrane formation for gas separation processes, in: *Polymeric gas separation membranes*, Paul, D.R., Yampol'skii, Y.P., (Eds.), CRC Press, (1994) 209-271
- [44] Ebert, K., Thin film composite membranes of glassy polymers for gas separation, Ph-D Thesis, University of Twente, The Netherlands, (1995)

- [45] Bondi, A., Physical properties of molecular crystals, liquids, and glasses, John Wiley & Sons, Inc., New York, (1968)
- [46] Van Krevelen, D.W., Group contribution techniques for correlating polymer properties and chemical structure, in: Computational Modeling of Polymers, Bicerano, J., (Ed.), Marcel Dekker, Inc., New York, (1992)
- [47] Slonimskii, G.L., Askadskii, A.A., Kitaigorodski, A.I., Vysokomolekularnie Soyedinia, 12 (1970) 494
- [48] Askadskii, A.A., Prediction of physical properties of polymers, in: Polymer Yearbook 4, R.A., Pethrick, Zaikov, G.E., Harwood Academic Publishers, London, (1987)
- [49] Askadskii, A.A., Influence of chemical structure on the properties of polymers, Pure & Appl. Chem., 46 (1976) 19-27
- [50] Van Krevelen, D.W., Hoftyzer, P.J., Properties of polymers - their estimation and correlation with chemical structure, Elsevier, Amsterdam, (1976)
- [51] Van Krevelen, D.W., Properties of polymers - their correlation with chemical structure; their numerical estimation and prediction from additive group contributions, Elsevier, Amsterdam, (1990)
- [52] Lee, W.M., Selection of barrier materials from molecular structure, Polym. Eng. Sci., 20 (1980) 65-69
- [53] Hensema, E.R., Polyoxadiazole and polytriazole gas separation membranes. Synthesis and properties, Ph-D Thesis, University of Twente, The Netherlands, (1991)
- [54] Coleman, M.R., Isomers of fluorine-containing polyimides for gas separation membranes, Ph-D Thesis, University of Texas, Austin, USA, (1988)
- [55] Kim, T.-H., Gas sorption and permeation in a series of aromatic polyimides, Ph-D Thesis, University of Texas, Austin, USA, (1988)
- [56] Okamoto, K.-i, Tanaka, K., Shigematsu, T., Kita, H., Nakamura, A., Kusuki, A., Sorption and transport of carbon dioxide in a polyimide from 3,3',4,4'-biphenyltetracarboxylic dianhydride and dimethyl-3,7-diaminodibenzothiophene-5,5'-dioxide, Polymer, 31 (1990) 673-678
- [57] Koros, W.J., Chern, R.T., Separation of gaseous mixtures using polymer membranes, in: Handbook of separation process technology, Rousseau, R.W., (Ed.), John Wiley & Sons, New York, (1987) 862-953
- [58] Koros, W.J., Walker, D.R.B., Gas separation membrane material selection criteria: weakly and strongly interacting feed component situations, Polymer J., 23 (1991) 481-490
- [59] Jean, Y.C., Yuan, J.-P., Liu, J., Deng, Q., Yang, H., Correlations between gas permeation and free-volume hole properties probed by positron annihilation spectroscopy, J. Polym. Sci., Polym. Phys. Ed., 33 (1995) 2365-2371
- [60] Koros, W.J., Hellums, M.W., Gas separation membrane material selection criteria: differences for weakly and strongly interacting feed components, Fluid Phase Eq., 53 (1989) 339-354

4

Suppression of CO₂ plasticization

Part 1: Crosslinking by thermal treatment

4.1. Introduction

In this thesis, the increase in permeability of a gas with increasing feed gas pressure is attributed to CO₂ induced plasticization of the polymer matrix. A high CO₂ concentration in the polymer film disrupts the chain packing which leads to a larger free volume and an enhanced segmental mobility. The increased permeability is therefore mainly determined by an increase in diffusivity. However, it is still difficult to obtain a detailed picture of the plasticization mechanism.

Since the CO₂-induced plasticization generally leads to a loss in selectivity of a membrane, plasticization should be minimized. CO₂ induced plasticization effects can be suppressed by various means. A method is defined as successful, if the permeability as a function of pressure does not increase anymore. It is also possible that the permeability-pressure curves still show a minimum, but at higher feed pressures. In that case, the film performance is only improved.

Hence, suppressing CO₂-induced plasticization in the sense that the permeability does not increase with pressure implies a suppression of the chain flexibility. From Chapter 3, it became clear that not all polymers show the same tendency to plasticize at pressures of up to 60 bar. However, just switching to a different polymer for a particular separation problem is not always a solution. Polymers with a low tendency to plasticize may not show the desired productivity combined with a sufficient selectivity or they may not be easily processed. It may as well be an option to modify the polymer of interest in such a way that it maintains its separating properties at a certain level, but does not plasticize. Two possibilities to suppress the flexibility of the polymer chains are:

- crosslinking of the polymer matrix,
- blending a polymer that is highly susceptible to plasticization with a polymer that does not plasticize.

This chapter presents the results obtained with crosslinking and the next chapter deals with blending of polymers.

4.2. Background on crosslinking methods

In this study polyimides are considered because of their good gas separation properties. Many possible crosslinking mechanisms of polyimides are described in the literature [1-3]. For example, crosslinking is possible with terminal amine groups or via the interaction of two neighbouring imide rings. Incompletely imidized polyimides are also highly susceptible to crosslinking. The carboxyl groups (-COOH) of the polyamic acid of different chains can react to form an imide group that simultaneously results in a crosslink. Angelo [4] modified the polyimide structure by introducing a carboxyl group in the main chain to create crosslinking possibilities. Furthermore, functional endgroups, in particular with double bonds, can form crosslinks at elevated temperatures [3]. An example of the crosslinking of an acetylene-encapped oligomeric polyimide will be given in Chapter 5. This subject is treated separately in the next chapter because the reaction is carried out in the presence of a second polymer, which in fact is a variation on blending.

UV irradiation is found to be effective in crosslinking too [5-9]. The main reason for the use of UV-treatments of films is to improve their gas separation performance. The result is usually an increase in selectivity after irradiation, but always at the expense of permeability. In particular BTDA-based polyimides are very photosensitive [10-13]. Pfeifer and Rohde [10] discovered that a BTDA-based polyimide with an ortho-alkyl-substituted diamine can be photocrosslinked at irradiation of light with a wavelength of 365 nm. However, the exact photochemical reaction mechanism was unknown. It was Lin et al. [12], who elucidated the mechanism of this photocrosslinking reaction, which is schematically given in Figure 4.1.

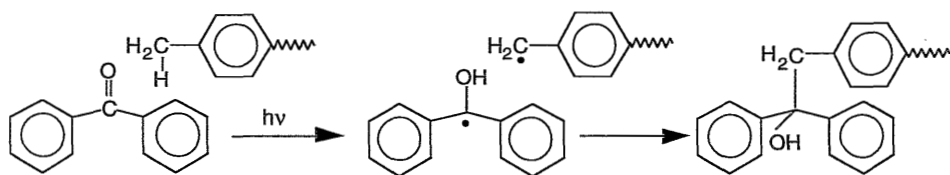


Figure 4.1. Mechanism of photocrosslinking of BTDA-based polyimides.

The benzophenone carbonyl group is excited by irradiation of light and will abstract a hydrogen from an alkyl group in a different polymer chain. The radicals so formed will couple into a new bond.

P84 is an excellent candidate to test this crosslinking mechanism. It is a BTDA-based copolyimide which contains the required ortho-alkyl substituted diamine. (see Table 2.1 in Chapter 2 for the chemical structure). Therefore, a film was irradiated under two normal UV-A lamps with a wavelength of 350-390 nm for

49 hours. The film was found to be crosslinked, as it did not dissolve in the original casting solvent anymore. However, the method was not effective enough to suppress CO_2 plasticization. The permeability as a function of pressure of the crosslinked P84 film is compared with an untreated one in Figure 4.2.

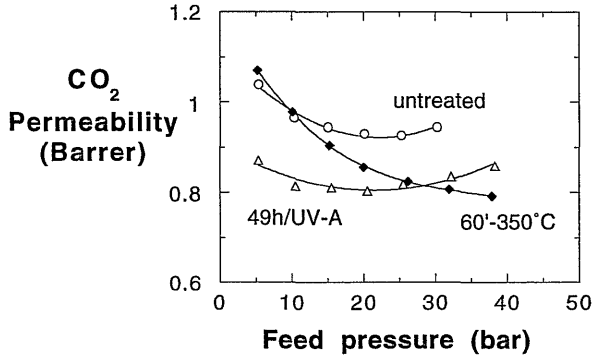


Figure 4.2. CO_2 permeation isotherms of an untreated, UV-A treated and a heat treated P84 film at 23, 23 and 22 °C, respectively.

The permeation curve still shows a minimum at 22 bar. The permeability of the treated film is lower compared to the untreated one, because crosslinking may lead to a densification of the polymer matrix. Similar results were obtained in UV-irradiation of PSF and PES at a wavelength of 254 nm. PSF and PES are crosslinked via a photodegradation reaction [10]. An explanation for the somewhat disappointing effects on the suppression of plasticization may be attributed to the low power of the light source, which was only 30 W. In the literature, mercury lamps of 450 W with the required wavelength are reported [5,7]. It is plausible that the crosslinking degree is too low to significantly change the plasticizing ability.

From P84 it is also known that it can be crosslinked by heating at a temperature of 350-380 °C [15,16]. The effect of a heat-treatment at 350 °C on the CO_2 permeability is also given in Figure 4.2. This method is more effective than the UV-irradiation. The permeability decreases with increasing pressure and does not show a minimum in the pressure range considered. However, it is not certain whether the permeability will increase again above 40 bar or not.

For research purposes, to allow better comparison of the effect of crosslinking on suppression of plasticization, a polymer with a high tendency to plasticize is preferred. As described in Chapter 1, Matrimid is therefore selected as a model polymer. Matrimid is also a BTDA-based polyimide with alkyl substituents in the diamine structure, but it did not crosslink by UV-irradiation. Several explanations for this result are possible. The power of the light source could be too low, but it is also possible that the methyl groups in Matrimid are insufficient

H-donors or that the alkyl groups are sterically hindered to be in close distance of the carbonyl group. As it was demonstrated with P84, a heat-treatment at 350 °C is expected to have more effect on the permeability. It is known that many polymers can be crosslinked in the solid state at such high temperatures [15-17]. The temperature is often well above the glass transition temperature and crosslinking is possible via a degradation mechanism [15,17]. This crosslinking method will therefore be applied to Matrimid. The disadvantage of this method is, that the exact crosslinking mechanisms are not known. Most reaction schemes are based on speculations, which are only partly elucidated. The crosslinking degree is often very low, but high enough to make the polymer insoluble. Unfortunately, this makes many analytical methods unsuitable for characterization of crosslinked films.

4.3. Film preparation

The typical procedure of preparing homogeneous dense films was described in Chapter 2. The crosslinking protocol described below starts after the nitrogen drying step in the procedure.

The crosslinked Matrimid films were prepared by treating the already dried film in a hot-air oven (Heraeus, K750/1) at 350 °C. The heat-treatment of 15, 30 or 45 minutes was carried out while the film still stuck to the glass plate. Since the ventilation system blew air in the oven chamber, the treatment was carried out in the presence of oxygen. After the treatment, the films were slowly cooled to room temperature. The cooled films were taken from the glass plate with a small amount of water and treated in a vacuum oven (Heraeus, RVT 220/180) at 150 °C for at least four days. Small pieces of the treated films were immersed in the original casting solvent to verify crosslinking. All treated films did not dissolve anymore, even at elevated temperatures of 100 °C, and were therefore indicated as being crosslinked.

The density and glass transition temperature of the untreated as well as the heat-treated films are determined as described in Chapter 2. Furthermore, the prepared films are characterized by single and mixed gas permeation and sorption experiments, described in Chapter 2 as well.

4.4. Characterization of the treated Matrimid films

Matrimid® 5218 composes of 3,3',4,4'-benzophenone tetracarboxylic dianhydride (BTDA) and diaminophenylindane (DAPI). To facilitate reading, the monomer unit is given again in Figure 4.3.

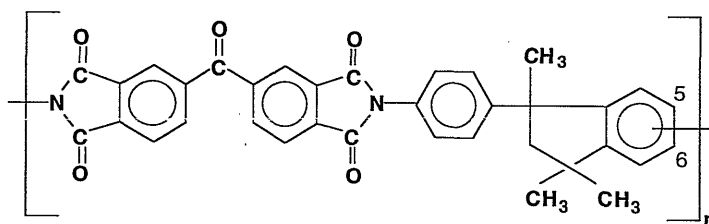


Figure 4.3. Chemical structure of the Matrimid[®] 5218 monomer unit.

The 15, 30 as well as 45 minutes heat-treated films were crosslinked as indicated by the solubility test. Neither of the films dissolved in the original casting solvent. A further swelling test was carried out in DMAc at 100 °C, but the films still did not dissolve. However, one should be careful by addressing the insolubility of the polymer film after treatment to crosslinking alone. The insolubility can also result from crystallinity in the film [3]. This was tested by DSC experiments. If crystallization takes place, one should see a melting peak in the DSC-curve. This was not the case for the treated Matrimid films. Additional evidence that no crystallization takes place is found in infrared measurements, which will be described in Chapter 6. Crystallization can therefore be dismissed.

The polymer is purchased as fully imidized, but it is possible that still a certain amount of polyamic acid is present in the material. The free carboxyl groups are then possible crosslinking sites. This is only one suggestion on a possible crosslinking mechanism. It was not possible to elucidate the exact crosslinking mechanism of Matrimid.

According to the information of Ciba-Geigy, crosslinking by a degradation reaction is most plausible because Matrimid degrades at 350 °C or higher. At temperatures above the glass transition both radical and chemical crosslinking can take place. Falcigno et al. [18] determined the insolubilization temperature of polyimides containing DAPI. Their results showed that Matrimid was insoluble in NMP after 1 hour treatment in a nitrogen atmosphere at 350 °C.

The films used in this thesis were treated in air. This means that oxygen may also contribute to the crosslinking reaction. It was suggested that oxygen would oxidize a methyl group of the indane group. To check this, the polyimide BTDA-PDA was treated under the same conditions. The chemical structure of this polyimide is very similar to Matrimid, except for the indane group (compare Figure 1.1 of Chapter 1 with Figure 4.3). However, BTDA-PDA appeared to be crosslinked too. Hence, the indane group does not necessarily contribute to the crosslinking reaction. Thermal oxidative degradation of the indane group has also been rejected by Bateman [19]. For such a reaction, the cycloaliphatic indane group should have benzylic hydrogens susceptible to oxidation. There are no two adjacent carbons bearing hydrogen, which excludes the oxidative degradation pathway.

In case of the heat-treatment of P84 at 350 °C, Yanagishita et al. [16] assumed that the crosslinking occurs in the way as in the reaction by UV irradiation. However, Rohde et al. [11] note that polyimides with structures such as P84 possess a photo-crosslinking as well as a thermal crosslinking mechanism. Both treatments must therefore be considered separately.

Notable changes in the treated films compared to an untreated one are changes in colour, density and glass transition temperature. The differences are presented in Table 4.1.

Table 4.1. *Changes in maximum in wavelength of light absorption (colour), density and glass transition temperature of the differently treated Matrimid films.*

Matrimid film	λ (UV) (nm)	ρ (g/cm ³)	T_g (°C)
untreated	391	1.23	313
15' 350 °C	394	1.25	319
30' 350 °C	406	1.28	323
45' 350 °C	412	1.29	339

The colour of an untreated Matrimid film is lightly yellow. The heat-treated films still have a yellow colour, but are darker. The longer the treatment the darker the film will be. After 45 minutes heat-treatment, the colour changed to lightly brown. The change in colour could be detected by UV-spectroscopy. The maximum in the wavelength representing light absorption increased with increasing heating time as given in Table 4.1.

The yellow colour is characteristic for most polyimides and is attributed to charge-transfer complexes [3,20]. In general, charge transfer complexes are formed by electron transfer between an electron rich-donor molecule and an electron-deficient acceptor molecule [20-22]. Since many aromatic polyimides have a highly conjugated chemical structure, alternating segments of electron-donating and electron accepting character result from delocalization of electrons. Charge transfer complexes (CTC's) are often formed between benzene rings (either in the dianhydride or diamine) and the five-membered imide rings provided that the rings are able to approach each other closely enough to allow transfer of π -electrons [20-23].

The density of the treated Matrimid films are higher compared to the untreated film and increased with heating time. This indicates a better packing of the polymer chains and a decrease in free volume. Furthermore, the glass transition temperature also increases with heating time. This can be interpreted as a reduction of the segmental mobility.

Summarizing, it is possible that a combination of crosslinking and the CTC formation is responsible for the changes in the Matrimid films. The crosslinking might be the reason for the insolubility of Matrimid after the heat-treatment. A few crosslinks in a polymer with a high molecular weight is often enough to make it insoluble. If the crosslinking degree is really low, the CTC's may be the main reason for the densification. Additionally, the CTC's may work as physical crosslinks, since they are strong enough, and therefore may prevent swelling of the polymer matrix.

4.5. CO₂ and CO₂/CH₄ permeation behaviour

Single gas permeation

The CO₂ permeation behaviour of a 15 and 30 minutes heat-treated Matrimid film is compared with an untreated film. The results are shown in Figure 4.4.

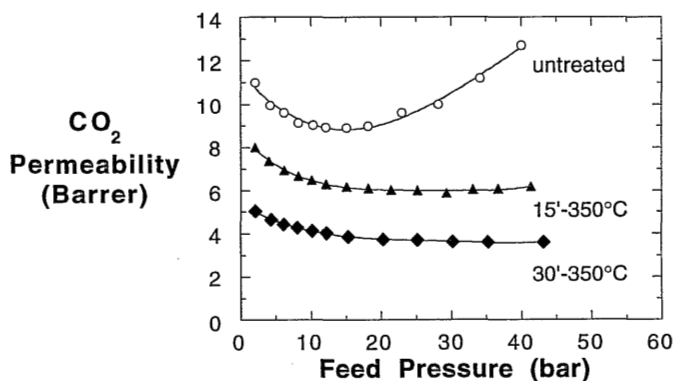


Figure 4.4. Permeability-pressure curves of an untreated and two heat-treated Matrimid films at 35 °C.

The untreated film shows a minimum at 15 bar in its permeability-versus-pressure curve. The permeability first decreases with increasing pressure and then increases with further increase of carbon dioxide pressure. The decrease in permeability at low pressures stems from a decreasing solubility with increasing pressure. The increase of permeability with increasing pressure is due to plasticization. A high CO₂ concentration in the polymer film disrupts chain packing. The free volume of the polymer matrix increases, which results in an increased segmental mobility. The crosslinked films do not show a minimum, but level off above 15 bar. The increase in segmental mobility is reduced, as indicated by the initially higher glass transition temperature. The permeability approaches a limiting value at high feed pressures. This result indicates therefore that the crosslinking method is successful in suppressing the CO₂-induced

plasticization. A disadvantage is that the permeabilities of the treated films are lower than the untreated one. A longer treatment time leads to decreasing permeability values. An explanation for this effect is the densification of the polymer matrix after crosslinking.

Another phenomenon attributed to the carbon dioxide plasticization is the time-dependent permeability at feed pressures above the plasticization pressure [24]. This behaviour is shown in Figure 4.5.

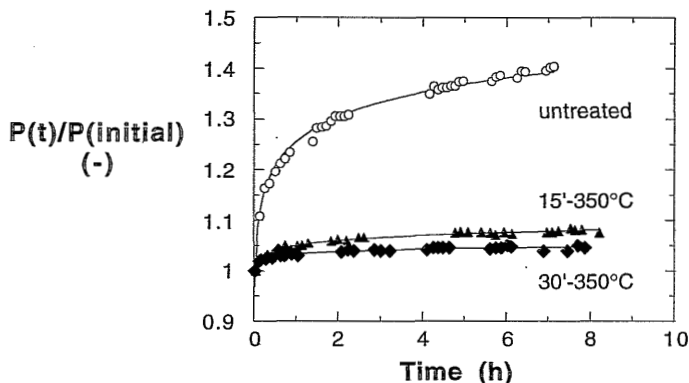


Figure 4.5. Time-dependent permeability of an untreated and two heat-treated Matrimid films at 30 bar CO_2 and 35 °C.

The CO_2 permeability is measured at 30 bar as a function of time for the untreated and the two heat-treated films. The 30 bar CO_2 pressure is applied directly on the film after vacuum evacuation of the test cells without intermediate pressure steps. All permeabilities are divided by their initial permeability (at $t \approx 1$ minute) to make comparison possible. The time-lag, representing the built-up of the concentration profile, of these experiments was about 30 seconds or less. Hence, the increase in permeability can be completely attributed to conditioning by sorbed CO_2 .

As it was indicated in Chapter 1, the CO_2 permeability of the untreated film does not reach a steady-state value within the given experimentation time. The total increase is more than 40% after 8 hours. The treated films on the other hand do reach a steady-state value. The film treated for 15 minutes reaches a permeability which is 8% higher than the initial permeability and the film treated for 30 minutes levels off at a 5% higher permeability. The fact that the treated films reach a steady-state value indicates again that the crosslinking method is effective in suppressing the CO_2 -induced plasticization. Furthermore, the conditioning effect of CO_2 in the treated films is lower compared to the untreated one, because the increase in permeability is less pronounced: 5 or 8% compared to 40% of the untreated film.

Mixed gas permeation

The mixed gas permeation experiments were carried out with a 55/45 mol % CO_2/CH_4 mixture. Over the pressure range considered, the partial CO_2 pressure is high enough to plasticize the untreated Matrimid film. Figure 4.6 shows the selectivity as a function of the total feed pressure for the untreated and the two heat-treated films.

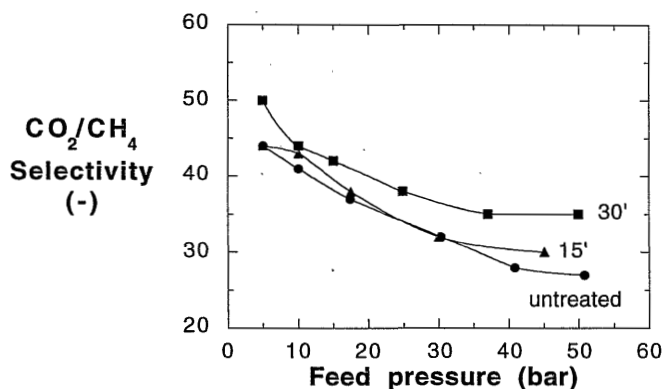


Figure 4.6. Selectivity as a function of total feed pressure of a 55/45 mol % CO_2/CH_4 mixture for an untreated film and two heat-treated films (15 and 30 minutes at 350 °C).

A clear trend in absolute values of the selectivities can be found among the differently treated films. At elevated pressures, the 15 and 30 minutes heat-treated films show up to 11 and 30% higher values, respectively, compared to the untreated film. This can be explained from the densification of the polymer matrix after crosslinking. The permeability of CH_4 decreases more than the CO_2 permeability, which results overall in an improved CO_2/CH_4 selectivity of a treated film.

Furthermore, the selectivity decreases with increasing feed pressure for the untreated as well as the treated films. In the past this was interpreted as a result stemming from CO_2 -plasticization [25,26]. The decreasing selectivity of the treated films suggest therefore no stabilization which is in contradiction to the single gas permeation experiments. However, for glassy polymers the decrease in selectivity stems from a decrease in permeability due to a decreasing solubility coefficient with increasing pressure. And because the CO_2 permeability decreases more pronounced with increasing pressure than the CH_4 permeability, the selectivity will decrease. In case of plasticization, it is hypothesized that the opposite occurs, however, only few literature data are available to support this. The polymer matrix swells by the highly sorbed carbon dioxide, which results in an increase in CO_2 permeability. Simultaneously, the methane permeability increases and as it increases more than the CO_2 permeability, the selectivity

decreases. Since these two counteracting effects are subtle, the two contributions to the decrease in selectivity cannot be distinguished in Figure 4.6. Therefore, an analysis of the (partial) permeabilities is necessary.

The results of the permeability analysis are given in Figure 4.7A, B and C. Figure 4.7A shows the total permeability of both gases. The partial CO₂ and CH₄ permeabilities, in Figure 4.7B and Figure 4.7C, respectively, are calculated from the total permeabilities as is given by Equation (2.6).

In Figure 4.7A, the permeation isotherm of the untreated film shows the increase in permeability typical for plasticization, whereas the permeation curves for the treated films do not show such an increase in permeability. In Figure 4.7B the permeation isotherm for pure CO₂ and an untreated Matrimid film is added for comparison. The partial CO₂ permeation behaviour in the mixture corresponds with the permeation behaviour of a single gas. Both permeation curves show the typical increase in permeability above 15 bar partial CO₂ pressure. The CO₂ permeability in the mixture is slightly lower compared to the pure CO₂ permeability, because the presence of CH₄ reduces the permeability of CO₂. This is also predicted by the dual-mode sorption theory. The permeability of a penetrant A in a binary mixture of gases A and B can be given by [27]:

$$P_A = k_{DA}D_{DA} \left(1 + \frac{F_A K_A}{1 + b_{AP_A} + b_{BP_B}} \right) \quad (4.2)$$

where $F_A = D_{HA}/D_{DA}$ and $K_A = C'_{HA} b_A / k_{DA} \cdot p_A$ and p_B are the partial pressures of gas A and B, respectively. C'_{HA} is the Langmuir affinity constant, b_A the Langmuir sorption capacity and k_{DA} the Henry's law constant of gas A. b_B is the Langmuir sorption capacity of gas B. D_{HA} and D_{DA} are the mobility of gas A in the Langmuir and the Henry mode, respectively. The permeability of gas A will be smaller in presence of gas B, because the denominator of the second term is larger compared to the single gas case. In fact Equation (4.2) is an extension of Equation (1.9) accounting for competition for sorption sites.

The permeation isotherms of the treated films do not show a minimum in permeability as a function of the partial CO₂ pressure. Because single and mixed gas permeation behaviour in the untreated films are very similar, it is expected that the permeability of the treated films will level off with further increase in pressure as it is measured in pure gas permeation experiments. This is also supported by Equation (4.2). The permeability P_A will approach the limiting value $k_{DA}D_{DA}$ as $p_A \cdot p_B \rightarrow \infty$. Hence, this result again is a clear indication of the successful suppression of plasticization.

An even superior evidence for the suppression of CO₂-induced plasticization is found in comparing the CH₄ permeability of the untreated and treated films. Figure 4.7C shows the partial CH₄ permeabilities. The untreated film shows a significant increase in the CH₄ permeability at higher partial CH₄ pressure which is due to CO₂ plasticization. A similar increase in CH₄ permeability is observed by

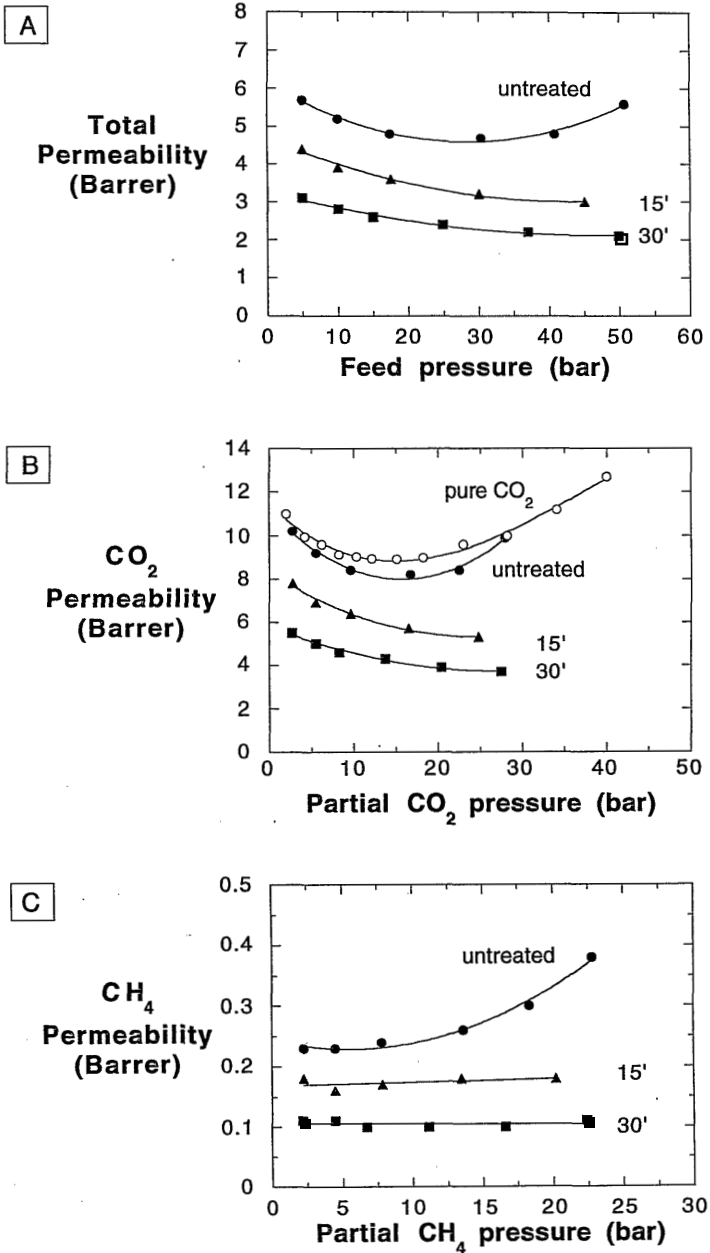


Figure 4.7. Permeability-pressure curves obtained with a 55/45 mol % CO₂/CH₄ mixture at 35 °C for an untreated and two heat-treated Matrimid films.

Coleman [28] for a 6FDA-based polyimide and by Sada et al. [29] for cellulose acetate. As reported by Li et al. [30], this is also the case in for CO_2/N_2 mixtures. Due to CO_2 plasticization, the N_2 permeability is increased. The CO_2 has loosened up the polymer matrix in such a way that relative CH_4 permeation increases more than the relative CO_2 permeation. On the other hand, the treated films show a constant CH_4 permeability. This truly supports the effectiveness of the applied crosslinking method to suppress plasticization.

Summarizing, crosslinking a Matrimid film by a heat-treatment at $350\text{ }^\circ\text{C}$ is a successful method to suppress CO_2 -induced plasticization. In a mixture both the CO_2 and the CH_4 permeabilities are constant at elevated feed pressures. It is therefore plausible to state that the crosslinked films will also show a constant selectivity at further increased pressure.

4.6. CO_2 sorption and diffusion behaviour

To obtain a better understanding of the CO_2 permeation behaviour as a function of pressure, the sorption and diffusion behaviour of CO_2 has been studied for an untreated and two heat-treated films. Sorption experiments are carried out as described in Chapter 2. To minimize differences due to film history, samples are taken from the same cast film and the permeation isotherms are remeasured with the same pressure increments as used for the sorption isotherm. As described in Chapter 2, the plasticizing ability of CO_2 is higher at lower temperatures. The experiments are therefore done at $25\text{ }^\circ\text{C}$ instead of $35\text{ }^\circ\text{C}$. The permeation and sorption results are given in Figure 4.8.

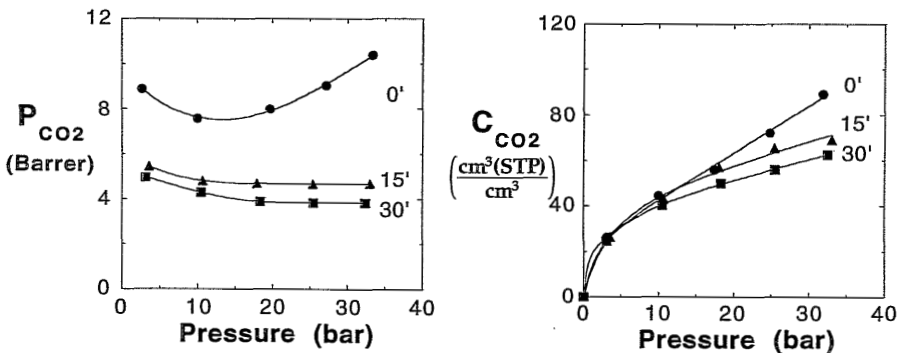


Figure 4.8. CO_2 permeability (P_{CO_2}) and concentration (C_{CO_2}) as a function of pressure for an untreated (0') and two heat-treated (15' and 30' at $350\text{ }^\circ\text{C}$) films at $25\text{ }^\circ\text{C}$.

The permeation and sorption isotherms are described phenomenologically by

fitting them to a suitable mathematical function. As was pointed out in Chapter 3, the permeation isotherms are fitted with a higher order polynomial. The sorption isotherms are fitted with a function in form similar to the dual-mode sorption equation, i.e., $y=ax+bx/(1+cx)$. The solid lines represent these numerical fits.

Despite the higher plasticizing ability of CO₂, the treated films show again a constant permeability at elevated pressures. This result emphasizes the success of the crosslinking method to suppress CO₂-induced plasticization. The differences in permeability of the differently treated films show the same trends as the permeabilities measured at 35 °C. The level of permeability decreases with longer heating time.

The sorption isotherms show the concave shape typical for gas sorption in glassy polymers. The CO₂ concentration sorbed by the differently treated films do not differ much at pressures up to 10 bar. No particular reason has been found to explain this. At higher feed pressures the CO₂ concentration in the treated films is lower compared to the untreated film and decreases further with longer heating time.

The permeability (P), the solubility (S) and the average diffusion coefficient (\bar{D}) at a pressure of 5 and 25 bar for the three films are given in Table 4.2. As defined in Chapter 3, the solubility coefficient (S) of CO₂ in the films is obtained by the ratio of the concentration and the corresponding pressure. The average diffusion coefficient is obtained from the ratio of permeability and solubility at the same pressure [31].

Table 4.2. Permeability, solubility and average diffusivity of the differently treated Matrimid films at 5 and 25 bar feed pressure and 25 °C.

Film	5 bar			25 bar		
	P (Barrer)	S $\left(\frac{\text{cm}^3(\text{STP})}{\text{cm}^3 \text{ bar}}\right)$	\bar{D} $*10^{-8} \left(\frac{\text{cm}^2}{\text{s}}\right)$	P (Barrer)	S $\left(\frac{\text{cm}^3(\text{STP})}{\text{cm}^3 \text{ bar}}\right)$	\bar{D} $*10^{-8} \left(\frac{\text{cm}^2}{\text{s}}\right)$
Untreated	8.3	6.3	1.0	8.7	2.9	2.3
15' 350 °C	5.2	6.2	0.63	4.7	2.6	1.4
30' 350 °C	4.8	6.2	0.58	3.8	2.2	1.3

From Table 4.2 it can be concluded that the differences in permeability among the differently treated films is mainly determined by diffusion and not or much less by solubility. At a pressure of 5 bar, the diffusion coefficients for the 15 and 30 minutes heat-treated films are, respectively, 37% and 42% lower compared to the untreated film, whereas the solubilities are almost the same. At 25 bar the

solubilities of the 15 and 30 minutes heat-treated films are, respectively, 10% and 24% lower compared to the untreated one. However, the differences in permeability are also mainly governed by the differences in diffusivity. The diffusion coefficients of the heat-treated films are 39% and 43 % lower than the untreated film.

In a first approach to elucidate the permeability values, the solubility and the average diffusion coefficients are useful parameters. However, in most cases the diffusion coefficient strongly depends on concentration of the penetrant. It is therefore more correct to evaluate a local concentration dependent diffusion coefficient at any arbitrary point between the feed and permeate side of the membrane [31]. As described in Chapter 3, for this purpose a phenomenological description of the permeation and sorption isotherms is sufficient. Although the fits do not have any physical basis, they are legitimate tools to determine the derivatives of the isotherms at any desired pressure. The local concentration dependent diffusion coefficient is then calculated by Equation (3.9) and is given here again to facilitate reading.

$$D(C) = \left[P(p) + p \left(\frac{dP}{dp} \right) \right] \left[\frac{dp}{dC} \right] \quad (4.3)$$

According to the dual mode theory, the general trend is an increase of the diffusion coefficient with increasing concentration. This increase is not caused by plasticization but reflects the saturation of the excess free volume and levels off at higher concentrations [32]. The local diffusion coefficient as a function of the CO₂ concentration in the differently treated films is calculated with Equation (4.3). The results are shown in Figure 4.9.

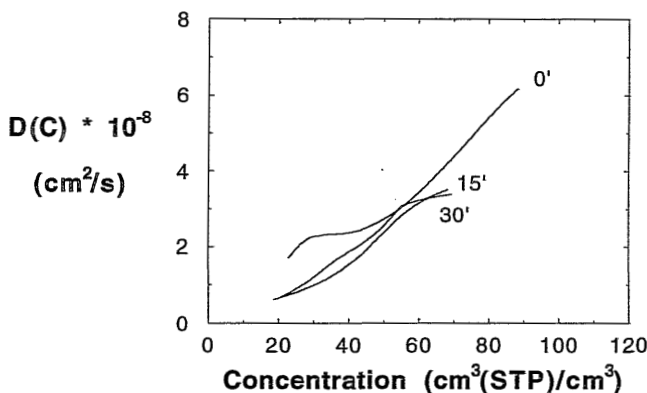


Figure 4.9. Local concentration dependent diffusion coefficient as a function of concentration for the untreated and two heat-treated Matrimid films at 25 °C. $D(C)$ is calculated with Equation 4.3.

The untreated film shows an increase in the local diffusion coefficient at lower concentrations and reaches a plateau level at concentrations of about 40

$\text{cm}^3(\text{STP})/\text{cm}^3$. Such a plateau level has also been observed by Koros and Hellums [28] for a polycarbonate series. The increase in the local diffusion coefficient after the plateau value is attributed to the effect of plasticization. The crosslinked films appear to reach a constant local diffusion coefficient. Unfortunately, the concentration range was too small to conclude that the diffusion coefficient remains constant with increasing concentration. However, taking a constant permeability (see Figure 4.4) and a linear increase in concentration as a function of pressure, Equation (4.3) predicts a constant local diffusion coefficient. It is therefore again concluded that the crosslinking method is successful in suppressing the CO_2 -induced plasticization.

4.7. Conclusions

Crosslinking of Matrimid films by a thermal treatment at $350\text{ }^\circ\text{C}$ is a successful method to suppress CO_2 -induced plasticization. This conclusion is supported by the following observations:

- In single gas permeation, a constant permeability at elevated pressures is obtained for the 15 and 30 minutes heat-treated films, whereas the untreated film shows an enormous increase in permeability due to plasticization.
- In time-dependent experiments at 30 bar CO_2 pressure no time dependency is observed in the permeability for the treated films after 4 hours of permeation, whereas the permeability of the untreated film still increases considerably.
- Mixed gas permeation experiments reveal that the partial CH_4 permeability remains constant for the treated films. For the untreated film the CH_4 permeability strongly increases at higher partial CH_4 pressure due to the CO_2 plasticization.
- The local diffusion coefficient as a function of the concentration of the treated films do not show the increase at higher concentrations typical for plasticization as observed in the untreated film.

4.8. References

- [1] Bessonov, M.I., Koton, M.M., Kudryavtsev, V.V., Laius, L.A., Polyimides. Thermally stable polymers, Consultants bureau, New York, (1987)
- [2] Bessonov, M.I., Zubkov, (Eds.), V.A., Polyamic acids and polyimides. Synthesis, transformations and structure, CRC Press, London, (1993)
- [3] Wilson, D., Stenzenberger, H.D., Hergenrother, P.M., Polyimides, Blackie, Glasgow, (1990)
- [4] Angelo, R.J., Crosslinkable polyamide-acids and polyimides and crosslinked polymeric products made therefrom, US Patent, 3:533.997, (1970)
- [5] Burgoyne, W.F., Langsam, M., Ford, M.E., Casey, J.P., Membranes formed from unsaturated polyimides, US Patent 4.931.182, (1990)
- [6] Hsu, K.K., Nataraj, S., Thorogood, R.M., Puri, P.S., O_2/N_2 selectivity improvement for polytrimethylsilylpropyne membranes by UV-irradiation and further enhancement by

- subambient temperature operation, *J. Membrane Sci.*, 79 (1993) 1-10
- [7] Meier, I.K., Langsam, M., Klotz, H.C., Selectivity enhancement via photooxidative surface modification of polyimide air separation membranes, *J. Membrane Sci.*, 94 (1994) 195-212
- [8] Kita, H., Inada, T., Tanaka, K., Okamoto, K.-i., Effect of photocrosslinking on permeability and permselectivity of gases through benzophenone-containing polyimide, *J. Membrane Sci.*, 87 (1994) 139-147
- [9] Liu, Y., Xu, J., Gas permeabilities and permselectivity of photochemically crosslinked polyimides, *J. Appl. Polym. Sci.*, 58 (1995) 4852-489
- [10] Pfeifer, J., Rohde, O., Direct photoimaging of fully imidized solvent-soluble polyimides, in: *Polyimides: materials, chemistry and characterization. Proceedings of second international conference on polyimides*, Ellenville, New York, (1985) 130-150
- [11] Rohde, O., Smolka, P., Falcigno, P.A., Novel auto-photosensitive polyimides with tailored properties, *Polym. Eng. Sci.*, 32 (1992) 1623-1629
- [12] Lin, A.A., Sastri, V.R., Tesoro, G., Reiser, A., Eachus, R., On the cross-linking mechanism of benzophenone-containing polyimides, *Macromolecules*, 21 (1988) 1165-1169
- [13] Scaiano, J. C., Netto-Ferreira, J.C., Baknell, A.F., Small, R.D., The mechanism of photocure of inherently photosensitive polyimides containing a benzophenone group, *Polym. Eng. Sci.*, 29 (1989) 942-944
- [14] Kuroda, S.-I., Nagura, A., Horie, K., Mita, I., Degradation of aromatic polymers-III. Crosslinking and chain scission during photodegradation of polysulphones, *Eur. Polym. J.*, 25 (1989) 621-627
- [15] Kuroda, S.-I., Mita, K., Degradation of aromatic polymer-II. The crosslinking during thermal and thermo-oxidative degradation of a polyimide, *Eur. Polym. J.*, 25 (1989) 611-620
- [16] Yanagishita, H., Maejima, C., Kitamoto, D., Nakane, T., Preparation of asymmetric polyimide membrane for water/ethanol separation in pervaporation by the phase inversion process, *J. Membrane Sci.*, 86 (1994) 231-240
- [17] Kuroda, S.-I., Terauchi, K., Nogami, K., Mita, I., Degradation of aromatic polymers-I. Rates of crosslinking and chain scission during thermal degradation of several soluble aromatic polymers, *Eur. Polym. J.*, 25 (1989) 1-7
- [18] Falcigno, P., Masol, M., Williams, D., Jasne, S., Comparison of properties of polyimides containing DAPI isomers and various dianhydrides, in: *Polyimides: materials, chemistry and characterization. Proceedings of third international conference on polyimides*, Ellenville, New York, (1989) 497-512
- [19] Bateman, J.H., Geresy, W., Neiditch, D.S., Soluble polyimides derived from phenylindane diamine: a new approach to heat resistant protective coatings, *Am. Chem. Soc., Div. Org. Coat. Plast. Chem.*, 35(2) (1975) 77-82
- [20] Dine-Hart, R.A., Wright, W.W., A study of some properties of aromatic imides, *Die Makromol. Chem.*, 143 (1971) 189-206
- [21] Foster, R., *Organic charge-transfer complexes*, Academic press, London, (1969)
- [22] Dinan, F.J., Schwartz, W.T., Wolfe, R.A., Hojnicky, D.S., St. Clair, T., Pratt, J.R., Solid-state ^{13}C -NMR spectral evidence for charge transfer complex formation in aromatic diimides and dianhydrides, *J. Polym. Sci., Polym. Chem. Ed.*, 30 (1992) 111-118
- [23] Kawakami, H., Mikawa, M., Nagaoka, S., Gas transport properties in thermally cured aromatic polyimide membranes, *J. Membrane Sci.*, 118 (1996) 223-230
- [24] Wessling, M., Huisman, I., v.d. Boomgaard, Th., Smolders, C.A., Time-dependent permeation of carbon dioxide through a polyimide membrane above the plasticization pressure, *J. Appl. Polym. Sci.*, 58 (1995) 1959-1966
- [25] Wessling, m., Schoeman, S., van der Boomgaard, Th., Smolders, C.A., Plasticization of gas separation membranes, *Gas Sep. & Purif.*, 5 (1991) 222-228
- [26] Koros, W.J., Fleming, G.K., Membrane-based gas separation, *J. Membrane Sci.*, 83 (1993) 1-80

-
- [27] Koros, W.J., Chern, R.T., Stannett, V., Hopfenber, H.B., A model for permeation of mixed gases and vapors in glassy polymers, *J. Polym. Sci., Polym. Phys., Ed.*, 19 (1981) 1513-1530
 - [28] Coleman, M.R., Isomers of fluorine-containing polyimides for gas separation membranes, PhD-thesis, University of Texas, Austin, USA, (1992)
 - [29] Sada, E., Kumazawa, H., Xu, P., Wang, S.-T., Permeation of pure carbon dioxide and methane and binary mixtures through cellulose acetate membranes, *J. Polym. Sci., Polym. Phys. Ed.*, 28 (1990) 113-125
 - [30] Li, K., Acharya, D.R., Hughes, R., Performance of a cellulose acetate permeator with permeability-influenced feed, *AIChE J.*, 36 (1990) 1610-1612
 - [31] Koros, W.J., Chern, R.T., Separation of gaseous mixtures using polymer membranes, in: *Handbook of separation technology*, Rousseau, R.W., (Ed.), John Wiley & Sons, New York, 862-953
 - [32] Koros, W.J., Hellums, M.W., Gas separation membrane material selection criteria: differences for weakly and strongly interacting feed components, *Fluid Phase Equilibria*, 53 (1989) 339-354

5

Suppression of CO₂ plasticization

Part 2: Blending and semi-interpenetrating polymer network

5.1. Introduction

Polymer blending is a possibility to modify material properties. A blend can show new properties not found in the single polymers. This is also true for membrane preparation. Ube prepare their membranes from BPDA-based polyimide blends [1]. Furthermore, blending is an option to reduce the price of the membranes. Considering Matrimid in particular, several examples can be found in the patent literature where membranes are prepared from Matrimid and the much cheaper PEI [2,3].

It is well known that many polymers do not mix on a molecular level. The blends contain the separate polymers as individual domains or phases [4]. Most blends consist of a matrix of one polymer containing the other polymer as a dispersed or co-continuous phase. However, it is found that Matrimid can be blended on a molecular level with PC [4], PSF [4,5], PES [6-8] and polybenzimidazole (PBI) [9,10]. Blending on a molecular level, for example, is indicated by a single glass transition temperature and optical transparency of the films.

In this thesis, blending is used as a method to change the susceptibility to plasticize the polymer film. It is hypothesized that blending of a polymer highly susceptible to plasticization with a polymer that hardly plasticizes will result in a material that shows a suppressed plasticization tendency. Permeation and sorption experiments will be carried out with a blend of Matrimid with PSF or P84. Matrimid is the polymer highly susceptible to plasticization and PSF and P84 the polymers that hardly plasticize. The results are presented in Section 5.2. Furthermore, Matrimid has been blended with an oligomer containing reactive acetylene groups. This blend results in a semi-interpenetrating polymer network (s-ipn) upon heating. In general, the latter type of blending is a concept to incorporate thermoplastics into a thermoset matrix. The toughness of a thermoplast is in this way combined with the thermal and chemical resistance of thermosets [11]. The influence of this type of blending on plasticization will be discussed in Section 5.3.

5.2. Matrimid/PSF and Matrimid/P84 blends

5.2.1. Film preparation

A 10% Matrimid/PSF (50/50 wt %) in CHCl_3 solution and a 20% Matrimid/P84 (60/40 wt %) in DMAc solution were cast on a glass plate and dried in a nitrogen atmosphere at room temperature. The dried films were removed from the glass plate with a small amount of water and further dried in a vacuum oven (Heraeus, RVT 220/180) at 150 °C for at least four days. The final film thickness was 18 μm for the Matrimid/PSF and 27 μm for the Matrimid/P84 blend.

5.2.2. Characterization of the films

The blends, Matrimid/P84 as well as Matrimid/PSF, were transparent. However, the Matrimid/PSF appeared to have two glass transition temperatures and are therefore indicated as inhomogeneous on a molecular level. The T_g 's of the blend appear to be slightly higher compared to the homopolymers. Optical clearness is therefore not a sufficient measure for determining blend homogeneity. For example, thin films of heterogeneous blends appear clear as the light encounters only one of the two phases in passing through the material [12]. Furthermore, the two polymers can have equal refractive indices or the dispersed phase has dimensions smaller than the wavelength of the visible light [12]. For the Matrimid/P84 blend one glass transition temperature was observed. Although it may not be completely obvious, the blend was indicated as homogeneous. It is possible that the second glass transition temperature is hard to detect, because the glass transition temperatures of the homopolymers do not differ much.

The glass transition temperatures and the densities are given in Table 5.1. The casting solvents used are also given as they may influence the results to a certain extent.

The densities of the different films varied from 1.221 g/cm^3 for the Matrimid/PSF blend to 1.336 g/cm^3 for P84. The density of the Matrimid/P84 blend is between the values of the homopolymers. The density of the Matrimid/PSF blend is lower compared to the homopolymers. This may be explained by the casting solvent used. The films prepared from the homopolymers were cast from DMAc, whereas the blend was cast from the more volatile CHCl_3 . A film cast from CHCl_3 will dry faster compared to a film cast from DMAc. In case of the CHCl_3 cast film, the polymer chains have less time to relax into a dense packing as in the case of the DMAc cast film, which results in a lower density for the CHCl_3 cast film.

Table 5.1. Glass transition temperatures and densities of the different films prepared.

Polymer	Solvent	ρ (g/cm ³)	T _g (°C)
Matrimid	DMAc	1.229	313
60%M/40%P84	DMAc	1.288	307
P84	DMAc	1.336	300
Matrimid	DMAc	1.229	313
50%M/50%PSF	CHCl ₃	1.221	191 and 319
PSF	NMP	1.236	182

5.2.3. CO₂ permeation, sorption and diffusion behaviour of Matrimid/P84 blend

Single gas permeation together with sorption experiments are only carried out with the Matrimid/P84 blend. Figure 5.1 shows the CO₂ permeation behaviour of the blend in comparison with the homopolymers at room temperature.

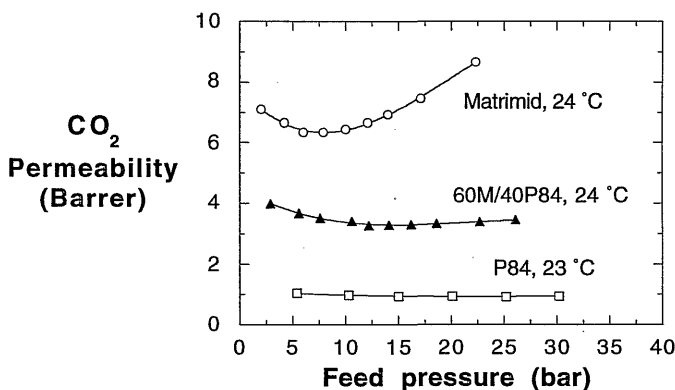


Figure 5.1. CO₂ permeability as a function of pressure for Matrimid, a Matrimid/P84 blend (60/40 wt %) and P84 at room temperature.

The permeability coefficients of the blend are found between the values of the homopolymers. On the basis of the film densities it can be concluded that blending Matrimid with P84 results in a densification of the polymer matrix and hence a reduction of free volume. And, as was found in Chapter 4, a densification of the polymer matrix results in lower permeability values. Compared to P84 the blend has a larger free volume and therefore a higher permeability. Similar results are found in the literature for polystyrene/poly(phenylene oxide) (PS/PPO) [13] and polystyrene/polymethylmethacrylate (PS/PMMA) blends [14]. The permeabilities of these blends also fall between the

values of the homopolymers.

The plasticization pressure of the Matrimid/P84 blend is shifted to higher feed pressures. The blend shows a plasticization pressure of 15 bar, which is between the plasticization pressure of 9 bar found for the Matrimid film and the 22 bar found for the P84 film. Kapantaidakis, et al. [15] found a similar shift in plasticization pressure for a Matrimid/PSF blend. The plasticization pressure of the blend shifted to higher pressures with increasing PSF content. Furthermore, only a slight increase in permeability of the Matrimid/P84 blend is observed at pressures above the plasticization pressure. Hence, blending of 60 % Matrimid and 40% P84 does not completely suppress plasticization at room temperature. The reason that the CO₂-plasticization is not completely suppressed as Matrimid is blended with P84 may be attributed to the concentration of P84 in the blend. The blend consists of only 40% of P84 and is expected to have more Matrimid than P84 character.

The sorption experiments are carried out with a different sorption set-up as described in Chapter 2. The main difference is that the cells in the set-up are connected through a differential pressure indicator instead of absolute ones on each cell [16]. Both cells are pressurized simultaneously. After closing the cells, a pressure decay in time in the sample cell with respect to the reference cell has been registered until equilibrium was reached. This sorption set-up is not used for all experiments in this thesis, because it is not suitable for high pressure sorption. During gas inlet the film starts to sorb the gas molecules immediately. This initial sorption cannot be registered as long as the cells are open. The missing initial sorption must be extrapolated. This extrapolation becomes very inaccurate at higher pressures. However, the sorption experiments up to 3 bar are very accurate and can be used for characterization purposes. The advantage of this sorption method is that sorption kinetics can be studied directly. An average diffusion coefficient is calculated from the slope of the relative mass uptake against the square root of time [17]:

$$\frac{M_t}{M_\infty} = \frac{4}{\pi^{1/2}} \left(\frac{\bar{D}t}{\ell^2} \right)^{1/2} \quad (5.1)$$

where M_t is the mass uptake at time t , M_∞ the mass uptake at infinite time, D the average diffusion coefficient and ℓ the membrane thickness. The diffusion coefficient is an average value over the concentration range determined by the corresponding initial and final pressure of the sorption step.

The sorption isotherms and the average diffusion coefficient as a function of concentration are given in Figure 5.2 for the Matrimid/P84 blend and the two homopolymers.

The CO₂ concentration in the P84 film is lower than the concentration in the Matrimid/P84 and Matrimid film at corresponding pressures. The sorption isotherms of Matrimid and the blend are comparable. It is not clear why the sorption isotherms of the Matrimid film and the blend coincide. The sorption

isotherm of the blend was expected to be between the isotherms of the homopolymers [13].

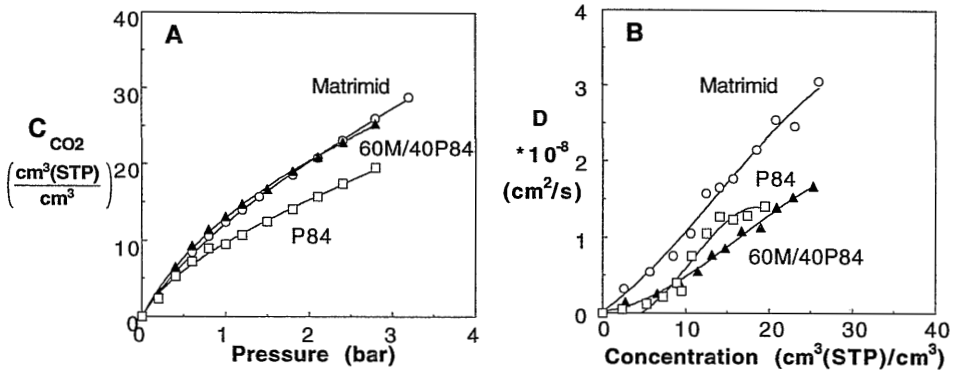


Figure 5.2. A. Sorption isotherms and B. average diffusion coefficients of the Matrimid/P84 blend and the homopolymers at 35 °C.

It should be noticed that the Matrimid/P84 is not a real blend from two homopolymers. P84 is a copolymer, which is in fact a blend itself. The sorption behaviour of a blend of a homopolymer and a copolymer may be different compared to a blend from two real homopolymers.

The diffusion coefficients of the blend correspond with the diffusion coefficients of P84, which is lower compared to Matrimid. This explains the lower permeability of the blend compared to Matrimid as the concentration in the blend is comparable to Matrimid. Hence, Matrimid blended with P84 results in a decrease of diffusivity. A decrease in diffusion is actually what is needed to suppress CO₂-induced plasticization. Blending Matrimid with a polymer showing a lower tendency to plasticize, such as P84, seems to be effective. However, a different ratio of Matrimid and P84 may be required to cause complete suppression of the CO₂ plasticization.

5.2.4. CO₂/CH₄ permeation behaviour

Mixed gas permeation experiments are carried out for the 60%Matrimid/40%P84 and 50%Matrimid/50%PSF blends. Figure 5.3 shows the CO₂/CH₄ selectivity obtained with a 55/45 mol % CO₂/CH₄ mixture as a function of the total feed pressure for both blends and the homopolymers Matrimid and PSF. The selectivity of P84 is not measured because of the very low fluxes and high selectivity. It would take too much time to collect enough permeate for an accurate gas chromatographic analysis. Because of the high selectivity, the determination of small CH₄ concentration in CO₂ is limited with the detection method used. To give an indication of the magnitude of the selectivity of P84, an

ideal selectivity of 89 was measured at 5 bar and 25 °C.

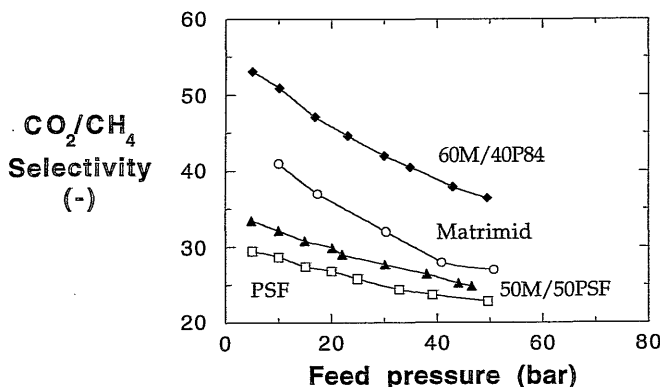


Figure 5.3. CO_2/CH_4 selectivity as a function of total feed pressure of the Matrimid/P84 and Matrimid/PSF blends and the homopolymer Matrimid obtained with a 55/45 mol % CO_2/CH_4 mixture at 35 °C.

The selectivities of the blends are between the values of the homopolymers. Raymond et al. [14] report similar trends for the selectivities of the PS/PMMA blends. The selectivity of PMMA was the highest and it decreased with increasing PS concentration. Furthermore, the selectivities shown in Figure 5.3. decrease with increasing feed pressure. As noticed in the previous chapter, it is not possible to draw conclusions from such selectivity trends about the plasticization behaviour of the films. Therefore, the partial CO_2 as well as CH_4 permeabilities are studied as a function of the partial feed pressure. The permeation isotherms are given in Figure 5.4.

Considering the Matrimid/P84 blend first, no increase in the total permeability and the partial CO_2 permeability at elevated pressures is observed. Apparently, the CO_2 permeation behaviour is somewhat different in the mixture compared to the pure gas (see Figure 5.1). However, the CH_4 still shows an increase (20%) in permeability indicating a small tendency to plasticize.

The total permeability curve of the Matrimid/PSF blend is between the permeability curves of the homopolymers as expected [13,14], although it is not clear on the basis of the densities of the films. The same behaviour is observed for the partial CO_2 permeation curve of the blend. The shape of the curve of the blend is similar to the curve of PSF. The permeability does not increase at higher feed pressures suggesting a suppression of plasticization. However, the partial CH_4 permeability of the blend still shows a slight increase (~5%) with increasing feed pressure. This indicates a tendency to plasticize. Considering the estimated error in the permeability measurement of 4 to 10 % (being larger at lower pressures), the increase in CH_4 permeability may not be significant. If it should be considered as significant, knowledge of the film morphology will be necessary.

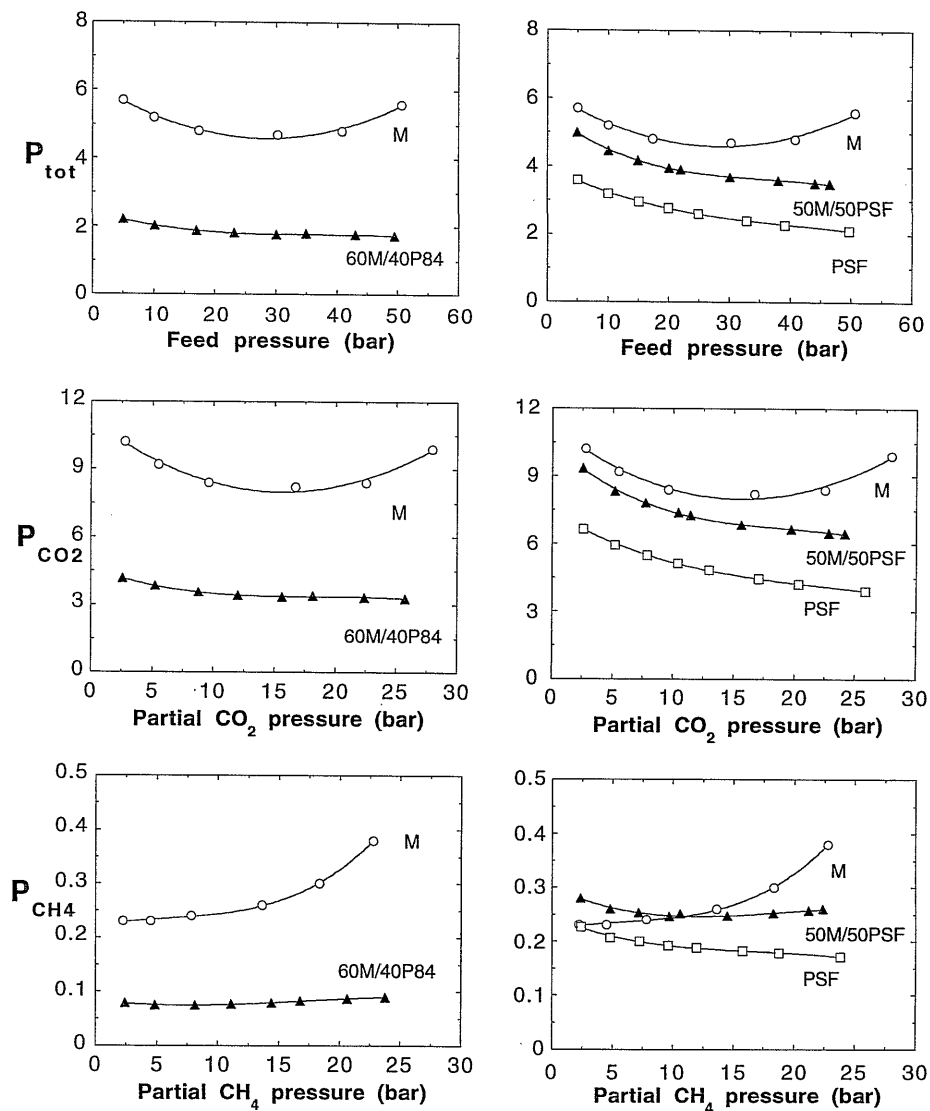


Figure 5.4. Permeability-pressure curves obtained with a 55/45 mol % CO_2/CH_4 mixture at 35 °C for the Matrimid/PSF and Matrimid/P84 blends and the homopolymers Matrimid (M) and PSF. The permeabilities are given in Barrer.

The Matrimid/PSF blend is not homogeneous on a molecular level. Either the PSF concentration may not be high enough to suppress the plasticizing ability of Matrimid completely or the plasticizing tendency is an effect of the inhomogeneity of the blend.

Summarizing, blending of a polymer highly susceptible to plasticization with a polymer that hardly plasticizes seems to be a promising method to suppress plasticization. A more accurate study on blends with different ratios of the homopolymers is necessary to predict the plasticization behaviour of the blends from the behaviour of the separate polymers.

5.3. Matrimid/Thermid blends: s-ipns

5.3.1. Background on semi-interpenetrating polymer network formation

A semi-interpenetrating polymer network can be obtained from the polymer Matrimid and the oligomer Thermid FA-700. Thermid FA-700 is manufactured by National Starch and Chemical Corporations and its chemical structure is given in Figure 5.5.

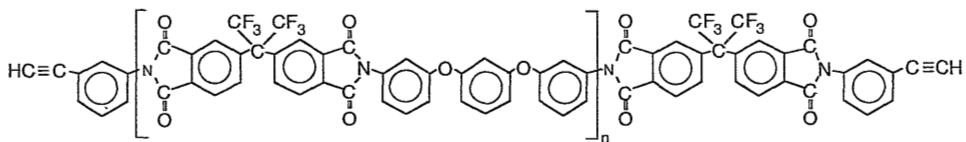


Figure 5.5. Chemical structure of Thermid FA-700.

This oligomer has the 6FDA-based polyimide structure of interest for gas separation. Furthermore, it has an acetylenic end group and can be crosslinked by heating at 250-275 °C without the evolution of volatile products [18]. Alam et al. [19] give a comprehensive review of possible reactions. Because of the acetylenic end groups the oligomer simultaneously polymerizes and crosslinks [18-20]. Two independent studies describe the chemistry of the crosslinking reaction. One study presumes a trimerization reaction of the acetylene groups, as schematically shown in Figure 5.6. Solid state ¹³C NMR experiments showed that about 30% of the structure formed during thermal curing indeed consisted of benzenoid rings. In another NMR study, naphthalenic units were detected in addition to benzenoid structures. The reaction is schematically given in Figure 5.7.

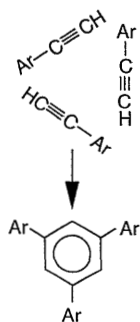


Figure 5.6. *Benzenoid cyclization (crosslinking) reaction.*

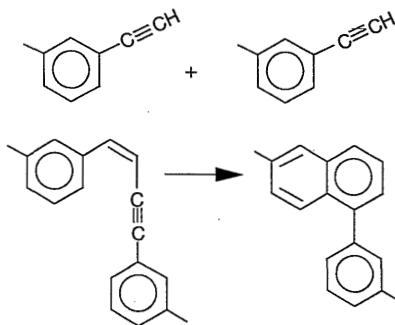


Figure 5.7. *Naphthalene formation (polymerization) reaction.*

It is known that the resulting material is inherently brittle due to a high degree of crosslinking. This renders the material less attractive as a gas separation material. This disadvantage can be overcome by controlling the degree of polymerization of the oligomer. The use of longer oligomer chains results in improved toughness. Another possibility, which is used in this thesis, is blending the oligomer with a tough linear thermoplastic polyimide (Matrimid). The polymerization and crosslinking of the oligomer in a mixture with the polymer results in a semi-interpenetrating polymer network (s-ipn) [19]. It appeared that blending Matrimid with the oligomer Thermid without a heat-treatment also results in a proper film suitable for gas permeation experiments. Such films are referred to as untreated or not crosslinked (NC). The treated films are referred to as crosslinked (C). The gas permeation behaviour of the untreated films is then compared with that of crosslinked ones.

Thermid is expected to be susceptible to CO_2 -plasticization. Its chemical structure is similar to the polyimide 6FDA-ODA, which has one ether-oxygen and benzene group less in the diamine structure (see Figure 1.1). 6FDA-ODA is known to show a high tendency to plasticize [21]. The same is true for Matrimid, as shown before. Hence, two materials susceptible to plasticization are mixed and subsequently crosslinked. This is again an excellent model to show whether this type of crosslinking can suppress plasticization too. No result in suppression of plasticization is expected from just blending Matrimid and Thermid, because both materials are susceptible to plasticization.

5.3.2. Film preparation

Semi-interpenetrating polymer networks were prepared from the polymer Matrimid and the oligomer Thermid. The polymer and oligomer were mixed in the desired ratios (90/10, 80/20 and 70/30 wt % Matrimid/Thermid, respectively) and dissolved in either DMAc or CH_2Cl_2 . Films with more than 20 wt %

Thermid could not be prepared with DMAc as solvent. Either the Matrimid/Thermid solution formed a gel or showed phase separation during drying. The highest concentration Thermid reached was 30% if the film was cast from CH_2Cl_2 . Homogeneous dense films are cast on glass plates and dried in a nitrogen atmosphere. The films, still stuck to the glass plate, are treated in a hot-air oven: 30 minutes preheating at 100 °C followed by a treatment for 15, 30, 60 or 120 minutes at 265 °C. Initially, the films were preheated at 100 °C to overcome the big temperature difference between room temperature and the curing temperature of 265 °C. Later it was found that no film damage occurred if the films were put directly in the hot oven without the preheating step, but to guarantee comparable film histories the same temperature program was applied to all Matrimid/Thermid films. Subsequently, the films were slowly cooled down to room temperature. They were then taken from the glass plate with a small amount of water. No post-treatment in the vacuum oven was carried out in order to prevent further crosslinking of the Thermid oligomer. It is assumed that during curing most solvent is removed from the films as the curing temperature is well above the boiling temperatures of the solvents. Final film thicknesses were 15 and 20 μm . The treated films were immersed in the original casting solvent to verify crosslinking, which was always the case.

The density and glass transition temperature of the different films are determined as described in Chapter 2. Furthermore, the films are characterized by single and mixed gas permeation experiments, as described in Chapter 2.

5.3.3. Characterization of the films

Different degrees of crosslinking are expected from either varying the curing time or changing the Matrimid/Thermid ratio. The films are treated mainly for 15, 30 and 60 minutes at 265 °C after the pretreatment step at 100 °C. Since the percentage acetylene-conversion into crosslinks depends on the curing time [22], the films are expected to have different degrees of crosslinking. Furthermore, the Matrimid/Thermid ratio is changed from 90/10, 80/20 to 70/30. Crosslinking was verified by swelling experiments in the original casting solvent. All treated films did not dissolve and were assumed to be crosslinked. The film with 10 weight percent Thermid did not crosslink after a heat-treatment up to 60 minutes, but appeared to be crosslinked after a 120 minutes heat-treatment.

Confirmation of the reaction involving the acetylene groups is found in FTIR analysis [22]. The intensity of the acetylenic C-H stretch vibration decreased with increasing treatment time and simultaneously the aromatic C=C skeletal stretch increased.

All films were transparent, the untreated as well as the treated films. The densities and glass transition temperatures of the different films are given in

Table 5.2. The casting solvent is again given, because it may influence the results to some extent.

Table 5.2. *Glass transition temperatures and densities of Matrimid and the different Matrimid/Thermid films prepared.*

Polymer	Solvent	ρ (g/cm ³)	Dissolves	T _g (°C)
Matrimid – untreated	DMAc	1.229	yes	313
80%M/20%T:				
15' 265 °C	DMAc	1.272	no	295
30' 265 °C	DMAc	1.266	no	297
60' 265 °C	DMAc	1.267	no	300
Matrimid – untreated	CH ₂ Cl ₂	1.223	yes	309
Matrimid – 30' 265 °C	CH ₂ Cl ₂	1.228	yes	317
90%M/10%T:				
untreated	CH ₂ Cl ₂	1.256	yes	293
120' 265 °C	DMAc	1.243	no	306
80%M/20%T:				
untreated	CH ₂ Cl ₂	1.267	yes	285
60' 265 °C	CH ₂ Cl ₂	1.222	no	296
70%M/30%T:				
untreated	CH ₂ Cl ₂	1.288	yes	283
60' 265 °C	CH ₂ Cl ₂	1.240	no	290
Thermid – 2h 280 °C	NMP	–*	no	272

* The film was too brittle and therefore not suitable for the measuring method used.

The densities vary from 1.222 g/cm³ for the crosslinked 80%Matrimid/20%Thermid blend cast from CH₂Cl₂ to 1.288 g/cm³ for untreated 70%Matrimid/30%Thermid blend cast from CH₂Cl₂. The Thermid film was too brittle and therefore not suitable for the density measurement method applied. The density of an untreated Matrimid film cast from DMAc is slightly higher compared to the film cast from CH₂Cl₂. As discussed in the previous section, the higher density of the DMAc cast film results from a slower drying process. Furthermore, the density of the Matrimid film cast from CH₂Cl₂ and heated at 265 °C for 30 minutes is slightly higher compared to the untreated Matrimid film cast from CH₂Cl₂. The heat-treatment has caused a densification of the polymer matrix.

The densities of most Matrimid/Thermid blends are higher compared to a Matrimid film. Apparently, the addition of the Thermid oligomer causes a

densification of the film. No obvious trend can be found among the densities of the crosslinked Matrimid/Thermid blends. The crosslinked 80%M/20%T blend cast from CH_2Cl_2 shows a lower density compared to the same blend cast from DMAc. This can be attributed to the casting solvent used as discussed in the previous section. Furthermore, a higher density can be expected from a higher degree of crosslinking. This is however not obvious for either the 80%M/20%T series cast from DMAc with different heating times or the Matrimid/Thermid series cast from CH_2Cl_2 . The crosslinked Matrimid/Thermid films cast from CH_2CH_2 show lower densities compared to the untreated blends. An explanation could be that the benzenoid rings formed after crosslinking of the Thermid contribute to a more open polymer matrix.

The glass transition temperature of Matrimid is found to be 313 °C. The film cast from CH_2Cl_2 showed a lower glass transition compared to the film cast from DMAc. As the T_g is often taken as a measure for chain stiffness, the higher T_g of the DMAc cast film may be attributed to a less flexible polymer matrix as a result of a more efficient packing (higher density).

A softening point of the Thermid *oligomer* of 175 °C is reported [20]. A homogeneous dense film of Thermid cast from NMP and crosslinked for 2 hours at 280 °C showed a T_g of 272 °C. Hence, the Thermid material is much stiffer after crosslinking. The Matrimid/Thermid blends, the untreated as well as the crosslinked films, showed single T_g 's. This indicates that the blends are mixed on a molecular level. The T_g values of the Matrimid/Thermid blends are between the values for the separate Matrimid and Thermid films. The glass transition temperature of the 80%Matrimid/20%Thermid series cast from DMAc increases with heating time. The increase in glass transition temperature may be interpreted as an increase in crosslink density. Furthermore, the glass transition temperature decreases with increasing Thermid concentration as the untreated and the crosslinked blends are considered separately. The Thermid oligomer contains two flexible ether linkages in its oligomer backbone, which can result in lower T_g 's of the Matrimid/Thermid blends compared to Matrimid. Furthermore, the untreated Matrimid/Thermid blends show lower T_g 's than the crosslinked Matrimid/Thermid films. Although the crosslinked blends show lower densities, the crosslinking may reduce chain flexibility resulting in higher T_g 's.

5.3.4. CO_2 permeation behaviour

This subsection discusses three topics concerning CO_2 permeation experiments with Matrimid/Thermid films:

- a. The effect of heat-treatment time and the Matrimid/Thermid ratio on the permeation behaviour of CO_2 .

- b. Comparison of untreated and heat-treated films.
 A 70%Matrimid/ 30%Thermid film treated at 265 °C is compared with an untreated 70%Matrimid/ 30%Thermid film. The same comparison is made for a Matrimid film.
- c. A closer look at the effect of a heat-treatment at 265 °C (annealing) on the permeation behaviour of a Matrimid film.

a. Effect of heat-treatment time and Matrimid/Thermid ratio

Figure 5.8A shows the permeability as a function of pressure at room temperature of 80%Matrimid/20%Thermid films cured for 15, 30 and 60 minutes at 265 °C, respectively. Figure 5.8B shows the permeability at 35 °C of Matrimid/Thermid films with the ratios 90/10, 80/20 and 70/30. The 80/20 and 70/30 films were heated for 60 minutes at 265 °C. The 90/10 film needed a 120 minutes heat-treatment at 265 °C to crosslink. In both figures the permeation curve of an untreated Matrimid film is added for comparison.

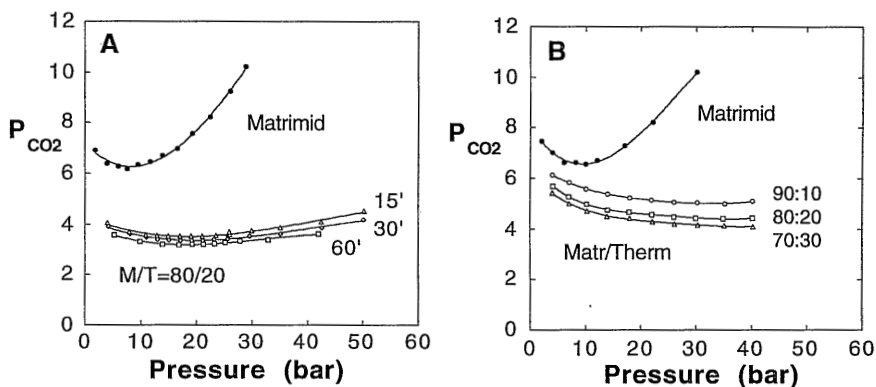


Figure 5.8.

- A. Permeability-pressure curves of an untreated Matrimid film (at 25 °C) and three 80%Matrimid/20%Thermid films (at 22 °C) cast from DMAc and cured for 15, 30 and 60 minutes at 265 °C, respectively.
- B. Permeability-pressure curves at 35 °C of an untreated Matrimid film and three Matrimid/Thermid films cast from CH_2Cl_2 with ratios of 90/10, 80/20 and 70/30, respectively. The 90/10 film was heated during 120 minutes at 265 °C and the 80/20 and 70/30 films during 60 minutes.

One can conclude from Figure 5.5A and 5.5B that the differences due to different curing times (Figure 5.5A) or different Matrimid/Thermid ratios (Figure 5.5B) are not large enough to be significant. The permeability values differ slightly, but the trends as a function of pressure are the same. Differences in permeability values between, for example, the 80/20 films cast from DMAc and CH_2Cl_2 can be attributed to differences in film history caused by film preparation. The

permeability of the DMAc cast film is lower compared to the CH_2Cl_2 film. In Chapter 2, this was also observed for a Matrimid film cast from DMAc compared to a Matrimid film cast from CHCl_3 . The film cast from the more volatile solvent, such as CH_2Cl_2 or CHCl_3 , has a slightly higher free volume compared to a film cast from DMAc and has therefore a higher permeability. The temperature also contributes to the difference in permeability. The permeabilities of the DMAc cast film are measured at room temperature, which results in lower permeabilities compared to the permeabilities of the CH_2Cl_2 cast film obtained at 35 °C.

Furthermore, the films cast from CH_2Cl_2 show no tendency to plasticize in the pressure range considered indicated by a constant permeability at elevated pressures, whereas the films cast from DMAc still show a slight increase in permeability at elevated feed pressures. This difference should be attributed to the difference in operating temperature. In Chapter 2 it was shown that a Matrimid film had a higher tendency to plasticize at 24 °C than at 35 °C. The plasticization pressure was shifted to higher feed pressures at 35 °C. This was also checked for the Matrimid/Thermid films cast from DMAc. The results are given in Figure 5.9. The crosslinked 80%Matrimid/20%Thermid films cast from DMAc show a lower plasticization tendency at 35 °C too.

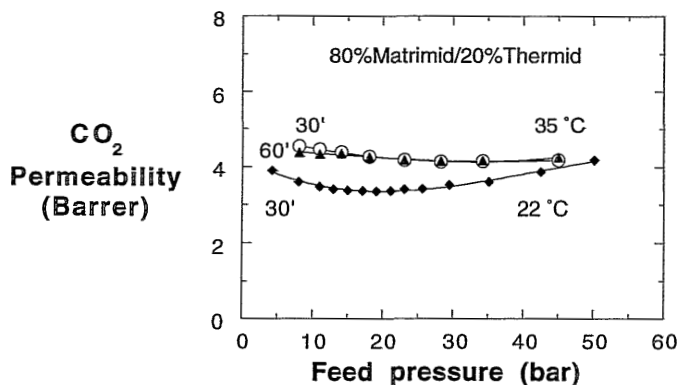


Figure 5.9. Comparison of the permeability-pressure curves of 80%Matrimid/20%Thermid films at 22 °C and 35 °C.

b. Comparison of untreated and heat-treated films

Blending the Matrimid polymer with the oligomer Thermid into a s-ipn seems to give the same results in suppressing plasticization as exposing the Matrimid films to a heat-treatment at 350 °C. However, the question arose what actually happened with the Matrimid polymer during the heat-treatment at 265 °C. Is the plasticization suppression really a result of the Thermid crosslinking or does

Matrimid also contribute to it? This was checked by measuring the permeation as a function of pressure of a Matrimid film which was treated at 265 °C for 30 minutes. In fact, this heat-treatment could be called annealing, because the temperature is just below the glass transition temperature. Additionally, a 70/30 film was taken which has had no heat-treatment at all as it appeared that a film suitable for permeation experiments can be obtained without any heat-treatment. The Matrimid films were cast from DMAc and the Matrimid/Thermid films from CH₂Cl₂. The results are given in Figure 5.10.

As the Matrimid/Thermid films are considered first, it is clear that crosslinking is necessary to suppress plasticization. The untreated Matrimid/Thermid film still shows the increase in permeability but at higher pressures compared to an untreated Matrimid film. The untreated Matrimid/Thermid film has not undergone any temperature treatment. Possible plasticization by the casting solvent is excluded, because of the low vapour pressure of CH₂Cl₂. It was assumed that drying the film in a nitrogen atmosphere for several days has reduced the remaining CH₂Cl₂ concentration to the same level as a film cast from DMAc treated at 265 °C. The solubility test showed that the Matrimid/Thermid film indeed was not crosslinked without heat-treatment.

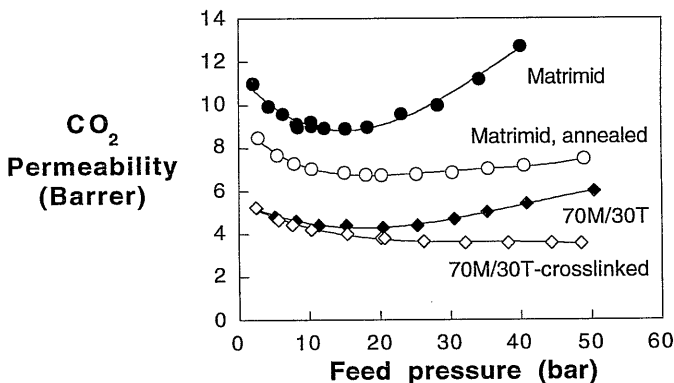


Figure 5.10. Permeability-pressure curves at 35 °C of respectively an untreated Matrimid film, an annealed Matrimid film (30 minutes at 265 °C), an untreated 70%Matrimid/30%Thermid film and a treated 70%Matrimid/30%Thermid film (30 minutes at 265 °C).

The annealed Matrimid film (treated for 30 minutes at 265 °C) was not crosslinked either. Surprisingly, the annealed Matrimid film does show a suppressed plasticization behaviour. The permeability as a function of pressure levels off. As indicated by an increased density, the annealing treatment results in a densification of the film. The densification results in a reduction of chain mobility and simultaneously in suppression of the CO₂ plasticization. The

densification can also be concluded from the lower permeability compared to an untreated film.

The time-dependency of the permeability of the annealed Matrimid film has been measured at 30 bar CO_2 pressure. The relative permeability as a function of time is given in Figure 5.11. The other three curves were obtained in earlier experiments and are described in the previous chapter.

All permeability values are normalized with the permeability value at 1 minute, the earliest time at which a permeability value was obtained. These relative values allow comparison of the different films. The permeability of the annealed Matrimid film increased 15% over 8 hours. This is two to three times higher as the films treated at 350°C , but still significantly lower than the untreated film. Furthermore, the permeability seems to increase slightly further after 8 hours of permeation which indicates plasticization.

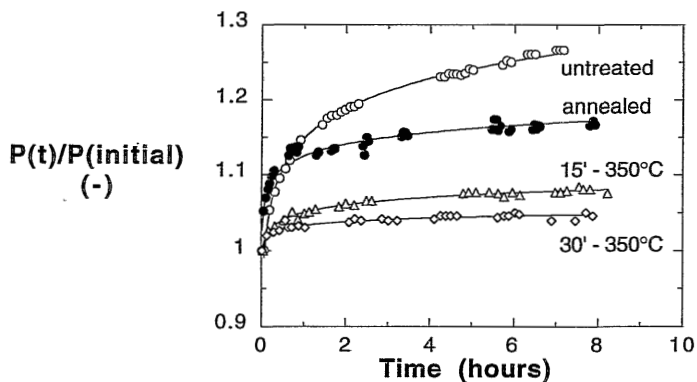


Figure 5.11. Time-dependent permeability at 30 bar CO_2 and at 35°C of the Matrimid film annealed at 265°C for 30 minutes (filled symbols); the untreated film and two heat-treated Matrimid films reported in Chapter 4 (open symbols) are also given.

c. Effect of annealing of a Matrimid film at 265°C

To obtain a reliable picture of the effect of the 265°C heat-treatment (annealing) of the Matrimid film, new films are prepared and the CO_2 permeation behaviour as a function of pressure is studied. All films appeared to be not crosslinked. The results of three additional experiments are given in Figure 5.12.

On a more detailed permeability scale, a definite minimum is observed in the CO_2 permeability isotherm already presented in Figure 5.10. The three additional curves show a similar minimum. From these results it can be concluded that simply annealing of the film is not enough to suppress CO_2 plasticization completely. Crosslinking of the film is a superior method.

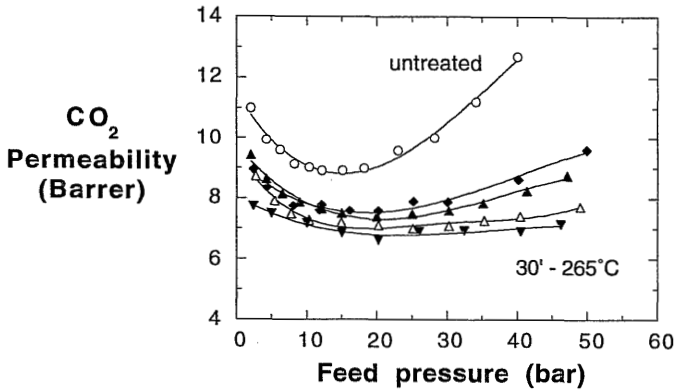


Figure 5.12. CO_2 permeability-pressure curves obtained at 35°C of similar Matrimid films treated for 30 minutes at 265°C (solid symbols). The permeation curve with the open triangles is the same curve as given in Figure 5.10 by the open circles.

To support the conclusion that no complete suppression of the plasticization is reached after a heat-treatment at 265°C , the partial CO_2 and CH_4 permeabilities obtained with a 55/45 mol % CO_2/CH_4 mixture are given in Figure 5.13.

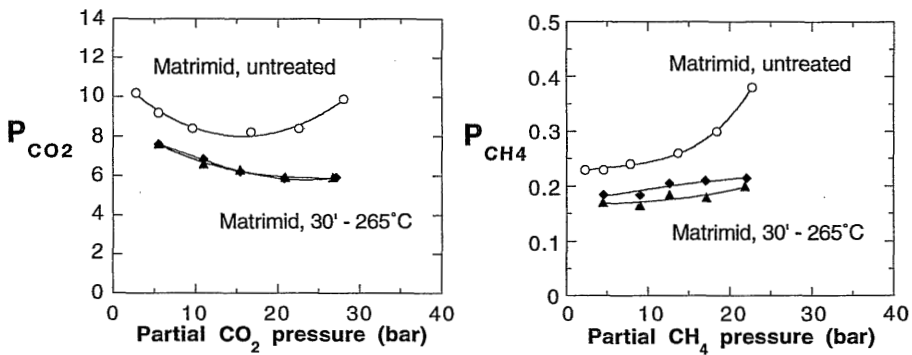


Figure 5.13. Partial CO_2 and CH_4 permeability-pressure curves of an untreated Matrimid film and two films treated at 265°C obtained with a 55/45 mol% CO_2/CH_4 mixture at 35°C .

Although it is not very clear in the figure, the partial CO_2 permeability-curves of the treated films suggest that the permeability will increase at further increase of the pressure. A better evidence can be found in the partial CH_4 permeation curves of the treated films. These curves still show a slight increase in CH_4 permeability with increasing partial CH_4 pressure, indicating plasticization.

5.3.5. CO_2/CH_4 permeation behaviour

70%Matrimid/30% Thermid films cast from CH_2Cl_2 were used for the mixed gas permeation experiments. An untreated as well as a crosslinked Matrimid/Thermid film is considered and compared with an untreated Matrimid film. The CO_2/CH_4 selectivities as a function of the total feed pressure obtained with a 55/45 mol % CO_2/CH_4 mixture are given in Figure 5.14.

Figure 5.14 shows the same trends as observed in previous experiments. The selectivity decreases with increasing feed pressure. The decrease in selectivity due to plasticization cannot be derived from these data. Furthermore, the Matrimid/Thermid blends show higher selectivities than the Matrimid film.

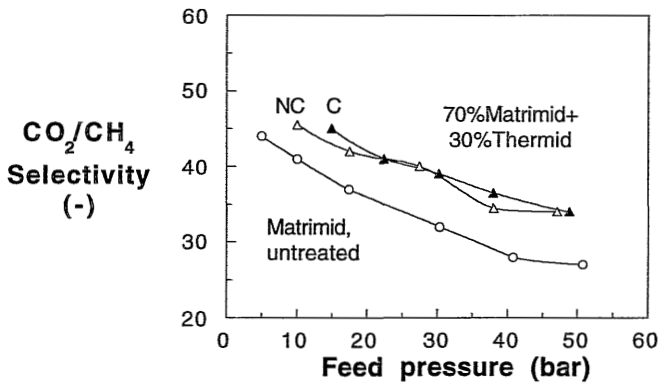


Figure 5.14. CO_2/CH_4 selectivity as a function of total feed pressure for an untreated Matrimid film, an untreated 70%Matrimid/30%Thermid blend (NC= not crosslinked) and a heat-treated (15' at 265 °C) 70%Matrimid/30%Thermid at 265 °C (C=crosslinked) obtained with a 55/45 mol % CO_2/CH_4 mixture at 35 °C.

This can be explained by the higher densities of the Matrimid/Thermid films compared to a Matrimid film. Permeabilities decrease with increasing film density. Apparently, the CH_4 permeability decreases more than the CO_2 permeability, which results in an improved CO_2/CH_4 selectivity. There is no significant difference found in the selectivities of the untreated or crosslinked Matrimid/Thermid films.

The results of the permeability analysis are given in Figure 5.15. The crosslinked Matrimid/Thermid film shows higher permeabilities than the untreated Matrimid/Thermid film. An explanation for this should be the lower density found for the crosslinked films compared to the untreated ones. This difference was not clear from the pure gas permeation experiments (see Figure 5.10). The pure gas permeabilities of the untreated and crosslinked film coincide at low

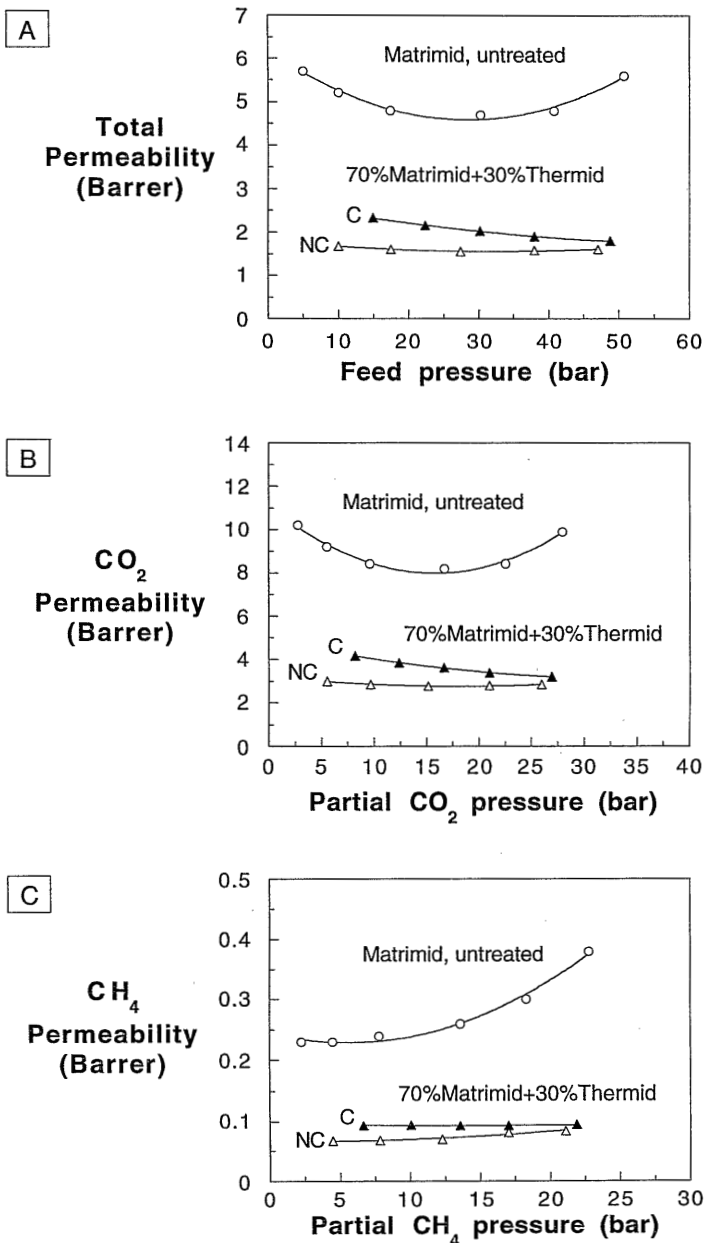


Figure 5.15. Permeability-pressure curves of an untreated Matrimid film, an untreated 70%Matrimid/30%Thermid (NC=not crosslinked) and a heat-treated (15' at 265 °C) 70%Matrimid/ 30%Thermid film (C=crosslinked) obtained with a 55/45 mol % CO₂/CH₄ mixture at 35 °C.

pressure. At higher feed pressures the untreated Matrimid/Thermid film showed higher permeabilities, but this could be attributed to plasticization.

Figure 5.15A shows the total permeability as a function of feed pressure. A small minimum is observed in the permeation curve of the untreated Matrimid/Thermid film. This indicates a small tendency to plasticize. The total permeability of the crosslinked film decreases with increasing feed pressure and does not show any plasticizing effect.

In Figure 5.15B, the CO_2 permeability as a function of the CO_2 partial pressure is given. The untreated Matrimid/Thermid film shows again a small minimum in the permeability. However, the increase in permeability is not as pronounced as in single gas permeation. Compared to the pure gas permeation experiments (see Figure 5.10), the untreated blend hardly shows plasticization in mixed gas permeation. A lower plasticization effect of CO_2 in mixed gas permeation experiments compared to pure gas permeation was also found for the Matrimid/P84 blend. Competition between the gases in the mixture influence their permeation behaviour. These effects may be more pronounced in blends than in, for example, a Matrimid film. Furthermore, in case of the Matrimid/Thermid film the difference may also be attributed to differences in film history, because the single and mixed gas permeation experiments are not carried out with the same cast film.

Figure 5.15C shows the CH_4 permeabilities as a function of partial CH_4 pressure for the untreated and crosslinked films. The slight increase in CH_4 permeability of the untreated film indicates effects of CO_2 plasticization behaviour. Also from these results it can be concluded that the plasticization effects in mixed gas permeation are less pronounced for the untreated blend compared to a Matrimid film. The increase in CH_4 permeability is about 25% for the blend, whereas the Matrimid film shows a relative increase of more than 60% over the same pressure range. The crosslinked blend shows a stabilized CH_4 permeability in the pressure range considered. From this result it can be concluded that the blending method with subsequent heat-treatment at 265 °C is successful in suppressing CO_2 induced plasticization.

5.4. Conclusions

Blending a polymer highly susceptible to plasticization (Matrimid) with a polymer with moderate (P84) or a low (PSF) tendency to plasticize is very promising in suppressing CO_2 -induced plasticization.

- A blend of 60% Matrimid and 40% P84 showed only a slight increase in CO_2 permeability at elevated pressures. The diffusion coefficient has been decreased significantly. It is suggested that an increase of the P84 concentration in the blend would result in more or complete suppression of plasticization.
- A blend of 50% Matrimid and 50% PSF did not show an increase in CO_2 permeability at elevated pressures. However, the CH_4 permeability still

showed a slight increase at higher partial CH₄ pressures. The possible plasticization effects may be attributed to the inhomogeneity of the blend.

Blending Matrimid and the oligomer Thermid with a subsequent heat-treatment at 265 °C is a successful method to suppress the CO₂-induced plasticization phenomena in Matrimid.

- The CO₂ and CH₄ permeation curves of the crosslinked blends (s-ipns) level off at elevated pressures. It was questioned whether the suppression was a result of annealing of the Matrimid. It is found that the crosslinking of the Thermid oligomer caused the suppression of plasticization, because the uncrosslinked s-ipn still showed an increase in permeability at elevated pressures. The annealed Matrimid films also showed a significant increase in permeability at elevated pressure.
- Differences in permeation behaviour due to different heating time or different polymer/oligomer ratios are too small to be significant.

5.5. References

- [1] Nakamura, A., Gas and vapor dehydration with the polyimide membranes, Report of the A.I.S.T.-A.F.M.E. expert meeting on energy conservation technology, Tokyo, (1989)
- [2] Simmons, J.W., Ikiner, O.M., Polyimide and polyamide-imide gas separation membranes, US Patent 5.232.472, (1993)
- [3] Macheras, J.T., Bikson, B., Nelson, J.K., Method of preparing membranes from blends of polyetherimide and polyimide polymers, US Patent 5.443.728, (1995)
- [4] Camargo, R., Mercer, F., Cheng, T.C., Compositions of poly(imides) having phenylindane diamines and/or dianhydride moieties in the poly(imide) backbone, US Patent 5.047.487, (1991)
- [5] Kapantaidakis, G.C., Kaldis, S.P., Dabou, X.S., Sakellaropoulos, G.P., Gas permeation through PSF-PI miscible blend membranes, *J. Membrane Sci.*, 110 (1996) 239-247
- [6] Grobelny, J., Rice, D.M., Karasz, F.R., MacKnight, W.J., High resolution solid state ¹³C nuclear magnetic resonance study of poly(ether sulphone)/polyimide blends, *Polymer Comm.*, 31 (1990) 86-89
- [7] Liang, K., Grebowicz, J., Valles, E., Karasz, F.E., MacKnight, W.J., Thermal and rheological properties of miscible polyethersulfone/polyimide blends, *J. Polym. Sci., Polym. Phys.*, 30 (1992) 465-476
- [8] Guerra, G., Choe, S., Williams, D.J., Karasz, F.E., MacKnight, W.J., Fourier transform infrared spectroscopy of some miscible polybenzimidazole/polyimide blends, *Macromolecules*, 21 (1988) 231-234
- [9] Cha, Y.J., Kim, E.-T., Ahn, T.-K., Choe, S., Mechanical and morphological phase behavior in miscible polyethersulfone and polyimide blends, *Polymer J.*, 26 (1994) 1227-1235
- [10] Musto, P., Karasz, F.E., MacKnight, W.J., Hydrogen bonding in polybenzimidazole/polyimide systems: a Fourier-transform infra-red investigation using low-molecular weight monofunctional probes, *Polymer* 30 (1989) 1012-1021
- [11] Lee, B.K., Kim, S.C., Morphology and properties of semi-ipns of polyetherimide and bisphenol A dicyanate, *Polym. Adv. Technol.*, 6 (1994) 402-412
- [12] MacKnight, W.J., Karasz, F.E., Fried, J.R., Solid state transition behavior of blends, in: *Polymer blends*, Paul, D., Newman, S., (Eds.), Academic Press, New York, V1 (1978) 185-242

-
- [13] Morel, G., Paul, D.R., CO₂ sorption and transport in miscible poly(phenylene oxide)/ polystyrene blends, *J. Membrane Sci.*, 10 (1982) 273-282
- [14] Raymond, P.D., Koros, W.J., Paul, D.R., Comparison of mixed and pure gas permeation characteristics for CO₂ and CH₄ in copolymers and blends containing methyl methacrylate units, *J. Membrane Sci.*, 77 (1993) 49-57
- [15] Kapantaidakis, G.C., Kaldis, S.P., Dabou, X.S., Sakellaropoulos, G.P., Gas permeation through PSF-PI miscible blend membranes, *J. Membrane Sci.*, 110 (1996) 239-247
- [16] Wessling, M., Schoeman, S., van der Boomgaard, Th., Smolders, C.A., Plasticization of gas separation membranes, *Gas Sep. & Purif.*, 5 (1991) 222-228
- [17] Crank, J., *The mathematics of diffusion*, Clarendon press, 2nd edition, Oxford, (1983)
- [18] Rossi, R.D., Polyimides, Reprint from: *Engineered Materials Handbook*, Vol. 3: Adhesives and sealants, ASM International, Materials Park, Ohio, (1992) 151-162
- [19] Alam, S., Kandpal, L.D., Varma, I.K., Ethynyl-terminated imide oligomers, *J. Macromol. Sci.-Rev. Macromol. Chem. Phys.*, C33(3) (1993) 291-320
- [20] Capo, D.H., Schoenberg, J.E., An acetylenic-terminated fluorinated polyimide, properties and applications, publ. in *SAMPE J.*, March/April (1987)
- [21] Koros, W.J., Walker, D.R.B., Gas separation membrane material selection criteria: weakly and strongly interacting feed component situations, *Polymer J.*, 23 (1991) 481-490
- [22] Huang, W.X., Wunder, S.L., FTIR investigation of cross-linking and isomerization reactions of acetylene-terminated polyimide and polyisoimide oligomers, *J. Polym. Sci., Polym. Phys. Ed.*, 32 (1994) 2005-2017
- [16] Wessling, M., Schoeman, S., van den Boomgaard, Th., Smolders, C.A., Plasticization of gas separation membranes, *Gas Sep. & Purif.*, 5 (1991) 222-228
- [17] Crank, J., *The mathematics of diffusion*, Clarendon press, 2nd edition, Oxford, (1983)

6

FTIR study of CO₂ in Matrimid films

6.1. Introduction

Chapter 4 and 5 demonstrate that crosslinking is the most successful method to suppress CO₂-induced plasticization of Matrimid films. Crosslinking of the Matrimid films could be achieved by thermal treatment at 350 °C or by blending Matrimid with the oligomer Thermid with subsequent thermal treatment at 265 °C to form a semi-interpenetrating polymer network. In case of the Matrimid films treated at 350 °C, the formation of charge transfer complexes (CTC's) might also play a role in suppressing the CO₂ plasticization. The colour change of the films upon heating is an indication of the existence of the charge transfer complexes.

The main effect of the crosslinking (and CTC formation) is a reduction in chain mobility due to a densification of the polymer matrix. The densification was indicated by a higher density of the treated compared to the untreated films. Furthermore, higher glass transition temperatures were observed for the treated films. The reduction of chain mobility was also demonstrated by a lower diffusivity of CO₂ in the treated films compared to the untreated ones. Additionally, the diffusivity of CO₂ in the crosslinked films did not increase at elevated pressures whereas the untreated film showed an enormous increase. Since the permeability of gases in glassy polymers is mainly determined by the diffusivity, the permeability of the treated films remained constant at elevated pressures whereas the permeability of the untreated films increased. The constant permeability at elevated pressure was an indication for the suppression of plasticization.

To obtain a better picture of the underlying reasons for the suppressed plasticization behaviour, Fourier transform infrared spectroscopy (FTIR) has been carried out. For this purpose the heat-treatment at 350 °C is chosen as the crosslinking method. To find possible changes in the chemical structure of Matrimid due to crosslinking, FTIR spectra of an untreated and a treated film are measured. The results are discussed in Section 6.2.

FTIR spectroscopy has been used extensively to investigate the interaction of CO₂

with polymers [1-8]. As has been discussed already in Chapter 3, Puleo et al. [1] and Fried and Li [2] observed dipole-induced-dipole interactions between polar groups in the polymer chain and between CO₂ and polar groups in the polymer chains, respectively. However, the changes in the spectra were small. Moreover, such interactions could not explain the plasticizing ability of a polymer completely, as was concluded in Chapter 3.

Another approach in studying the CO₂ behaviour in polymers is found in analyzing the spectrum of CO₂ dissolved in the polymers [3-8]. Differences in the CO₂ peaks imply differences in polymer properties and vice versa. In section 6.3, the results obtained from measurements with an untreated and a treated Matrimid film impregnated with CO₂ are presented. The CO₂ behaviour in an untreated film will be compared with a treated one and studied by determining the desorption of CO₂. Furthermore, possible CO₂-polymer interactions are studied.

6.2. FTIR of Matrimid films

6.2.1. Background on FTIR spectroscopy

The energy of a molecule is given by the sum of the electronical, vibrational and rotational energy:

$$E_{\text{molecule}} = E_{\text{electr}} + E_{\text{vibr}} + E_{\text{rot}} \quad (6.1)$$

where $E_{\text{electr}} \gg E_{\text{vibr}} \gg E_{\text{rot}}$. Absorbance of infrared radiation provides changes in the vibrational, rotational and vibration-rotation energy in the ground state. [9-11]. The electronic energy remains the same ($\Delta E_{\text{electr}}=0$), because the foton energy of infrared radiation is not high enough to excitate an electron to a higher electronic level. The absorbed radiation gives a value of the energy change involved. The change in energy, ΔE , is related to the wavelength (λ) of the radiation by the equation:

$$\Delta E = h.c/\lambda = h.v \quad (6.2)$$

where h is Planck's constant, v the frequency and c the velocity of light. Transitions due to rotation are only observed for small molecules in the gas phase.

An infrared spectrum is recorded in wavenumbers (v (cm⁻¹)), which is the reciprocal of the wavelength. Hence, the wavenumber is directly proportional to the energy and vibrational frequency of the absorbing unit. A criterion for the absorption of vibrational energy by a molecule in the infrared region is that a change of electric dipole moment must occur during the vibration [9-11]. Many vibrational origins of group frequencies are already elucidated and tabulated [9-11]. In more complex molecules, it is found empirically that certain submolecular groups of atoms consistently produce absorption bands in the same frequency region. These bands are the characteristic group frequencies. For example the

carbonyl group (-C=O) always absorbs at a frequency around 1700 cm^{-1} . With this knowledge on group frequencies an infrared spectrum of a sample can be analyzed. Shifts found in the characteristic group frequencies can give information about the position of the group in the molecule and about possible interactions with other groups.

6.2.2. Experimental methods

A Matrimid film with a final thickness of $5\text{ }\mu\text{m}$ was cast from DMAc as described in Chapter 2. A piece of the film was mounted in a holder with an opening of a diameter of 2 cm. The holder was placed in a Bio-Rad FTS-60 spectrophotometer. The chamber with the holder was continuously flushed with nitrogen. FTIR absorbance spectra were measured at room temperature from 4000 cm^{-1} to 400 cm^{-1} with a spectral resolution of 2 cm^{-1} and averaged over 200 scans.

The film still mounted in the holder was put in a hot-air oven (Heraeus, K750/1). The Matrimid film was then treated at $350\text{ }^\circ\text{C}$ for 30 minutes. After it was slowly cooled down to room temperature, the holder was placed in the spectrophotometer again. A FTIR absorbance spectrum of the treated film was measured at the same conditions as the untreated film.

6.2.3. Interpretation of the FTIR-spectrum of Matrimid

The spectrum of Matrimid obtained at room temperature is given in Figure 6.1 and corresponds well with the Matrimid spectra obtained by other investigators [12]. The spectra of the untreated and treated Matrimid films were identical, therefore only one spectrum is shown.

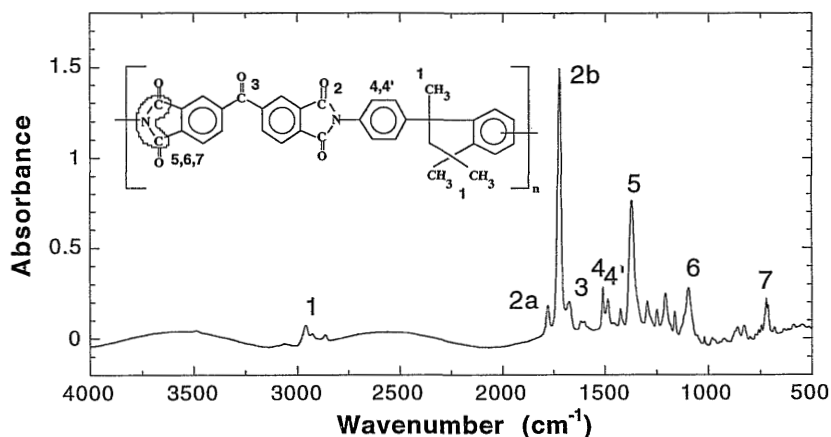


Figure 6.1. Chemical structure of Matrimid and FTIR absorption spectrum of a Matrimid film ($5\text{ }\mu\text{m}$) at room temperature.

It was thought that as a result of crosslinking existing peaks would (partly) disappear or that new peaks would show up. The crosslinking density is probably too low so that no change is visible in the infrared spectrum. A similar phenomenon was observed by White et al. [13]. They treated a 6FDA-based polyimide at 350 °C and observed no change in the infrared spectrum, whereas the colour of the film changed and the polymer became insoluble indicating that the film properties had changed. Nevertheless, in the following the spectrum of Matrimid will be discussed in some detail because this will be of use in the discussion of the next section.

The most characteristic group frequencies of a polyimide are the vibrations of the carbonyl group (C=O) and the C–N–C group of the imide bond. Anti-symmetric and symmetric stretching vibrations of the carbonyl group can be distinguished. Furthermore, the C–N–C vibration modes are distinguished in axial and transverse vibration (in-plane) modes and an out-of-plane bending mode [14]. The carbonyl groups coupled through the five-membered ring are indicated with the imide I band. These are of interest because of their absolute position and their relative intensity. The symmetric stretch of the carbonyl groups are found at 1770-1780 cm^{-1} and the anti-symmetric stretch at 1720-1730 cm^{-1} . The other three imide absorption bands are found at 1370-1380 cm^{-1} (imide II), 1070-1140 cm^{-1} (imide III) and 710-730 cm^{-1} (imide IV) [10,14] The frequencies observed in Figure 6.1. and the corresponding assignments are given in Table 6.1.

The wavelength at which a specific group absorbs depends largely on the direct neighbouring groups. For example, the carbonyl group of the benzophenone absorbs at a lower wavenumber (1673 cm^{-1}) than the carbonyl groups of the imide moiety (1725 and 1779 cm^{-1}) because of its highly conjugated state. Delocalization of the π -electrons of the carbonyl group reduces its double bond character, which results in a lower absorption frequency [9-11].

Table 6.1. Wavenumbers (ν) and band assignments for Matrimid obtained from Figure 6.1.

Number	ν (cm^{-1})	Band assignment
1	2960-2860	ν (C-H) stretch of methyl groups
2a	1779	ν (C=O) symmetric stretch [imide I]
2b	1725	ν (C=O) anti-symmetric stretch [imide I]
3	1673	ν (C=O) stretch of benzophenone carbonyl
4 & 4'	1512 & 1488	ν (C=C) aromatic stretching
5	1374	ν (CNC) axial stretch [imide II]
6	1096	ν (CNC) transverse stretch [imide III]
7	717	ν (CNC) out-of-plane bending [imide IV]

With this knowledge it is also possible to give additional evidence that crystallization of the Matrimid film upon heating does not occur. In case of crystallization the carbonyl group frequency of the treated Matrimid film would have shifted to lower frequencies. Ishida and Huang [15] observed a shift of 18 cm^{-1} for the benzophenone carbonyl in a BTDA-based polyimide. Such a shift can be understood as follows. The high packing density in a crystalline part of the polymer matrix can cause electronic interactions between polar groups of different segments, thereby changing the delocalization of the π -electrons and hence the absorption frequency.

In the same way, possible interactions of CO_2 with polar groups in the polymer chain can be analyzed. If CO_2 interacts with a certain group, a shift to lower frequencies of the vibration band of that particular group in the infrared absorption spectrum is expected.

6.3. FTIR in the presence of CO_2

6.3.1. Background on infrared spectra of CO_2

Carbon dioxide is a linear triatomic molecule and has in theory four fundamental vibration modes as derived from the number of vibrational degrees of freedom ($3N-5=3*3-5=4$) [9-11]. The four vibration modes are schematically presented in Figure 6.2.

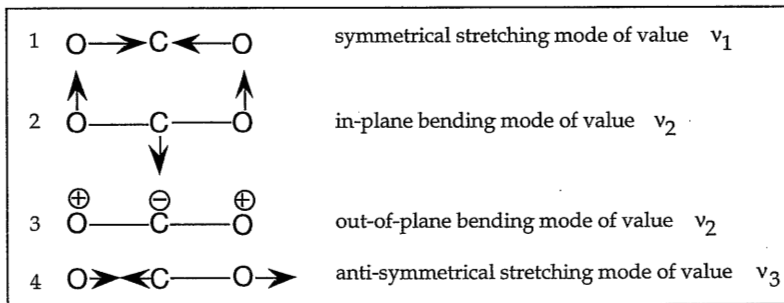
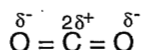


Figure 6.2. Fundamental vibration modes of CO_2 .

The symmetrical stretching mode (ν_1) is not infrared active since CO_2 has no dipole moment and no dipole moment will be induced either during this stretching vibration. This is clear as the delocalization of the electrons on the CO_2 molecule is considered:



Because the oxygen atoms are more electronegative than the carbon atom, they will withdraw electrons, which results in an electron-deficiency at the carbon atom. The centre of the negative and positive charge coincide and no dipole moment is present. The bending mode (ν_2) results in a dipole moment through the vibration and is therefore infrared active. This deformation mode is doubly degenerate. The in-plane bending motion and the out-of-plane bending have the same energy and vibrate therefore at the same frequency (ν_2). The anti-symmetric stretching mode (ν_3) induces also a dipole moment and is therefore infrared active too. The FTIR absorption bands of gaseous CO_2 that correspond to the bending and the anti-symmetric stretching mode are given in Figure 6.3.

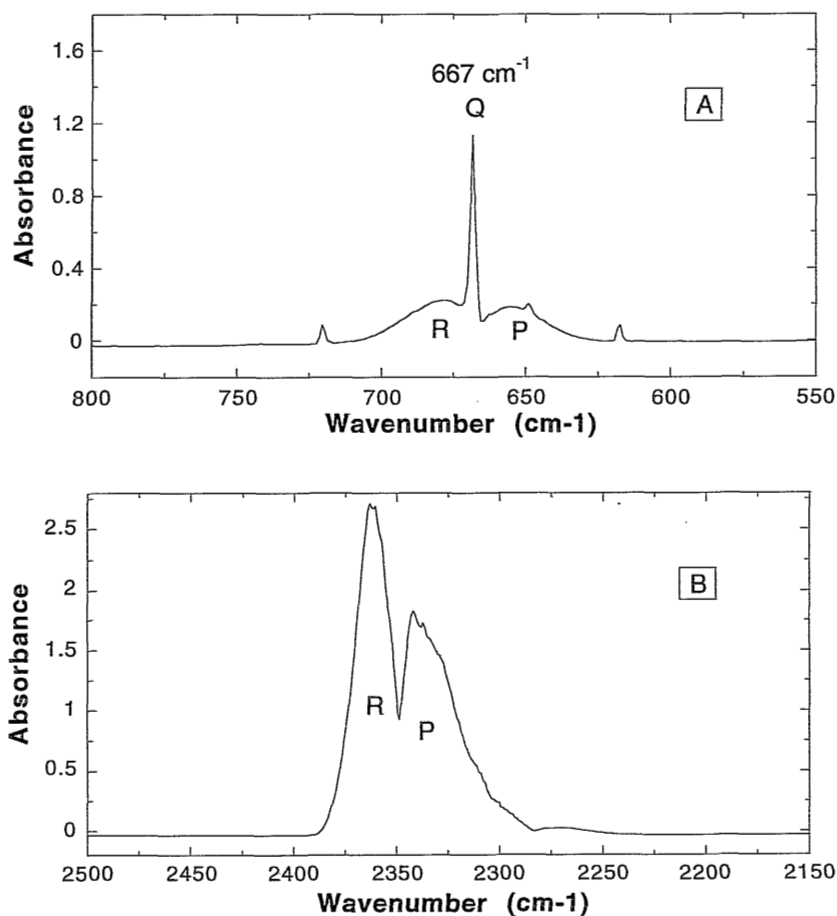


Figure 6.3. FTIR absorption spectra of gaseous CO_2 obtained at room temperature in: A. the bending mode (ν_2) and B. the anti-symmetric stretching mode (ν_3).

The anti-symmetrical stretching mode is observed at a wavenumber of 2349 cm^{-1} and the bending mode at 667 cm^{-1} . The split peaks and band broadening are a result of rotational changes associated with vibrational transitions. If the spectral resolution was higher (0.5 cm^{-1} instead of 2 cm^{-1}), individual rotation peaks could be observed [9-11].

In Figure 6.3A as well as 6.3B, the peak to the left is known to be the R-branch and the peak to the right as the P-branch. The bending mode (Figure 6.3A) has a sharp peak in the middle, which is known as the Q-branch [9-11]. No Q-branch can be observed in the anti-symmetric stretching mode because this transition is quantum mechanically forbidden. The classification of the transitions into P, Q and R branches is made in the quantum mechanical theory of infrared spectroscopy. However, it is beyond the scope of this thesis to go in further detail about the quantum mechanics.

6.3.2. Experimental methods

Conditioning of the film

A special high pressure cell was prepared for the FTIR experiments to allow measurements in the presence of CO_2 . The cell is shown schematically in Figure 6.4. It contains two parallel KBr disks spaced at 1 cm distance. A gas inlet was made on top of the cell.

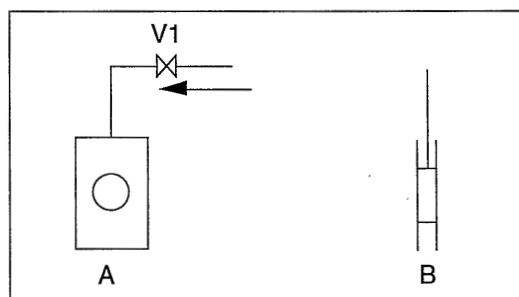


Figure 6.4. *High pressure FTIR-cell: A. Front view, B. Side view.*

The KBr disks were pressed from dried KBr powder and had a diameter of 2 cm and a thickness of 2 mm. The actual diameter of the KBr windows in the cell was 1.2 cm. On one of the KBr disks a homogeneous dense Matrimid film was cast from DMAc and dried in a nitrogen atmosphere. The final film thickness was $25\text{ }\mu\text{m}$. The coated KBr disk and an uncoated one were mounted in the cell, the coated layer facing at the inside. The cell was then placed in a set-up as schematically shown in Figure 6.5.

The cell was kept in a nitrogen atmosphere to prevent water absorption by the

KBr windows. The film was evacuated with an Edward vacuum pump during 16 hours. After evacuation the cell was pressurized at 8 bar CO_2 . The film was conditioned at this pressure during 16 hours. The cell was then disconnected from the set-up at the right side of valve V1 maintaining the pressure in the cell. The cell was placed into the spectrofotometer with the KBr windows in the centre of the light beam. The chamber of the spectrofotometer was again flushed with nitrogen during the FTIR run.

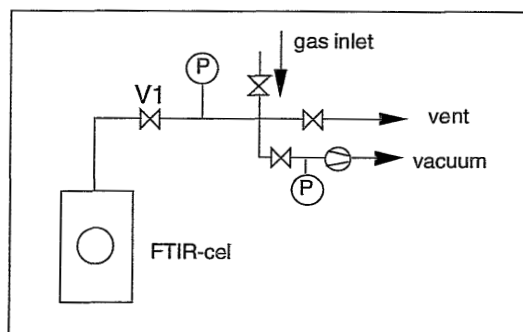


Figure 6.5. High pressure set-up for conditioning the film with CO_2 (P =pressure indicator).

FTIR measurements in the presence of CO_2

The cell, placed in the spectrofotometer, was connected with an Edward vacuum pump at the right side of valve V1. By opening valve V1, the CO_2 was sucked from the cell by the vacuum pump. The desorption of the dissolved CO_2 could be measured in time. Data collection was performed with the Bio-Rad FTS-60 Win IR software. Valve V1 was opened simultaneously while starting the measuring program.

FTIR absorbance spectra were measured in the wavenumber range of 4000 cm^{-1} to 400 cm^{-1} with a spectral resolution of 2 cm^{-1} . 200 scansets were taken, which results in 200 spectra. Each scanset resulted in a spectrum consisting of the average of 5 scans. Thus the number of scans per scanset was 5. To provide small time differences between the obtained spectra, the number of scans per set was kept low. The time difference between two spectra was 11.5 seconds.

At the end of the 200 scansets, the coated KBr disk was removed from the cell and was put in a hot-air oven (Heraeus, K750/1). The coated film was then treated at $350\text{ }^\circ\text{C}$ for 30 minutes. The sample was mounted in the cell again after it was slowly cooled down to room temperature. The conditioning procedure was repeated as described above: evacuation at vacuum for 16 hours and conditioning at 8 bar for 16 hours. Subsequently, the FTIR measurements were carried out with the treated film in the same way as with the untreated one.

6.3.3. Results and discussion of FTIR in the presence of CO₂

CO₂-polymer interactions

The FTIR absorption spectrum of a Matrimid film impregnated with CO₂ is shown in Figure 6.6. At this scale no difference was observed in the spectra of an untreated and a treated Matrimid film impregnated with CO₂. Therefore only one spectrum is shown.

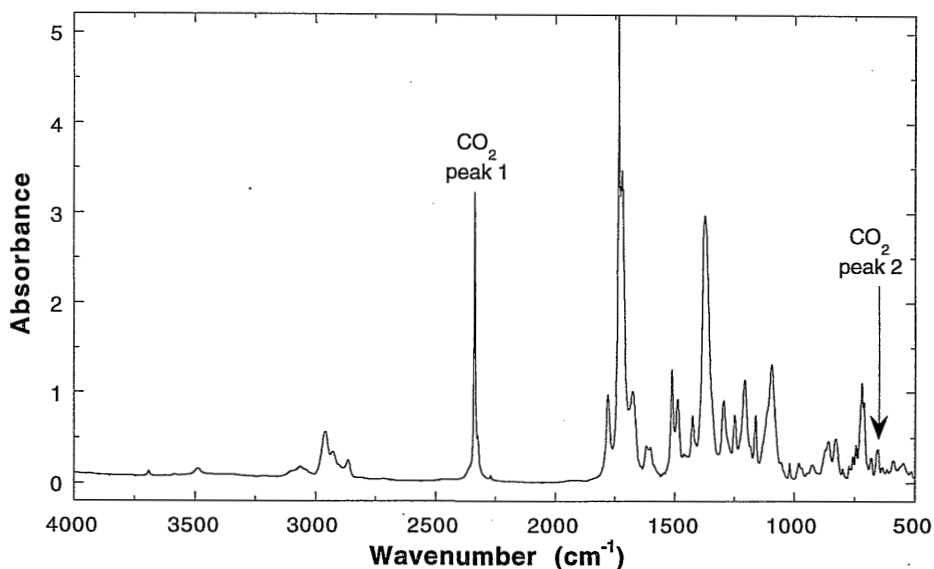


Figure 6.6. FTIR absorption spectrum of a Matrimid film with CO₂ obtained at room temperature. Peak 1 corresponds with the anti-symmetric stretching mode of CO₂ and peak 2 with the bending mode of CO₂.

The anti-symmetric stretching (peak 1) and the bending mode (peak 2) of CO₂ can be distinguished clearly. It is of advantage that the polymer does not absorb in the CO₂ frequency range. A more detailed look at the frequencies of the peaks in the spectra of the untreated and treated Matrimid spectrum did not result in frequency shifts of group frequencies compared to the CO₂ free films. This would suggest no interactions of CO₂ with the polymer chain. This result is in contradiction with the findings of Fried and Li [2] and Puleo et al. [1]. Fried and Li [2] studied cellulose acetate (CA) and polymethylmethacrylate (PMMA) under high CO₂ pressure. In both polymers, the presence of CO₂ caused a shift in the carbonyl peak to higher frequency. A maximum shift of 2 cm⁻¹ was observed at 55 atm. Because the shift was small, Fried and Li [2] attributed the shift to *weak* dipole-dipole interactions between the carbonyl group and CO₂. This interpretation may not be right. If CO₂ interacts with the carbonyl group, the C=O

bond of the carbonyl would become weaker and therefore a shift to lower frequencies should be observed. Puleo et al. [1] observed a shift of 4 cm^{-1} of the carbonyl frequency to higher wavelength in a similar experiment with CA under high CO_2 pressure. They interpreted the frequency shift as follows. The dissolved CO_2 molecules disrupt dipolar interactions between the acetyl groups, which results in an increasing amount of 'free' acetyls. Hence, the $\text{C}=\text{O}$ bond becomes stronger which results in an increase in energy and thereby a frequency shift to a higher wavenumber. However, the significance of the shifts observed by Puleo et al. [1] and Fried and Li [2] may be questionable. Although the spectra are averaged over 100 and 150 scans, the resolution was only 2 cm^{-1} .

It is thought that the CO_2 -polymer interaction might be of a Lewis acid-base type [2,5,16]. CO_2 acts as a Lewis acid (electron acceptor) in the presence of a basic polymer group (electron donor). For example, a free electron pair on the carbonyl oxygen in the polymer chain might interact with the carbon atom of CO_2 . However, no shifts are observed in the Matrimid spectra probably due to the low CO_2 concentration (8 bar) and the low resolution (2 cm^{-1}).

Actually, the carbonyl peak (imide I) and the CNC peak (imide II) show small doublets. This might indicate some interaction of CO_2 with the polymer. However, a more intensive study is necessary to make this plausible.

Comparison of gaseous CO_2 and dissolved CO_2

Since it is difficult to find clear evidence of possible CO_2 -polymer interaction in the polymer part of the spectrum, the remaining discussion in this chapter will focus on the CO_2 absorption peaks. In Figure 6.7, the FTIR absorption spectrum of free CO_2 is compared with the spectrum of CO_2 dissolved in Matrimid.

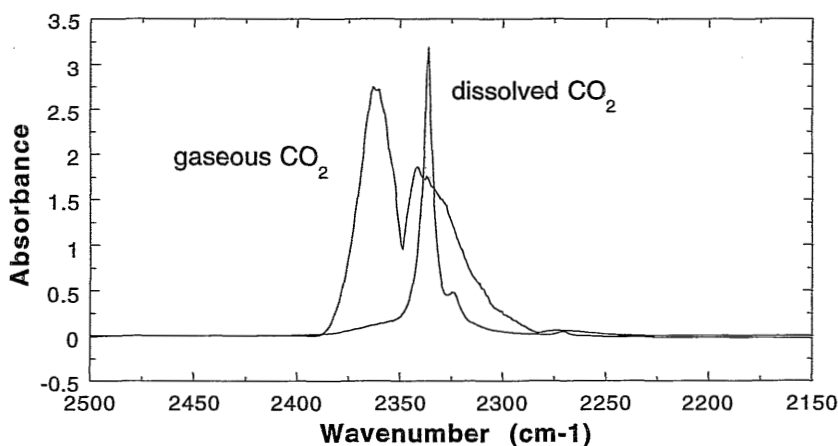


Figure 6.7. FTIR absorption spectrum of gaseous CO_2 and CO_2 dissolved in a Matrimid film in the ν_3 anti-symmetric stretching mode region.

A relatively sharp peak of CO₂ in the Matrimid film is observed when compared to the peak of CO₂ in the gas phase. Several investigators have observed the same change in peak shape when CO₂ changes from the gaseous state to a dissolved state [5,6,17,18]. The centre of the peak is found to be at 2336 cm⁻¹, which is 13 cm⁻¹ lower than the centre of the peak of free CO₂. No P and R branches are observed for the dissolved CO₂. This is due to a loss in rotational freedom of CO₂ dissolved in the polymer. As rotation is hindered, the P and R branches evolve to a single peak that shift to lower frequency as the density or the dielectric environment increases [18].

Higuchi and Nakagawa [6] found different anti-symmetrical stretching frequencies of dissolved CO₂ in different polymers. The wavenumbers varied from 2338.5 cm⁻¹ for CO₂ in polydimethylsiloxane (PDMS) to 2336.5 cm⁻¹ for CO₂ in PDMA-ODA. The frequency shift may be explained again by CO₂-polymer or CO₂-CO₂ interactions. Dipole-dipole interactions weaken the C=O bond and thereby lower the bond energy.

The peak at 2271 cm⁻¹ is the asymmetric stretching mode of the ¹³CO₂ isotope. The spectral width is also smaller for ¹³CO₂ in the dissolved state compared to the gaseous state. The reason is that no peak broadening appears due to rotation, as it is the case with the normal isotope. The new peak at 2324 cm⁻¹ is assigned as a 'hot-band' [17]. The origin of this band will be explained later.

Following the physical picture suggested by the dual-mode sorption theory, one may think that the peaks at 2336 cm⁻¹ and 2324 cm⁻¹ correspond to CO₂ dissolved in the Henry and the Langmuir mode, respectively. However, this interpretation can be rejected because both peaks are observed in rubbery polymers as well [6]. Furthermore, the ratio of the absorbance of the peaks (A_{2336}/A_{2324}) decreased with increasing temperature even for a polymer that passes through its glass transition in the considered temperature range [7]. Hence, if one of the peaks refers to CO₂ in the Langmuir mode that particular peak should disappear as the polymer changes from the glassy to the rubber state. Higuchi and Nakagawa [6,7] interpret therefore that the two postulated states of CO₂ in the Henry and the Langmuir mode in the glassy polymer are similar in the spectroscopic measurements.

CO₂ in the bending mode

If the CO₂-polymer interactions are of the Lewis acid-base type, Kazarian et al. [5] would not expect significant differences in the CO₂ anti-symmetric stretching mode. An explanation may be that a CO₂ molecule can stretch in the same way since only the carbon atom is fixed. Therefore, Kazarian et al. [5] discussed extensively the changes anticipated in the bending mode of CO₂ dissolved in PMMA.

The absorbance spectrum of the bending mode of CO₂ in an untreated and a treated Matrimid film are given in Figure 6.8.

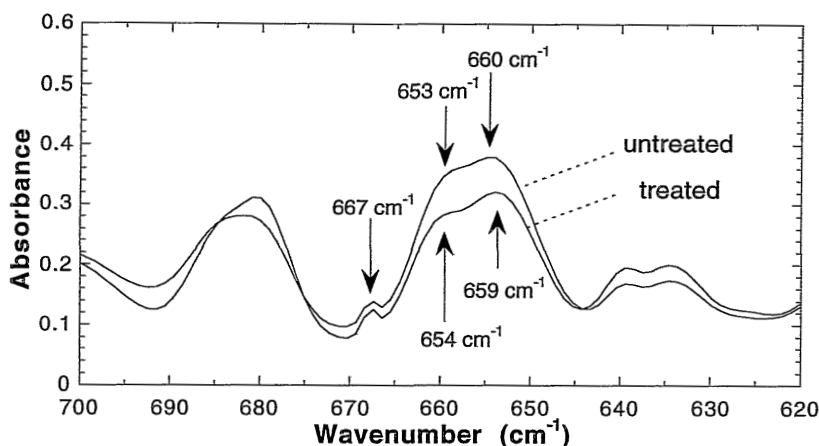


Figure 6.8. FTIR absorption spectrum of CO_2 in the ν_2 bending mode region: Comparison of the bending vibration of CO_2 dissolved in an untreated and a treated Matrimid film.

Three bands can be distinguished. Following the interpretation of Kazarian et al. [5], the small peak at 667 cm^{-1} is from the Q-branch, presumably due to gaseous CO_2 at the the surface of the Matrimid films. The broad absorption bands at 660 and 653 cm^{-1} (659 and 654 cm^{-1} for the treated film) are new compared to gaseous CO_2 and are shifted to lower frequency with respect to the gaseous CO_2 Q-branch. The shift to lower frequency may be attributed again to interaction. If CO_2 interacts with a polar group in the polymer chain then its bond will become weaker and has a lower energy. Kazarian et al. [5] attribute the split ν_2 peaks to the in-plane (higher frequency) and to the out-of-plane (lower frequency) bending mode. The degeneracy of the ν_2 mode should be released due to the different positions of CO_2 with respect to the carbonyl group during interaction as shown in Figure 6.9. These type of interactions are supported by ab-initio calculations [5].

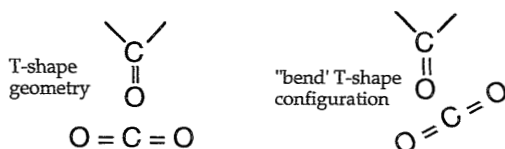


Figure 6.9. Schematic representation of the T-shaped interaction carbonyl- CO_2 interaction configurations [5].

In Figure 6.8, the CO_2 in the treated film shows a clearer splitting of the bending mode than the CO_2 in the untreated film. The significance of the difference between the spectra is not clear at this moment.

No detailed interpretation will be further given at this stage. The wavenumber range below 1000 cm^{-1} (the 'finger-print region') is a very interesting part of the spectrum, because it can give many details, but it is therefore also the most difficult part to interpret. For example no peaks of the polymer are observed in absence of CO_2 , but it may be possible that peaks of the polymer arise in the presence of CO_2 . Their absorbance may be small, but if they are completely masked by the CO_2 band, it can lead to wrong interpretation of the CO_2 absorption bands.

CO_2 in the anti-symmetric stretching mode

The anti-symmetric stretching spectrum of dissolved CO_2 was already shown in Figure 6.7. Compared to gaseous CO_2 , the band-width is narrower in the dissolved state, which is due to a loss in rotational freedom of CO_2 dissolved in the polymer. The more the rotational motion of CO_2 is impeded the narrower the band width will be [17]. Furthermore, only one band appears in the spectrum that correspond to the ν_3 mode. According to Kazarian et al. [5], this suggests that all sorbed CO_2 molecules have the same environment in the polymer matrix. If there were two or more unequal sites for the CO_2 molecules within the polymer matrix, Kazarian et al. [5] would expect more than one band in the anti-symmetric stretching region. Kazarian et al. [5] also observed a weak low-frequency band at 2326 cm^{-1} (2324 cm^{-1} for Matrimid). As mentioned earlier, the band is assigned to be the $(\nu_3-\nu_2)-\nu_2$ hot-band [17]. If the band width of the ν_3 peak is small enough, this absorption band is always observed about 12 cm^{-1} towards lower frequency than the main band [17]. A hot-band transition is a transition from an excited level of one vibration (usually of low frequency) to an excited level of another higher frequency vibration [10]. Due to interactions, the higher energies levels are lowered, which makes transition of electrons in excited states possible. This can also be understood as follows. Vibrations of nuclei are never strictly harmonic, because the stretching of the vibrating bond is not perfectly elastic. Most vibrations are therefore nonharmonic. The vibrational energy levels are no longer equally spaced, as in the case of a harmonic vibration, but they gradually converge as the frequency increases [9]. If a molecule is already in a vibrational excited state it can easily undergo further excitation. Because the energy difference is smaller compared to a transition from the ground state, an absorbance at lower frequency is then obtained.

In the following, the anti-symmetric stretching mode of CO_2 dissolved in an untreated Matrimid film is compared with CO_2 dissolved in a treated Matrimid film. In both cases the hot-band transition is observed, indicating similar interactions between CO_2 and the polymer chain in both cases. No shift in the frequency of the main band was observed for CO_2 in the treated Matrimid film compared to the untreated one. The half band-width (which is the band-width at half of the peak intensity) of the CO_2 peak corresponding to CO_2 in the untreated film was slightly lower than the half band-width of CO_2 in the treated film. A

half band-width of the 2336 cm^{-1} band of 7 and 7.4 was found for CO_2 in the untreated and treated Matrimid film, respectively. For the hot-band, half band-widths of 10 and 10.4 are found for CO_2 dissolved in the untreated and treated Matrimid, respectively.

As stated by Kazarian et al. [5], no significant differences are observed in the ν_3 spectra of CO_2 at the first sight. However, more information is obtained in studying the kinetics of CO_2 in an untreated Matrimid film compared to a treated one. For this purpose the desorption of CO_2 is followed in time for an untreated and a treated Matrimid film. The desorption is measured during 40 minutes in which every 11.5 seconds a spectrum is obtained. The absorption spectra of CO_2 in the anti-symmetric stretching mode in an untreated film are shown in Figure 6.10. For clarity not all 200 spectra are shown, but only 12 covering the whole measurement. Again only the spectra of the untreated film are shown, because without accurate numerical analysis of the peaks no difference can be observed.

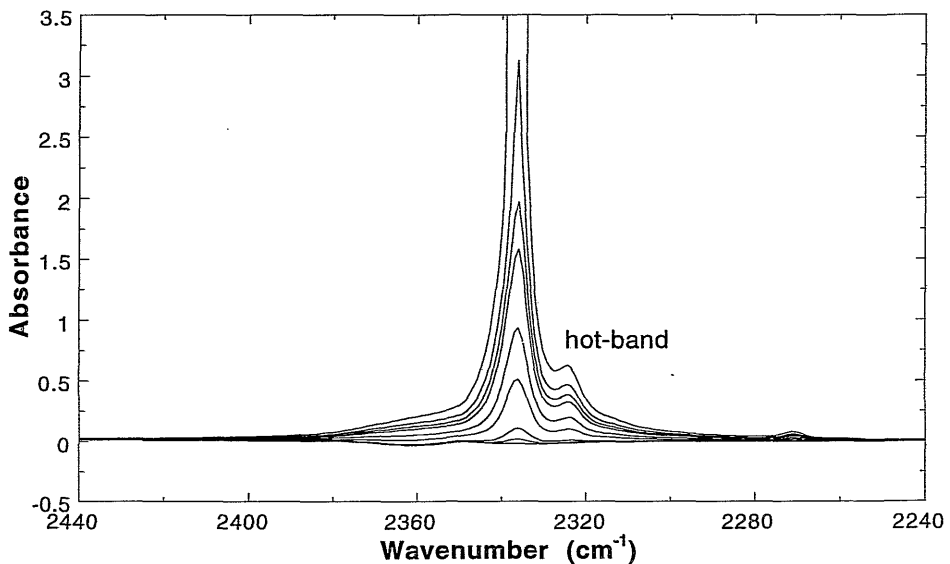


Figure 6.10. FTIR absorption spectrum of the anti-symmetric stretching (ν_3) of CO_2 dissolved in an untreated Matrimid film: Desorption of CO_2 as function of time.

The decrease in CO_2 concentration due to desorption is clearly shown in Figure 6.10. To compare the desorption behaviour of CO_2 in an untreated Matrimid film with a treated film, the peak heights are measured. For quantitative interpretation the peak areas should be measured. However, for qualitative purposes the peak heights are a good approximation considering also that the half band-width of the peaks hardly change during desorption. And, as pointed

out above, the half band-width of the CO_2 absorption peaks in the untreated film are comparable to the CO_2 absorption peaks in the treated film.

The peak intensities of the 2336 and the 2324 cm^{-1} band are plotted as function of time for CO_2 in the untreated as well as in the treated Matrimid film. The peak intensity of the C=C aromatic stretching ($\nu=1488 \text{ cm}^{-1}$) is taken as an internal standard [19,20]. It is assumed that no significant changes occur at this vibration, neither due to the heat-treatment and neither due to interactions. The results are given in Figure 6.11.

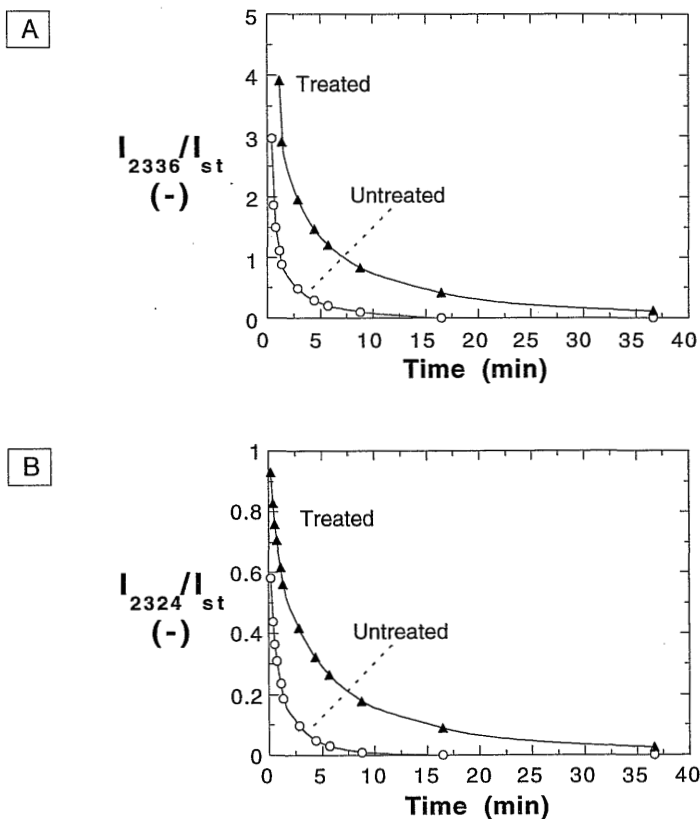


Figure 6.11. Relative absorbance of CO_2 peaks as function of time for: A. the anti-symmetric stretching mode ($\nu=2336 \text{ cm}^{-1}$), B. the 'hot-band' ($\nu=2324 \text{ cm}^{-1}$).

In Figure 6.11A, the relative intensity of the normal anti-symmetric stretching mode of CO_2 in an untreated and a treated Matrimid film is given as function of time. In both cases the relative intensity decreases exponentially. It is clear from this figure that with respect to the polymer the desorption of CO_2 out of the untreated film is quicker compared to the treated film. In case of the untreated

film, no CO₂ absorbance was detected after 17 minutes, whereas the treated film still contains CO₂. Furthermore, with respect to the polymer the initial CO₂ concentration is higher in the untreated film compared to the treated film (see also Figure 4.8). But during desorption the concentration of CO₂ in the untreated film will decrease faster compared to the CO₂ concentration in the treated film. Since more CO₂ desorps from the untreated film, the CO₂ concentration observed in the FTIR measurement is higher for the treated film. A slower desorption of CO₂ out of the treated film could be expected since the diffusion coefficient of CO₂ in the treated film is lower compared to the untreated film (see Chapter 4). In Figure 6.11B, a similar trend is observed for the hot-band transition. It can be concluded from these results that CO₂ behaves differently in an untreated Matrimid film compared to a treated film which is in accordance with the results from the permeation experiments.

Since the hot-band transition occurs due to interaction of CO₂ with its surroundings [17], one may compare the intensity of the hot-band transition of CO₂ in the untreated and the treated Matrimid film. Figure 6.11B would suggest more CO₂-polymer interactions in the treated film compared to the untreated one because the intensities of the hot-band absorbance are higher for CO₂ in the treated film. However, the absorbance of the main band (2336 cm⁻¹) is also higher for CO₂ in the treated film compared to the untreated one. Therefore, the ratio of the intensity of the main band and the hot-band are compared for CO₂ in the untreated and treated film. The ratio (I_{2336}/I_{2324}) as function of time is given in Figure 6.12

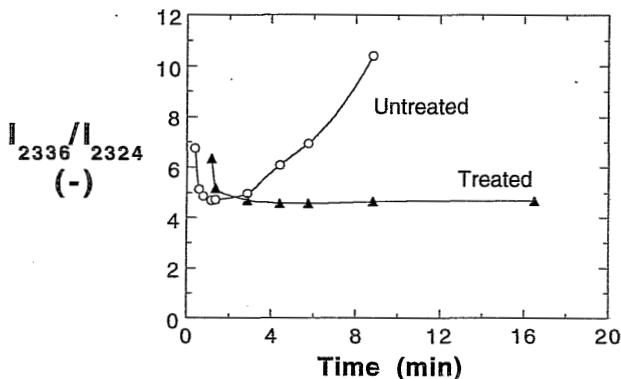


Figure 6.12. Ratio of the anti-symmetric stretching ($\nu=2336\text{ cm}^{-1}$) and the 'hot-band' ($\nu=2324\text{ cm}^{-1}$) intensity of CO₂ as function of time in an untreated and a treated Matrimid film.

At short times, the ratio (I_{2336}/I_{2324}) is slightly higher for the treated film. Furthermore, both films show the same decrease in the ratio of I_{2336}/I_{2324} at short times. This may indicate similar interactions of CO₂ with the untreated

Matrimid matrix and the treated one at short desorption times, i.e. high CO₂ concentration. However, at longer times the ratio increases for the untreated film whereas the ratio for the treated film remains constant. Apparently, the tendency of CO₂ to interact with the untreated polymer becomes lower as desorption time proceeds. This phenomenon may be interpreted in terms of the energy involved in occupying certain positions in the polymer matrix related to the available free volume.

Initially at $t=0$, both films contain a high CO₂ concentration in the polymer matrix. In both cases interaction of CO₂ is present with the interaction sites (polar groups) on the polymer chain. In the infrared spectra these interactions are represented by the hot-band absorption at 2324 cm⁻¹.

When desorption starts, the concentration of CO₂ in both films will decrease. For short times, interaction of CO₂ with the interaction sites on the polymer are still there as supported by the hot-band in the spectrum. However with respect to the peak at 2336 cm⁻¹, the concentration of the interacting CO₂ has decreased more, resulting in a decrease in the ratio of I_{2336}/I_{2324} . Apparently, the intensity of the hot-band transition (2324 cm⁻¹) with respect to the normal anti-symmetrical stretching vibration (2336 cm⁻¹) remains similar for the untreated compared to the treated Matrimid film. This is shown in Figure 6.12 by a similar decrease in the ratio I_{2336}/I_{2324} .

As desorption proceeds, the hot-band intensity of CO₂ in the untreated film decreases faster compared to the intensity corresponding to the normal anti-symmetric stretching. Hence, less CO₂ molecules are in the neighbourhood of the interaction sites of the polymer chain. Apparently, occupying the sorption sites in a near distance of the interaction sites is not the only possibility to lower the energy. Occupying a sorption site further away from the interaction site seems to be competitive. In case of the untreated film the CO₂ molecules have the possibility to move to a sorption site of lower energy away from the interaction sites because of the high free volume which was already present or has been created due to plasticization. In case of the treated film this exchange of sorption sites is less likely because of the lower free volume. Also, the polymer matrix of the treated film does not have the possibility to create a larger free volume since it is a network. The polymer morphology is kept by the crosslinks or the charge transfer complexes. In case of the treated film the interaction sorption sites are occupied as long as there are CO₂ molecules in the film, which might be an explanation for the simultaneous decrease in intensity of the ratio I_{2336}/I_{2324} .

The qualitative picture of the available free volume is supported by Wessling et al. [21]. They gave a qualitative model for the hysteresis phenomenon between the dilation and the consolidation isotherm induced by sorption and desorption. The remaining free volume right after desorption is larger than the initial free volume before sorption as indicated by a higher CO₂ concentration in the polymer film in the consolidation cycle compared to the dilation cycle. The larger free volume as a result of dilation does not collapse to the original free volume because chain relaxation is much slower than the desorption of the CO₂

molecules.

To obtain a picture of the underlying reasons why an untreated Matrimid film plasticizes and a treated one not, the above interpretation should be considered for the sorption process as well. However, no infrared spectra are available for the sorption process of CO₂ into the polymers. Although there is no direct evidence for the fact that the first CO₂ molecules will not occupy the interaction sites first, the desorption experiments support the fact that the number of polar groups in the polymer chain is not a measure for the tendency of a polymer to plasticize. From the desorption experiments one may conclude that the sorption sites at the interaction sites of the polymer chain are not energetically favourable. The fact that the polymer plasticizes is therefore a matter of concentration as hypothesized in Chapter 3. Chapter 3 suggests that a critical CO₂ concentration is necessary to plasticize the polymer. At that concentration the CO₂ molecules have the ability to increase the free volume in case of the untreated film to such an extent that the permeability increases significantly absolutely and in time. The chain mobility increases because there is more space to move and a higher chain mobility is defined as plasticization. In case of the treated film, an increase in free volume and chain mobility is suppressed due to the network resulting in no plasticizing ability.

6.4. Conclusions

- The infrared analysis did not result in further elucidation of the crosslink mechanism of the Matrimid film, because no differences are observed in the spectra of the untreated compared to the treated film.
- The spectra of CO₂ dissolved in the Matrimid film could clearly be distinguished from gaseous CO₂. The peaks corresponding to the anti-symmetric stretching mode of CO₂ dissolved in the film have smaller bandwidths compared to gaseous CO₂ and are shifted to lower frequency.
- The peak corresponding to CO₂ dissolved in the Matrimid film showed a small peak at lower frequency attributed to a hot-band. The observed hot-band transition indicates interaction of CO₂ with the polymer matrix and is observed for the untreated as well as the treated Matrimid film.
- The change in the ratio of the peak intensity of the asymmetrical stretching vibration of CO₂ and the hot-band transition for CO₂ dissolved in the untreated Matrimid film differs significantly from the ratio of the treated film. At longer desorption time the ratio increased for untreated film. The increase indicates a faster disappearance of the interaction sorption sites. The interaction sorption sites may be not energetically favourable. From these results, it is concluded that the plasticization is not determined by the amount of polar groups in the polymer chain. The hypothesis that a critical concentration is necessary to induce plasticization is supported here.

6.5. References

- [1] Puleo, A.C., Paul, D.R., Kelley, S.S., The effect of degree of acetylation on gas sorption and transport behavior in cellulose acetate, *J. Membrane Sci.*, 47 (1989) 301-332
- [2] Fried, J.R., Li, W., High-pressure FTIR studies of gas-polymer interactions, *J. Appl. Polym. Sci.*, 41 (1990) 1123-1990
- [3] Brolly, J.B., Bower, D.I., Ward, I.M., Diffusion and sorption of CO₂ poly(ethylene terephthalate) and poly(ethylene naphthalate), *J. Polym. Sci., Polym. Phys. Ed.*, 34 (1996) 769-780
- [4] Webb, J.A., Bower, D.I., Ward, I.M., Cardew, P.T., Infra-red study of diffusion of CO₂ in highly oriented polyethylene films, *Polymer*, 33 (1992) 1321-1322
- [5] Kazarian, S.G., Vincent, M.F., Bright, F.V., Liotta, C.L., Eckert, C.A., Specific intermolecular interaction of carbon dioxide with polymers, *J. Am. Chem. Soc.*, 118 (1996) 1729-1736
- [6] Higuchi, A., Nakagawa, T., Infrared spectroscopic studies of CO₂ sorbed in glassy and rubbery polymeric membranes, *J. Polym. Sci., Polym. Phys. Ed.*, 32 (1994) 149-157
- [7] Higuchi, A., Nakajima, T., Morisato, A., Ando, M., Nagai, Nakagawa, T., Estimation of diffusion and permeability coefficients of CO₂ in polymeric membranes by FTIR method, *J. Polym. Sci., Polym. Phys. Ed.*, 34 (1996) 2153-2160
- [8] Pyrkov, A.V., Makrova, N.I., Bednykh, E.I., IR spectroscopy of carbon dioxide dissolved in poly(methyl methacrylate), *Polymer Sci., Ser. B.*, 36 (1994) 1005-1006
- [9] Straughan, B.P., Walker, S., (Eds.), *Spectroscopy*, John Wiley & Sons, New York, V2 (1976)
- [10] Colthup, N.B., Daly, L.H., Wiberley, S.E., *Introduction to infrared and Raman spectroscopy*, third edition, Academic press, New York, (1990)
- [11] Schrader, B., (Ed.), *Infrared and Raman spectroscopy. Methods and applications*, VCH Publishers, New York, (1995)
- [12] Guerra, G., Choe, S., William, D.J., Karasz, F.E., MacKnight, W.J., Fourier transform infrared spectroscopy of some miscible polybenzimidazole/polyimide blends, *Macromolecules*, 21 (1988) 231-234
- [13] Dine-Hart, R.A., Wright, W.W., A study of some properties of aromatic imides, *Die Makromol. Chemie*, 143 (1971) 189-206
- [14] White, L.S., Blinka, T.A., Kloczewski, H.A., Wang, I-f., Properties of a polyimide gas separation membrane in natural gas streams, *J. Membrane Sci.*, 103 (1995) 73-82
- [15] Ishida, H., Huang, M.T., Molecular level study of the crystallization of a thermoplastic polyimide by infrared spectroscopy, *J. Polym. Sci., Polym. Phys. Ed.*, 32 (1994) 2271-2282
- [16] Meredith, J.C., Seminario, J.M., Kazarian, S.G., Eckert, C.A., Quantitative equilibrium constants between CO₂ and Lewis-bases from FTIR spectroscopy, *J. Phys. Chem.*, 100 (1996) 10837-10848
- [17] Cunliffe-Jones, B.D., Perturbation of some vibrational bands in solution, *Spectrochim. Acta*, 25A (1969) 779-791
- [18] Yee, G.G., Fulton, J.L., Smith, R.D., Fourier transform infrared spectroscopy of molecular interactions of heptafluoro-1-butanol or 1-butanol in supercritical carbon dioxide and supercritical ethane, *J. Phys. Chem.*, 96 (1992) 6172-6181
- [19] Pryde, C.A., FTIR studies of polyimides. II. Factors affecting quantitative measurement, *J. Polymer Sci. Polym Chem. Ed.*, 31 (1993) 1045-1052
- [20] Wilson, D., Stenzenberger, H.D., Hergenrother, P.M., *Polyimides*, Blackie & Son, Glasgow, (1990)
- [21] Wessling, M., Huisman, I., Boomgaard, Th. v.d., Smolders, C.A., Dilation kinetics of glassy, aromatic polyimides induced by carbon dioxide sorption, *J. Polym. Sci., Polym. Phys. Ed.*, 33 (1995) 1371-1384

Process calculations

7.1. Introduction

The efficiency of a gas separation process is mainly determined by the flux, the purity of the product gas and the recovery. The latter is the fraction of the gas in the feed stream recovered as product. Intrinsic membrane properties such as permeability and selectivity determine these parameters. Furthermore, processing parameters such as the total and partial pressures on the feed and permeate side and the feed flow rate influence the separation efficiency. The arrangement or staging of the membrane elements is also important. It is often impossible to separate two components adequately in one pass through a membrane module because of the limitations of membrane selectivity and achievable pressure ratio. Thus multistage processes may be required and an optimization of the process is necessary to achieve product costs which are as low as possible

The basic membrane separation unit is the permeator or the separator providing a one-stage process. A permeator is generally considered as a 'black box' with two compartments separated by a membrane. A feed stream enters the permeator and is divided into two outlet streams. The part that passes through the membrane is referred to as permeate and the non-permeated part as the retentate. Depending on the application either the permeate or the retentate can be the product. In natural gas treatment, the retentate stream enriched in methane is the product. In hydrogen separations, hydrogen is concentrated in the permeate and is the product.

The relative directions of the feed and permeate flow inside the module may affect the performance of a membrane separator as well. For membrane performance analysis some idealized flow patterns are commonly used: perfect mixing, cross flow, countercurrent and cocurrent flow. The mathematical analysis of these flow patterns has been described extensively in the literature [1-4]. Sengupta and Sirkar [5] summarized the papers describing the different permeation models.

In the literature few studies are available on multistage processes because they are difficult to evaluate and optimize, even with the aid of computer programs [6]. In general, calculations based on a single-stage membrane configuration give a good indication on the importance of process parameters and their optimization. Multistaged processes are often used when product recovery and/or high product purity are important. Further optimization is then achieved by permeate recycling or using the retentate as feed in a next stage. Spillman [6] and Bhide and Stern [7,8] explain a series of process design options and illustrate the importance of factors such as single- versus multistage configuration, feed compression and permeate recycle. Recently, Lababidi et al. [9] developed optimization models and cost functions for three gas separation systems, which include single stage, two stage and a continuous membrane column.

The main objective of the work reported in this chapter is to compare the CO₂/CH₄ separation performance in case of an untreated Matrimid membrane and a membrane stabilized against plasticization. Simple process calculations may reveal valuable information to what extent stabilized membranes show improved process performance. This study is limited to a parametric evaluation based on an equal inlet stream of 1 m³/h. Since gas separation membrane systems scale linearly with gas feed volumes, the process can be scaled-up simply by adding more membrane area [6]. Furthermore, a certain product purity (% CH₄) and product flow (m³/h) is always demanded. The desired product purity is achieved by calculating the membrane area required to reach that purity. The result of the calculations are product flow, product recovery and methane losses. Another approach is to postulate a required product stream for example 1 m³/h. However, the calculations principally lead to the same information as the calculations with constant feed flow, only the direction of calculation is reversed. To achieve a certain product purity the membrane area should be calculated. This will then lead to different inlet streams in case of an untreated or a stabilized membrane. Outputs of the calculations are also recovery and methane losses.

In Section 7.2 the permeator analysis based on experimental permeation data are presented and the economics are considered in Section 7.3.

7.2. Permeator analysis

7.2.1. Background

To compare the gas separation performance of the untreated and heat-treated Matrimid membranes, a single-stage membrane process with cross flow configuration is considered in the analysis. A schematic drawing is given in Figure 7.1. The feed stream that enters the module is divided into a permeate stream perpendicular to the feed stream and a retentate stream. The CO₂ permeates the membrane more readily than CH₄ and therefore the retentate

stream is the product.

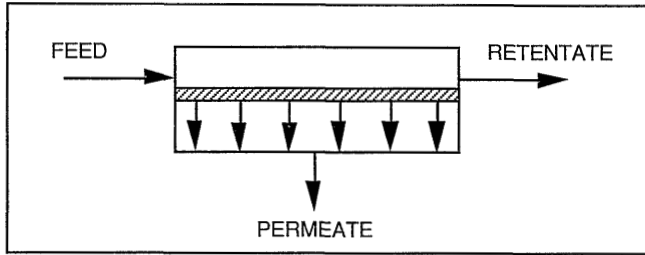


Figure 7.1. Schematic representation of a single-stage membrane process with cross flow configuration.

The aim of this work is to compare the module performance of membranes having a tendency to plasticize with stabilized membranes. The partial CO_2 pressure should therefore be high enough to induce plasticization of the unstabilized membrane. In natural gas upgrading, gas pressures up to 140 bar with carbon dioxide compositions ranging from 5-40% are reached [6]. The maximum operating pressure in this work is 50 bar. This is more than a factor two lower. However, the field situation can be simulated with a mixture containing higher CO_2 concentration than in the field case. A feed stream consisting of 45 mol % CH_4 in CO_2 is considered. At 50 bar total feed pressure, the partial CO_2 pressure corresponds, for example, with 100 bar field gas containing 27.5 mole % CO_2 . The gas mixture considered in this work is upgraded to a pipe line quality level of 98 % [6].

As the gas mixture traverses over the membrane surface its composition changes in any point along the membrane surface. The CO_2 gas molecules are removed from the feed stream so that the CH_4 is concentrated in the retentate. Due to these changes in mole fractions of the gases along the membrane surface, the partial pressures of the gases also change from one unit area to the other. The partial pressure decreases for CO_2 and increases for CH_4 . Consequently, the permeability changes from one unit of area to the other, because in most cases the permeability depends on pressure. The permeate flow equation must therefore be evaluated as an integral over the entire flow path [3,10]:

$$Q_{P,i} = \int \frac{P_i(p_i^f)}{\ell} (p_i^f - p_i^p) dA \quad (7.1)$$

where $Q_{P,i}$ is the total molar permeate flow of component i , $P_i(p_i^f)$ the partial pressure dependent permeability of component i , ℓ the membrane thickness, p_i^f the partial feed pressure and p_i^p the partial permeate pressure of component i . This integral can be approximated by a summation over as many as possible small intervals with the differential area dA . For each unit area or element, a

new feed gas composition has to be determined. The feed flow of the next element is identical to the retentate flow from the previous element. The retentate flow of the last element is the retentate flow of the whole module. The permeate flow of the whole module is the sum of all permeate flows of the elements. This principle is schematically given in Figure 7.2.

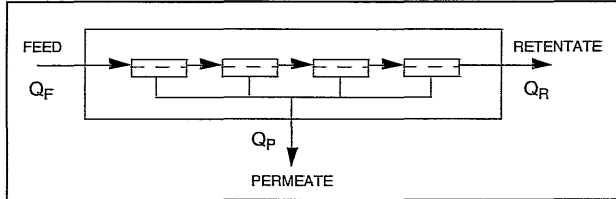


Figure 7.2. Schematic representation of a membrane system divided in differential elements.

The total feed flow (Q_F) equals the sum of the total permeate flow (Q_P) and the retentate flow (Q_R):

$$Q_F = Q_P + Q_R \quad (7.2)$$

where the total permeate flow is the sum of the CO_2 permeate flow ($Q_{\text{CO}_2}^P$) and the CH_4 permeate flow ($Q_{\text{CH}_4}^P$):

$$Q_P = Q_{\text{CO}_2}^P + Q_{\text{CH}_4}^P \quad (7.2a)$$

$$\text{and} \quad Q_{\text{CO}_2}^P = \sum_{i=1}^n q_{\text{CO}_2}^P(i) \quad (7.2b)$$

$$Q_{\text{CH}_4}^P = \sum_{i=1}^n q_{\text{CH}_4}^P(i) \quad (7.2c)$$

In Equations (7.2b) and (7.2c), n is the number of elements. The flow rate of CO_2 through the membrane in an element (n) is:

$$q_{\text{CO}_2}^P(n) = \left[\frac{P_{\text{CO}_2}(p_{\text{CO}_2}^f(n))}{\ell} (X_{\text{CO}_2}^f(n) p^f - X_{\text{CO}_2}^P(n) p^P) \right] dA \quad (7.3)$$

where P_{CO_2} is the permeability of carbon dioxide at partial pressure $p_{\text{CO}_2}^f(n)$, ℓ the membrane thickness, $X_{\text{CO}_2}^f(n)$ and $X_{\text{CO}_2}^P(n)$ the mole fraction of CO_2 in the feed and permeate, respectively, p^f is the feed pressure, p^P the permeate pressure and dA is the membrane area of element (n). A corresponding equation is valid for the flow rate of CH_4 through the membrane.

The mole fraction of CO_2 in the permeate of element (n) is then given by Equation (7.4):

$$X_{\text{CO}_2}^P(n) = \frac{q_{\text{CO}_2}^P(n)}{q_{\text{CO}_2}^P(n) + q_{\text{CH}_4}^P(n)} \quad (7.4)$$

For a binary mixture, Equation (7.5) for the mole fraction of CH_4 in the permeate of element (n) is valid:

$$X_{\text{CH}_4}^{\text{p}}(n) = 1 - X_{\text{CO}_2}^{\text{p}}(n) \quad (7.5)$$

By combining Equation (7.3), (7.4) and (7.5), the mole fraction of CO_2 in the permeate of element (n) can be written as:

$$X_{\text{CO}_2}^{\text{p}}(n) = B - \left[B^2 - \frac{\alpha}{(\alpha-1)} \frac{P^{\text{f}}}{P^{\text{p}}} X_{\text{CO}_2}^{\text{f}}(n) \right]^{0.5} \quad (7.6)$$

$$\text{with } B = 0.5 \left[1 + \frac{1}{(\alpha-1)} \frac{P^{\text{f}}}{P^{\text{p}}} + \frac{P^{\text{f}}}{P^{\text{p}}} X_{\text{CO}_2}^{\text{f}}(n) \right] \quad (7.6a)$$

$$\text{and } \alpha^* = \frac{P_{\text{CO}_2}}{P_{\text{CH}_4}} \quad (7.6b)$$

Weller and Steiner [1] were the first who derived this analytical expression for the enrichment of a binary mixture in a single-stage membrane process with complete mixing of the feed flow. Equation (7.6) is known as the Weller-Steiner Case I. This equation can also be used for cross flow configuration if the module is divided in an infinite number of small modules in which the complete mixing case can be considered. This is known as the Weller-Steiner Case II solution. For large differences between the mole fraction in the feed and retentate ($X^{\text{f}}/X^{\text{r}} < 0.5$), Hogsett and Mazur recommend to use the natural log mean average of the CO_2 mole fraction in the feed in stead of $X_{\text{CO}_2}^{\text{f}}$:

$$\bar{X}_{\text{CO}_2}^{\text{f}} = \frac{X_{\text{CO}_2}^{\text{f}} - X_{\text{CO}_2}^{\text{r}}}{\ln(X_{\text{CO}_2}^{\text{f}}/X_{\text{CO}_2}^{\text{r}})} \quad (7.7)$$

In this work, each element is made small enough ($X^{\text{f}}/X^{\text{r}} \gg 0.5$) to use the complete mixing approximation.

When the mole fractions in the permeate and the permeate flow of an element (n) are known the retentate mole fractions can be calculated with the mass balance of CO_2 :

$$X_{\text{CO}_2}^{\text{f}}(n) * Q_{\text{F}}(n) = X_{\text{CO}_2}^{\text{p}}(n) * Q_{\text{P}}(n) + X_{\text{CO}_2}^{\text{r}}(n) * Q_{\text{R}}(n) \quad (7.8)$$

$$\text{or } Q_{\text{CO}_2}^{\text{f}}(n) = Q_{\text{CO}_2}^{\text{p}}(n) + Q_{\text{CO}_2}^{\text{r}}(n) \quad (7.9)$$

The mole fraction of CH_4 in the retentate is then given by:

$$X_{\text{CH}_4}^{\text{r}}(n) = 1 - X_{\text{CO}_2}^{\text{r}}(n) \quad (7.10)$$

The retentate stream is the product stream. An important question is therefore how much of the initially present methane is recovered in the retentate. The

recovery is defined as:

$$\text{Recovery} = \frac{Q_{\text{CH}_4}^{\text{R}}}{Q_{\text{CH}_4}^{\text{F}}} * 100\% \quad (7.11)$$

In many design calculations, constant permeabilities are assumed. As was shown in the single and mixed gas permeation experiments, this assumption is not justified. The permeabilities are a function of the partial feed pressure. Consequently, the selectivity changes. These factors were taken into account in calculating the mole fraction of CO₂ in the permeate with Equation (7.6). As Li et al. [11] and Ettouney et al. [12] have done, permeation functions are composed from the experimentally determined permeabilities as function of the partial feed pressure. All data are fitted with a second order polynomial of the form:

$$P_i(p_i) = A + B * (X_i^f * p^f) + C * (X_i^f * p^f)^2 \quad (7.12)$$

where A, B and C are the adjustable parameters. This equation has no physical meaning, but is a mathematical tool to interpolate the permeability at any desired pressure. For the CH₄ permeability of the stabilized membrane a constant value is taken, because no pressure dependence of the permeability was observed.

7.2.2. Results and discussion

A single-stage membrane module is divided in 200 elements. This number was found sufficient enough to reach convergence in the calculations. The pressure loss inside the permeator has been neglected, because the exact configuration of the permeator is not known. The total feed flow is 1 m³/h and the permeate pressure 1 bar. The membrane thickness is assumed to be 1 μm, the operating temperature 35 °C and the gas mixture to be separated consists of 55% CO₂ and 45% CH₄. The following permeation functions are derived from the permeation curves presented in Figure 4.7 of Section 4.5:

Untreated Matrimid membrane:

$$P_{\text{CO}_2}(p_{\text{CO}_2}^f) = 11.112 - 0.39673 p_{\text{CO}_2}^f + 0.012591 (p_{\text{CO}_2}^f)^2 \quad (7.13a)$$

$$P_{\text{CH}_4}(p_{\text{CH}_4}^f) = 0.24421 - 0.005494 p_{\text{CH}_4}^f + 0.00049382 (p_{\text{CH}_4}^f)^2 \quad (7.13b)$$

Stabilized Matrimid membrane:

$$P_{\text{CO}_2}(p_{\text{CO}_2}^f) = 5.8085 - 0.15427 p_{\text{CO}_2}^f + 0.002863 (p_{\text{CO}_2}^f)^2 \quad (7.13c)$$

$$P_{\text{CH}_4}(p_{\text{CH}_4}^f) = 0.11 \quad (7.13d)$$

In these functions $p_{\text{CO}_2}^f$ and $p_{\text{CH}_4}^f$ are the partial pressure for CO₂ and CH₄, respectively, and are given in bar. The permeabilities are given in Barrer (1 Barrer=10⁻¹⁰ cm³(STP)cm/cm² s cmHg). The functions are valid for a pressure

range up to 50 bar at 35 °C. The stabilized membrane has experienced a heat-treatment for 30 minutes at 350 °C.

The membrane area required to achieve 98% CH₄ purity in the retentate was calculated as a function of the total feed pressure. Simultaneously, the corresponding CH₄ recovery and the total product stream in m³/h were calculated. The results are given in Figure 7.3.

Figure 7.3A shows the membrane area needed as a function of total feed pressure for the untreated and stabilized membrane. The membrane area decreases with increasing feed pressure and is higher for the stabilized membrane because of the lower permeabilities. In Figure 7.3B the CH₄ recovery is given as function of feed pressure. For both membranes the recovery first increases with increasing feed pressure. This is due to a decreasing permeability with increasing feed pressure. Then the membrane area decreases with increasing pressure as shown in Figure 7.3A. If less gas permeates more gas remains in the retentate stream. In case of the untreated membrane the recovery decreases for pressures higher than 20 bars due to CO₂ plasticization. Above the plasticization pressure the permeabilities of CO₂ as well as CH₄ increase with increasing feed pressure. More CH₄ permeates, resulting in a lower recovery in the retentate stream. The stabilized membrane showed constant permeabilities at pressures where an untreated membrane plasticized. And since the decrease in membrane area is relatively less at elevated pressures, the recovery of the stabilized membrane remains constant with further increasing feed pressure. If recovery of more than 90% is required the single-stage membrane must be changed into a multi-stage system.

Figure 7.3C shows the product streams as function of feed pressure of the untreated and stabilized membrane. At low feed pressures the product stream increases because the permeabilities decrease with increasing feed pressure. The module always permeates more gas with increasing feed pressure, but it permeates relatively less with increasing pressure due to the decreasing permeability. With further increase in feed pressure the untreated membrane starts to permeate more gas due to CO₂ plasticization. The remaining retentate stream is therefore lower. The stabilized membrane shows an almost constant product flow at higher feed pressures. Caution, however, has to be taken, as the product streams are obtained with different membrane areas at different pressures. Figure 7.3C therefore cannot be interpreted without Figure 7.3A.

Additionally the influence of product purity on the membrane required area and the corresponding CH₄ recovery are studied. The product purity was varied between 90 to 99% at 50 bar total feed pressure. The results are given in Figure 7.4.

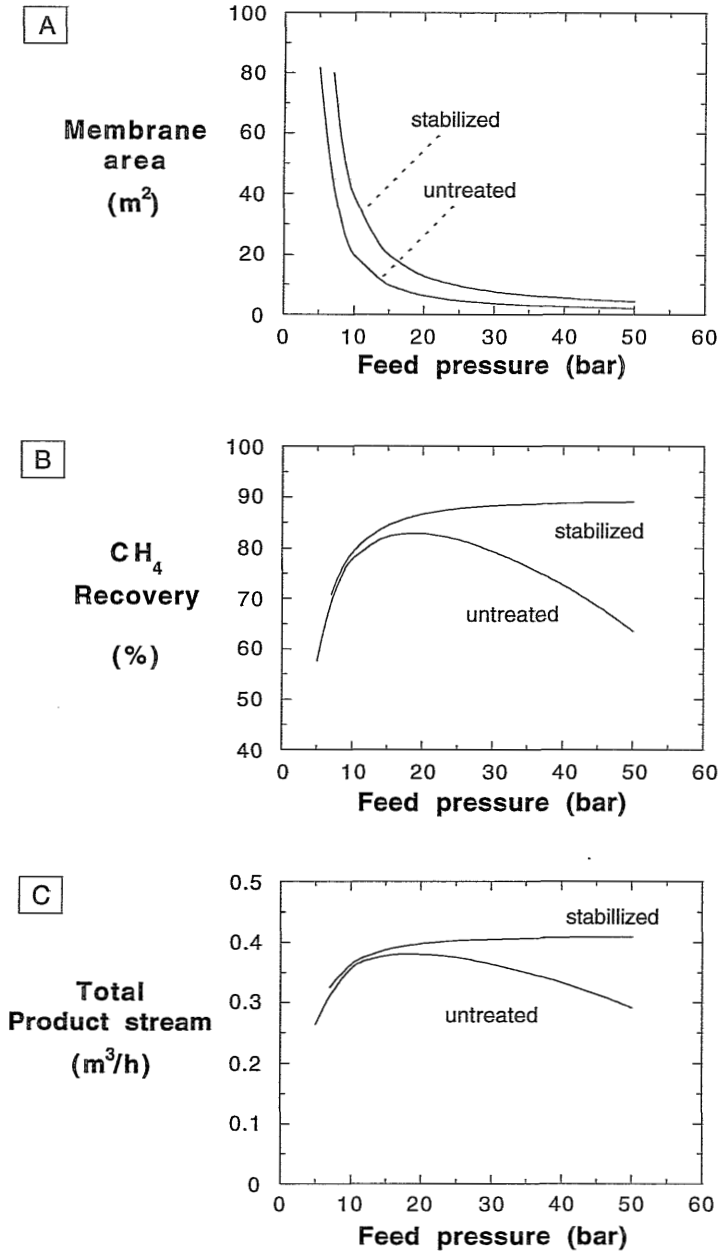


Figure 7.3. Membrane area, CH₄ recovery and product stream as a function of feed pressure for an untreated and a stabilized Matrimid membrane. Feed flow: 1 m³/h containing 55% CO₂, CH₄ purity in the retentate: 98%.

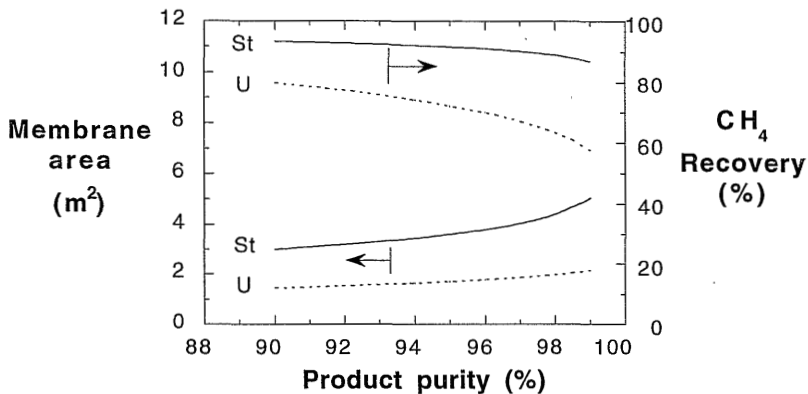


Figure 7.4. Membrane area and CH_4 recovery as function of product purity for an untreated (dashed lines) and a stabilized Matrimid membrane at 50 bar total feed pressure (U= untreated, St=treated). Feed flow: $1 \text{ m}^3/\text{h}$.

To achieve higher product purities more membrane area is needed for the untreated as well as the stabilized membrane. Simultaneously the recovery decreases with increasing product purity. An explanation for this is that more gas must permeate to remove more CO_2 . From these results one can conclude that an untreated membrane is favoured because much lower membrane area is needed to achieve high purity. On the other hand the recovery for the untreated membrane decreases more drastically than for the stabilized membrane resulting in a larger loss of the desired methane. The trade-off between higher purity with less membrane area but lower CH_4 recovery and the benefit of higher CH_4 recovery but larger membrane area can be evaluated by simple cost accounting calculation.

7.3. Cost accounting

7.3.1. Background

As shown in the previous section, simple design calculations gave insight in the parameters that play a role in optimizing an enrichment process, such as feed pressure, required membrane area, demanded retentate purity and resulting product recovery. To find the optimal combination of these parameters, a cost price analysis must be carried out. The analysis will show the importance of the different contributions to the total cost. For example, how the cost compare with the income from gas sales when the value of methane losses is taken into account. Extensive and detailed case studies are carried out by Spillman [6] and

Bhide and Stern [7,8].

Two cost items that can be distinguished are: capital investment and operating cost. The first is the sum of installed membranes, compressors, piping and valves. In practice, the membrane installation costs often determine 25% of the total capital investment. Hence, without every detail of the system, four times the membrane cost is a good approximation for the investment. The second, the total operating cost are the yearly expenses, which include membrane replacement, product losses, power for the compressors and maintenance. The economic parameters used in the calculations are summarized in Table 7.1.

Table 7.1. *Assumed economic parameters.*

Cost price membrane module:	Dfl 200.00/m ² [8]
Investment	4* price membrane module
Depreciation	10% of investment/year
Labour and maintenance	5% of investment/year
Energy price	Dfl 0.20/kWh
Membrane life time	5 years
Gas sales (pipe line quality: 98% CH ₄)	Dfl 0.50/m ³ and Dfl 1.00/m ³

In this economic analysis the benefit from gas sales are compared with the annual operational cost in case an untreated Matrimid membrane is used and a stabilized one.

The annual operational cost is calculated by the sum of the following items:

- Membrane replacement = (1/life time) * area (m²) * 200 (Dfl/m²)
- Labour and maintenance = 0.05 * 4 * area (m²) * 200 (Dfl/m²)
- Product loss = CH₄ loss (m³) * price/m³
- Energy consumption = power (P) * 24 * 365 * Dfl 0.20/kWh.

The power requirement can be calculated with Equation (7.14) as isothermal compression is assumed [13]:

$$P = \frac{nRT}{\eta} \ln \left(\frac{P^f}{P^i} \right) \text{ (kW)} \quad (7.14)$$

with n = number of moles to be compressed per second
 η = compressor efficiency (=0.7).

The benefit from gas sales is expressed as the pay-back time, which is defined as :

$$\text{Pay-back time} = \frac{\text{Investment}}{\text{Cash-flow}} \text{ (year)} \quad (7.15)$$

$$\text{with Investment} = \text{area (m}^2\text{)} * 4 * 200 \text{ (DFI/m}^2\text{)} \quad (7.15a)$$

$$\text{Cash-flow} = \text{gas sales} - \text{operational cost (DFI/year)} \quad (7.15b)$$

$$\text{gas sales} = \text{product (m}^3\text{)} * \text{price/m}^3 \text{ (DFI/m}^3\text{)} \quad (7.15c)$$

The pay-back time is the time necessary to obtain the initial investment back from the cash-flow. The disadvantage of this pay-back time is that the depreciation is not accounted for. However, it is a useful criterion for an initial judgement of projects [14].

The capital investment as well as the annual operating cost are dominated by the membrane area required. Some general trade-offs can be made. Low membrane area requirements can reduce both costs. In case of the operating cost, membrane replacement is a large item if membrane life time is short. As was shown in the previous section, the membrane area is determined by the operating pressure. Membrane area requirements decrease with increasing pressure. A high operating pressure should therefore be favourable. However, with increasing feed pressure the compressor power needed also increases. Hence, the energy consumption increases. To optimize the process, the increase in cost due to energy consumption and methane loss should be balanced against the benefit of lower membrane area requirements. In the following, the contributions to the annual operating costs are compared in case an untreated and a stabilized membrane is used.

7.3.2. Results and discussion

The annual operation cost are calculated as the sum of the cost for membrane replacement, labour and maintenance, energy consumption and cost for CH₄ loss. A membrane life time of five years is considered. All calculations are carried out for an enrichment of the product up to 98% CH₄. The data of the membrane area requirements, volume of the product stream and methane losses obtained in Subsection 7.2.2 are used as input for the economic calculations.

Figure 7.5 shows the annual operating cost as function of feed pressure for an untreated and a stabilized Matrimid membrane at gas prices of DFI 0.50/m³ and DFI 1.00/m³. The actual gas price per m³ is about DFI 0.50. In the future this price may be twice as high as it is today. In the calculations a gas price of DFI 1.00/m³ is therefore considered for comparison.

The annual operational cost initially decrease with increasing feed pressure for both membranes irrespectively of the gas price. As was shown in the previous section, the membrane area needed to achieve a product purity of 98% decreases with increasing feed pressure. The operational cost decrease therefore because a large part of the cost is determined by the required membrane area. At lower feed

pressures, the untreated membrane has lower annual cost compared to the stabilized membrane because it needs less membrane area due to higher permeabilities, see also Figure 7.3A. At higher feed pressures, the annual cost of the untreated membrane increase whereas the cost for the stabilized membrane still decrease. Hence, at feed pressures up to 22 bar the untreated membrane is more attractive than the stabilized membrane. However, the target was to select a membrane material for use at much higher feed pressure, such as 50 bar or higher. At these conditions the stabilized membrane becomes attractive irrespective of the gas price. The annual cost of the stabilized membrane are then lower compared to the untreated membrane for both gas prices.

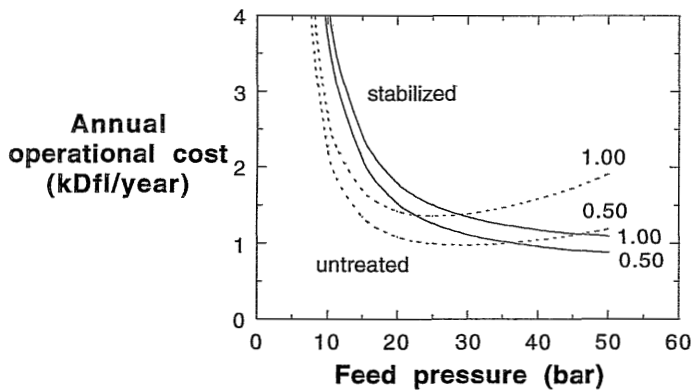


Figure 7.5. Total annual cost as function of feed pressure for an untreated (dashed lines) and a stabilized Matrimid membrane (solid line) at gas prices of Dfl 0.50/m³ and Dfl 1.00/m³.

The annual cost are lower for both membranes at a gas price of Dfl 0.50 compared to a gas price of Dfl 1.00. The gas price determines the magnitude of the cost caused by CH₄ loss. The higher the gas price the higher the price that must be paid for the CH₄ loss. To get more information about the contribution of CH₄ loss cost, the total annual cost is split in the contributions of CH₄ loss cost and the remaining cost. The results are given in Figure 7.6 for a gas price of Dfl 0.50/m³ and Dfl 1.00/m³.

The contribution of CH₄ loss cost for the untreated membrane exceeds the remainder at a pressure of 38 bar for a gas price of Dfl 0.50/m³ and already at 22 bar for a gas price of Dfl 1.00/m³. At 50 bar feed pressure or higher it even exceeds the remainder cost for the stabilized membrane. The contribution of CH₄ loss cost for the stabilized membrane is lower compared to the remainder over the entire pressure range for both gas prices. Hence, the enormous contribution of the CH₄ loss cost for the untreated membrane is the reason for the high annual operational cost at elevated pressures. The stabilized membrane is therefore

more attractive at high feed pressures compared to the untreated membrane.

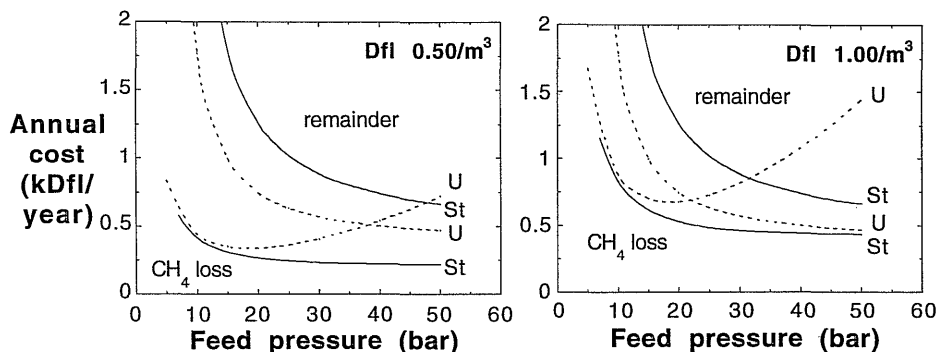


Figure 7.6. Annual operating cost split in CH₄ loss cost and the remainder for an untreated (dashed lines) and a stabilized membrane (solid lines) at gas prices of DfI 0.50/m³ and DfI 1.00/m³ (U= untreated, St=stabilized).

The stabilized membrane is also favoured if the total product streams (m³/year) are compared at high feed pressure. As was shown in the previous section the stabilized membrane gives larger product streams than the untreated membrane. A higher product stream means more gas product for sale. The benefit from gas sales is expressed by the pay-back time as defined by Equation (7.15). Figure 7.7 shows the pay-back time as function of feed pressure for the untreated and the stabilized Matrimid membrane for gas prices of DfI 0.50/m³ and DfI 1.00/m³.

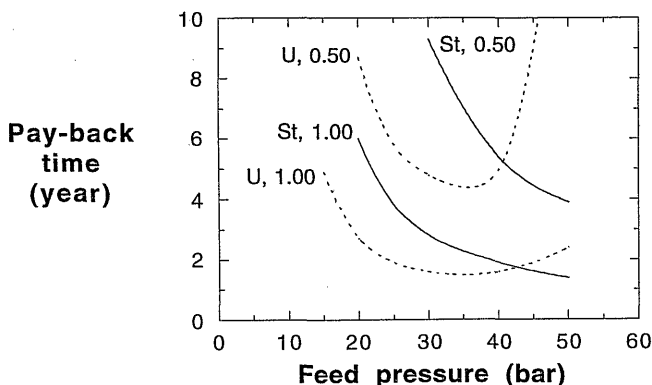


Figure 7.7. Pay-back time of an untreated (dashed lines) and a stabilized membrane (solid line) at gas prices of DfI 0.50/m³ and DfI 1.00/m³ (U= untreated and St=stabilized).

The pay-back time decreases with increasing feed pressure for the stabilized membrane over the entire pressure range irrespective of the gas price. The pay-back time is shorter for a gas price of DfI 1.00 m³ because of higher profits from gas sales. The untreated membrane shows similar trends at feed pressures up to about 35 bar. The pay-back time of the untreated membrane is lower compared to the stabilized membrane as the same gas price is considered. An explanation for this is that the annual cost of the untreated membrane are lower. However, above 35 bar the untreated membrane shows an increasing pay-back time with increasing feed pressure. The annual cost of the untreated membrane increases. Additionally, the product stream decreases with increasing feed pressure. Hence, the increase of the annual cost cannot be compensated by the profit from gas sales, because of the decreasing product stream.

The annual operational cost also depend on membrane life time. The membrane replacement cost are higher with shorter membrane life. For membrane life times of 3, 5, 7 and 10 years, the annual operational cost per m³ product are calculated for the untreated and stabilized Matrimid membrane for gas prices of DfI 0.50/m³ and DfI 1.00/m³. These calculations are done for a feed pressure of 50 bar. Additionally, the pay-back time is calculated for each case. Some fixed parameters and costs are given in Table 7.2.

Table 7.2. Fixed process and cost parameters for an untreated and a stabilized membrane with a membrane life of 5 years.
Process conditions: feed pressure = 50 bar, temperature = 35 °C.

	Untreated	Stabilized
Feed: 45% CH ₄ (m ³ /year)	8760	8760
Product: 98% CH ₄ (m ³ /year)	2558	3583
CH₄ loss (%)	37	11
Membrane cost (DfI/year)	396	880
Investment (DfI/year)	1584	3520
Energy (DfI/year)	311	311

The calculations are based on the basic assumption of equal feed flow rates. From this point of view the stabilized membrane produces more product gas with 98% methane purity than the untreated one since the methane loss is lower for the stabilized membrane. The membrane cost are lower for the untreated one, because less membrane area is required to reach a product purity of 98%. The investment cost is therefore lower for the untreated membrane. The energy consumption is the same for both membranes because the operating pressure is the same.

The annual cost and pay-back times for different membrane life times at 50 bar feed pressure are given in Table 7.3. The annual operational cost are lower than the gas price for all calculated cases. The cost per volume product of the stabilized membrane are about a factor two lower compared to a gas price of Dfl 0.50/m³ and even a factor three compared to a gas price of Dfl 1.00/m³. The membrane life times considered do not contribute much to the annual operation cost in most cases, except for the stabilized membrane as a gas price of Dfl 1.00/m³ is considered. The cost per volume product are about 18% lower in case the membrane life is ten years instead of three. However, a membrane life of ten years is unrealistic. A life time of 3 to 5 years is more realistic.

Table 7.3. Annual operational cost and pay-back time for an untreated (U) and a stabilized membrane (St) operating at 50 bar feed pressure as function of membrane life time for gas prices of Dfl 0.50/m³ and Dfl 1.00/m³.

		Membrane life time (year)			
		3	5	7	10
<i>gas = Dfl 0.50/m³</i>					
Annual operational cost (Dfl/m ³ product)	U	0.49	0.46	0.46	0.45
	St	0.28	0.25	0.23	0.22
Pay-back time (year)	U	42	18	14	12
	St	4.4	3.9	3.7	3.5
<i>gas = Dfl 1.00/m³</i>					
Annual operational cost (Dfl/m ³ product)	U	0.77	0.75	0.74	0.73
	St	0.34	0.31	0.29	0.28
Pay-back time (year)	U	2.7	2.4	2.4	2.3
	St	1.5	1.4	1.4	1.4

The largest contribution of membrane life to the pay-back time is observed for both membranes for a gas price of Dfl 0.50/m³. The pay-back times of the untreated membrane are unacceptably high. The reason is the high methane loss cost caused by membrane plasticization. Because these data are not realistic, they will not be discussed further. The pay-back time of the stabilized membrane is about 20% shorter at a membrane life of 10 years as compared to 3 years. But as noticed above, a life time of ten years is not realistic. Considering the pay-back time of about 4 years of the stabilized membrane at a membrane life of 3 to 5 years, it must be admitted that this is too long to make the process technically viable. [14]. Pay-back times of 2-3 years are more realistic and economical. This means that the process needs optimization to reach higher recoveries. With higher recoveries the benefit from gas sales will increase and the pay-back time may decrease. For gas prices of Dfl 1.00/m³ and membrane life of 3 years, pay-back times of 1.5 years for the stabilized and 2.7 years for the untreated

membranes are calculated. From this point of view, the stabilized membrane is again the most attractive one.

7.4. Conclusions

Permeator analysis

- The stabilized membrane has a lower permeability than the untreated membrane. More membrane area is therefore needed to achieve the same product purity, but a higher CH₄ recovery is obtained.
- The stabilized membrane shows an almost constant product flow at higher feed pressures, whereas the product flow of the untreated membrane decreases with increasing feed pressure.

Cost accounting

- At low feed pressures the annual operational cost decrease with increasing feed pressure for the untreated as well as the stabilized membrane. At elevated pressures the annual operation cost increase with further increase of pressure for the untreated membrane.
- If the actual gas price of DfI 0.50/m³ is considered, the untreated membrane is favoured at pressures up to 20 bar. The annual operational cost as well as the pay-back time are lower for pressures below 20 bar if a membrane life of 5 years is assumed. However, as we are interested in operating pressures of 50 bar or higher, the stabilized membrane is attractive. Although more membrane area is required resulting in a higher initial investment, the stabilized membrane shows lower operational cost and a shorter pay-back time at 50 bar feed pressure compared to the untreated membrane. The better performance of the stabilized membrane can be attributed to less methane loss and therefore a higher recovery resulting in higher profit from gas sales.

7.5. List of symbols

In this list i stands for the gas component CO_2 as well as CH_4 .

Permeator analysis

A	= total membrane area	m^2
dA	= differential membrane area	m^2
ℓ	= membrane thickness	m
P_i	= permeability of component i	$\frac{\text{m}^3(\text{STP})\cdot\text{m}}{\text{m}^2\cdot\text{s}\cdot\text{bar}}$
p^f	= total feed pressure	bar
p_i^f	= partial pressure in the feed of component i	bar
p^P	= permeate pressure	bar
Q_F	= total feed flow	m^3/h
Q_P	= total permeate flow	m^3/h
Q_R	= total retentate flow	m^3/h
Q_i^F	= total feed flow of component i	m^3/h
Q_i^P	= total permeate flow of component i	m^3/h
Q_i^R	= total retentate flow of component i	m^3/h
q_i^f	= feed flow of component i per element	m^3/h
q_i^P	= permeate flow of component i per element	m^3/h
q_i^R	= retentate flow of component i per element	m^3/h
X_i^f	= mole fraction of component i in feed in element	–
X_i^P	= mole fraction of component i in permeate/element	–
X_i^R	= mole fraction of component i in retentate/element	–
α	= separation factor	–

Cost accounting

n	= number of moles to be pumped per second	mol/s
P	= power	kW
R	= gas constant	J/mol K
T	= temperature	K
η	= compressor efficiency	–

7.6. References

- [1] Weller, S., Steiner, W.A., Separation of gases by fractional permeation through membranes, *J. Appl. Phys.*, 21 (1950) 279-283
- [2] Stern, S.A., Walawender, W.P., Analysis of membrane separation parameters, *Sep. Science*, 4(2) (1969) 129-159
- [3] Hwang, S.-T., Kammermeyer, K., *Membranes in separations*, John Wiley & Sons, New York, (1975)
- [4] Rautenbach, R., Albrecht, R., *Membrane separation processes*, Wiley, (1989)
- [5] Sengupta, A., Sirkar, K.K., Analysis and design of membrane permeators for gas separation, Chapter 11 in: *Membrane separations technology. Principles and applications*, Noble, R.D., Stern, S.A., (Eds.), Elsevier, Amsterdam, (1995)
- [6] Spillman, R., Economics of gas separation membranes, *Chem. Eng. Prog.*, (1989) 41-62; Economics of gas separation membrane processes, Chapter 13 in: *Membrane separations technology. Principles and applications*, Noble, R.D., Stern, S.A., (Eds.), Elsevier, Amsterdam, (1995)
- [7] Bhide, B.D., Stern, S.A., Membrane processes for the removal of acid gases from natural gas. I. Process configurations and optimization of operating conditions., *J. Membrane Sci.*, 81 (1993) 209-237
- [8] Bhide, B.D., Stern, S.A., Membrane processes for the removal of acid gases from natural gas. II. Effect of operating conditions, economic parameters, and membrane properties, *J. Membrane Sci.*, 81 (1993) 239-252
- [9] Lababidi, H., Al-Enezi, G.A., Ettouney, H.M., Optimization of module configuration in membrane gas separation, *J. Membrane Sci.*, 112 (1996) 185-197
- [10] MacLean, D.L., Stookey, D.J., Metzger, T.R., *Fundamentals of gas permeation*, Hydrocarbon Processing, August (1993) 47-51
- [11] Li, K., Acharya, D.R., Hughes, R., Performance of a cellulose acetate permeator with permeability-influenced feed, *AIChE Journal*, 36(10) (1990) 1610-1612
- [12] Ettouney, H.M., Al-Enezi, G., Hughes, R., Modelling of enrichment of natural gas wells by membranes, *Gas Sep. Purif.*, 9(1) (1995) 3-11
- [13] Genereaux, R.P., Mitchell, C.J.B., Hempstead, C.A., Curran, B.F., Transport and storage of fluids, Section 6 in: *Perry's chemical engineers' handbook*, Perry, R.H., Green, D., Maloney, J.O., (Eds.), sixth edition, McGraw-Hill Book Company, New York, (1984)
- [14] Coulson, J.M., Richardson, J.F., Sinnott, R.K., *Chemical Engineering, Vol. 6: Design*, Pergamon, (1983) 206

Summary

The main research objective was to develop a highly selective polyimide membrane for the separation of CO₂/CH₄ mixtures that maintains its separation performance at high feed pressures. Polyimide gas separation membranes have a significantly better permselective performance than membranes made from conventional glassy polymers such as cellulose acetate and polysulfone. Problems arise in applications where the polymer sorbs one or more species to such an extent that plasticization phenomena occur. The polymer matrix swells upon sorption of one species which accelerates the permeation of the other. As a consequence, the polymer membrane loses its selectivity. In CO₂/CH₄ separations CO₂ acts as a plasticizer. A typical effect of plasticization is that the permeability-versus-pressure curves go through a minimum. The pressure corresponding with the minimum permeability is called the plasticization pressure. The minimum partial carbon dioxide pressure, which is necessary to induce plasticization is easily exceeded in for example natural gas upgrading, enhanced oil recovery and landfill gas cleaning.

To prevent plasticization, understanding of the phenomenon is necessary. This thesis focuses firstly on understanding of CO₂-induced plasticization on a molecular level and secondly on identifying methods, such as crosslinking, to suppress plasticization. For the first task, different glassy polymers are characterized. For the second task, mainly the polyimide Matrimid 5218 (Ciba Geigy) is used. Although Matrimid is not as permeable as some of the polyimides of interest, it is chosen as a model polymer. It has the advantages that it is commercially available and also soluble in many common solvents. Furthermore, it has a high tendency to plasticize and is therefore a useful candidate to demonstrate possible effects of suppressing plasticization.

All experiments are carried out with solution cast homogeneous dense films. Since glassy polymer films are non-equilibrium materials, the effect of casting solvent and film thickness are described in Chapter 2. It has been concluded that the casting solvent used or the membrane thickness do not influence the study on the plasticization behaviour of CO₂.

CO₂-induced plasticization phenomena in eleven different glassy polymers are described in Chapter 3. The main objective was to search for relationships between the plasticization pressure and the chemical structure of the polymer. No trends are found based on glass transition temperature or fractional free volume. The plasticization pressure does not depend on the polar carbonyl or

sulfone density of the polymers considered either. However, it was found that the polymers studied needed the same critical CO₂ concentration to plasticize. Depending on the polymer, different pressures (the plasticization pressure) are required to reach the critical concentration.

Two options to suppress plasticization are: crosslinking or blending a polymer highly susceptible to plasticization with a polymer that hardly plasticizes. Chapter 4 describes the results obtained in thermally crosslinking Matrimid films at 350 °C. This heat-treatment has proven to be a successful method to suppress CO₂-induced plasticization. In single gas permeation, a constant permeability at elevated pressures is obtained for the treated film, whereas the untreated film shows an enormous increase in permeability due to plasticization. Mixed gas permeation experiments reveal that the partial CH₄ permeability remains constant for the treated films. For the untreated film the CH₄ permeability strongly increases at higher partial CH₄ pressure due to the CO₂ plasticization.

Chapter 5 describes the influence of blending on plasticization. Blending of Matrimid (highly susceptible to plasticization) with the copolyimide P84 (moderate tendency to plasticize) or with polysulfone (low tendency to plasticize) is very promising in suppressing CO₂-induced plasticization. However, to get a clear picture more research is necessary to study the effect of different ratios of the polymers in the blend and the effect of possible blend inhomogeneity. Blending of Matrimid and the oligomer Thermid with a subsequent heat-treatment at 265 °C is found to be a more successful method to suppress the CO₂-induced plasticization phenomena in Matrimid. As in the case of the thermal treatment at 350 °C, the network formed prevents the polymer matrix to swell and thereby suppresses plasticization.

Fourier transform infrared (FTIR) measurements are described in Chapter 6. FTIR is a useful method to study the behaviour of CO₂ in a polymer film. The peak corresponding to the anti-symmetrical stretching vibration of CO₂ shows an additional small peak at lower frequency which is attributed to a 'hot-band' transition. This 'hot-band' indicates interaction of CO₂ with the polymer matrix and is observed for CO₂ dissolved in an untreated as well as a treated (350 °C) Matrimid film. However, in studying the desorption of CO₂ from the untreated and the treated film, a significant difference in the ratio of the 'hot-band' intensity and the normal anti-symmetrical stretching vibration is observed. At longer desorption time, the intensity of the 'hot-band' of CO₂ dissolved in the untreated film decreases faster than the intensity measured in the treated film. This indicates that the interaction with polar groups is not necessarily favoured, which supports the findings in Chapter 3 where no correlation is found between the plasticization pressure and the density of polar groups in the polymer structure. Furthermore, these FTIR measurements support the hypothesis that plasticization is a matter of concentration. A critical CO₂ concentration is

necessary to loosen up the polymer matrix. Evidence for the increase in free volume is the fact that the CO₂ molecules in the untreated film have the possibility to move to sorption sites other than the polar interaction sites. In case of the treated film, the network created prevents the polymer matrix to increase its free volume by plasticization. More CO₂ molecules are located in close distance of the polar interaction sites as indicated by the longer existence of the 'hot-band' transition.

Chapter 7 describes membrane process simulations with a CO₂/CH₄ gas mixture. The calculations are based on mixed gas permeation data obtained with an untreated and a stabilized (thermally treated at 350 °C) Matrimid membrane. A gas mixture containing 45 mole % CH₄ is upgraded to 98 mole % CH₄. Compared to an untreated membrane, the stabilized membrane has a lower permeability and requires therefore more membrane area to achieve the same product purity, at the gain of a higher CH₄ recovery. Furthermore, the stabilized membrane shows an almost constant product flow at higher feed pressures, whereas the product flow of the untreated membrane decreases with increasing feed pressure. A cost price analysis shows lower operational costs and shorter pay-back times at high feed pressures for the stabilized membrane compared to the untreated membrane. The economically favourable performance of the stabilized membrane can be attributed to less methane loss and therefore a higher recovery, resulting in higher profit from gas sales.

Samenvatting

Het onderzoek beschreven in dit proefschrift is gericht op het ontwikkelen van een hoog selectief polyimide membraan voor de scheiding van CO_2/CH_4 mengsels dat zijn scheidende eigenschappen behoudt bij hoge druk. Gasscheidingsmembranen gemaakt van polyimides hebben beduidend betere eigenschappen dan membranen gemaakt van conventionele glasachtige polymeren zoals cellulose-acetetaat en polysulfon. Problemen ontstaan in toepassingen waar het polymeer één of meerdere componenten in een zodanige mate absorbeert dat verweking optreedt. De polymeermatrix zwelt ten gevolge van de hoge sorptie van die component(en), met als gevolg dat de doorlaatbaarheid van de andere component wordt vergroot. Het polymeermembraan verliest dan zijn selectiviteit. CO_2 veroorzaakt de verweking in CO_2/CH_4 -scheidingen. Typend effect van verweking is dat de permeabiliteit-versus-druk curven door een minimum gaan. De druk die overeenkomt met de minimum-permeabiliteit wordt de verwekingsdruk genoemd. De minimale partieldruk van CO_2 nodig om verweking te induceren wordt snel overschreden in bijvoorbeeld aardgas-opwerking, verhoogde olieterugwinning en het opwerken van stortgas.

Om verweking te voorkomen is een beter begrip van het verschijnsel nodig. Het onderzoek beschreven in dit proefschrift is daarom geconcentreerd op het begrijpen van CO_2 -geïnduceerde verweking op een moleculair niveau en op het identificeren van methoden, zoals vernetting, die verweking kunnen onderdrukken. Voor het eerste doel zijn verschillende glasachtige polymeren gekarakteriseerd. Voor het tweede doel is hoofdzakelijk het polyimide Matrimid 5218 (Ciba Geigy) gebruikt. Hoewel een Matrimid membraan niet het meest doorlaatbare polyimide membraan is, is het toch gekozen als modelpolymeer. Het heeft als voordeel dat het commercieel verkrijgbaar is en dat het oplosbaar is in verschillende gangbare oplosmiddelen. Matrimid is tevens eenvoudig te verweken met CO_2 , waardoor het een geschikt materiaal is om de mogelijke effecten van het onderdrukken van de CO_2 -verweking te testen.

Alle experimenten zijn uitgevoerd met homogene dichte films gestreken uit een polymeeroplossing. Omdat glasachtige polymeerfilms thermodynamisch niet in evenwicht zijn, is het effect van het gebruikte oplosmiddel en van de filmdikte bestudeerd. Uit de resultaten in hoofdstuk 2 kan geconcludeerd worden dat het gebruikte oplosmiddel en de filmdikte geen invloed hebben op het bestuderen van het verwekingsgedrag van CO_2 .

In hoofdstuk 3 is het verwekingsgedrag van elf verschillende glasachtige polymeren beschreven. Het voornaamste doel was een verband te vinden tussen de verwekingsdruk en de chemische structuur van het polymeer. Verbanden

tussen de verwekingsdruk en de glasovergangstemperatuur of het fractioneel vrije volume zijn niet gevonden. De verwekingsdruk blijkt ook niet af te hangen van het aantal polaire groepen in de polymeerketen. Gebleken is echter dat de bestudeerde polymeren dezelfde kritische CO₂-concentratie nodig hebben om te kunnen verweken. Deze kritische concentratie wordt, afhankelijk van het polymeer, bij verschillende drukken (de verwekingsdruk) bereikt.

Twee manieren om verweking te onderdrukken zijn: vernetting of mengen van een polymeer dat eenvoudig verweekt met een polymeer dat niet of nauwelijks verweekt. In hoofdstuk 4 zijn de resultaten beschreven die verkregen zijn met Matrimid films die vernet zijn bij 350 °C. Deze methode blijkt een goede manier te zijn om verweking te onderdrukken. Uit permeatiemetingen met puur CO₂ blijkt dat de behandelde film bij hoge druk een constante permeabiliteit geeft als functie van de druk, terwijl de onbehandelde film een enorme toename in de permeabiliteit geeft ten gevolge van verweking. Permeatiemetingen met menggas geven een constante partiële CH₄-permeabiliteit voor de behandelde film. De partiële permeabiliteit van CH₄ voor de onbehandelde film neemt enorm toe met toenemende druk.

In hoofdstuk 5 is de invloed van het mengen van polymeren op het verwekingsgedrag beschreven. Matrimid, het polymeer dat verweekt, is gemengd met de copolyimide P84 en met polysulfon (PSF). P84 en PSF zijn polymeren die beduidend minder verwekende eigenschappen vertonen. De permeabiliteit van de blends lijken constant te worden bij hoge druk. Er is echter meer onderzoek nodig naar het effect van de verhoudingen waarin de polymeren gemengd kunnen worden en naar het effect van mogelijke inhomogeniteit van de polymeerblends om een goed beeld te krijgen van het succes van deze methode. Het mengen van Matrimid met het oligomeer Thermid gevolgd door een thermische behandeling bij 265 °C blijkt een betere methode te zijn om verweking te onderdrukken. Net als bij de vernetting bij 350 °C zorgt een netwerk ervoor dat de polymeermatrix niet kan zwellen, waarmee de mogelijkheid tot verweken onderdrukt wordt.

Met behulp van Fourier-getransformeerde infrarood (FTIR) metingen met CO₂ kan het verschil in het verwekingsgedrag van CO₂ in een onbehandelde en een behandelde film nader bestudeerd worden. De resultaten zijn beschreven in hoofdstuk 6. De piek die overeenkomt met de asymmetrische rekvibratie van CO₂ heeft een extra piek bij een lager golfgetal. De extra piek wordt toegeschreven aan een 'hot-band' overgang en duidt op interactie van CO₂ met het polymeer. Deze overgang is te zien voor CO₂ dat is opgelost in zowel een onbehandelde als een behandelde (350 °C) film. Opmerkelijke verschillen in de verhouding van de intensiteiten van de 'hot-band' en de normale asymmetrische rekvibratie zijn waargenomen wanneer de desorptie van CO₂ uit de onbehandelde film wordt vergeleken met de desorptie van CO₂ uit de behandelde film. De 'hot-band' verdwijnt veel sneller in het geval van de onbehandelde film, wat aangeeft dat de interactie met de polaire groepen in de polymeerketen niet bij voorkeur optreedt. Dit ondersteunt de bevinding in hoofdstuk 3 waar geen verband is gevonden tussen de verwekingsdruk en het aantal polaire groepen in de

polymeerketen. De FTIR-metingen ondersteunen tevens de hypothese dat verweking door een component wordt bepaald door de hoeveelheid van die component in het polymeer. Een kritische CO_2 concentratie is nodig om de polymeerketens uit elkaar te drukken. Dit is alleen mogelijk voor een onbehandelde film. Bij het desorptie-experiment hebben de CO_2 -moleculen de mogelijkheid om andere plaatsen dan die bij een polaire groep te bezetten, omdat door verweking voldoende vrij volume is gecreëerd. Bewijs hiervoor is het verdwijnen van de 'hot-band' piek. Bij de behandelde film blijft de 'hot-band' piek veel langer waarneembaar. Het CO_2 blijft in de buurt van de polaire groepen. Er is geen groter vrij volume gecreëerd omdat de mogelijkheid tot verweking is onderdrukt door het netwerk. Als in dit geval de interactie tussen CO_2 en het polymeer is opgeheven dan is het CO_2 tevens uit de film verdwenen. In hoofdstuk 7 zijn procesberekeningen beschreven die gebaseerd zijn op permeatiemetingen met menggas (CO_2/CH_4) voor een onbehandelde en een gestabiliseerd (behandeld bij 350°C) Matrimid membraan. Een mengsel met 45% CH_4 wordt opgewerkt naar 98% CH_4 . Het gestabiliseerde membraan heeft een lagere permeabiliteit dan de onbehandelde en vereist daarom een groter oppervlakte om dezelfde produktzuiverheid te halen. Daartegenover staat dat met het gestabiliseerde membraan een hogere opbrengst verkregen kan worden. Het gestabiliseerde membraan geeft tevens een vrijwel constante produktstroom bij hogere voedingsdrukken, terwijl de produktstroom van het onbehandelde membraan daalt met toenemende druk. Uit een kostprijsanalyse blijkt dat de totale operationiële kosten voor het gestabiliseerde membraan lager zijn en de terugbetaaltijden korter. Deze betere resultaten voor het gestabiliseerd membraan kunnen worden toegeschreven aan minder methaan verlies, waardoor meer produkt en dus een hogere opbrengst uit de verkoop van gas wordt verkregen.

Levensloop

Alie Bos werd geboren op 23 maart 1968 te Emmen. In juni 1986 behaalde zij het VWO-diploma aan de Gemeentelijke Scholengemeenschap aldaar. In augustus van datzelfde jaar begon zij aan de HLO-opleiding van de Hogeschool Drenthe eveneens in Emmen. Stage en afstuderen vond plaats in de onderzoeksgroep Membraantechnologie van (toen) prof. dr. C.A. Smolders aan de Universiteit Twente. Gedurende de stageperiode heeft ze het sorptiegedrag van organische oplosmiddelen in siliconenrubber en ethyleen-propyleen-rubber bestudeerd. De afstudeeropdracht bestond uit het bestuderen van het permeatiegedrag van gechloreerde koolwaterstoffen door siliconenrubber. In juni 1990 behaalde zij het ingenieursdiploma. In september van datzelfde jaar vervolgde zij haar opleiding aan de Katholieke Universiteit Nijmegen met de studie Scheikunde. De afstudeeropdracht, getiteld 'Kwantitatieve interpretatie van ^{27}Al -spectra m.b.v. puls- en sweepmethoden', werd uitgevoerd in de vakgroep molecuul-spectroscopie onder leiding van prof. dr. E. de Boer. Het doctoraal diploma behaalde zij in december 1992.

Vanaf 1 januari 1993 tot 1 januari 1997 was zij als onderzoekster in opleiding in dienst van NWO. In de onderzoeksgroep Membraantechnologie van (nu) prof. dr. ing. H. Strathmann aan de Universiteit Twente werd het in dit proefschrift beschreven onderzoek verricht.



ISBN 90-3650905-X